

MQM-1A ROAD RUNNER

Max Johnson

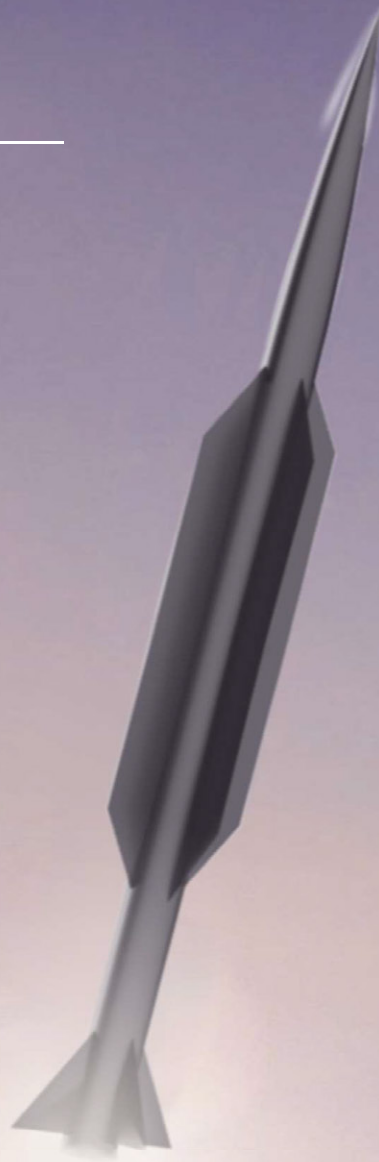
Jacob Gorman

Justin Matt

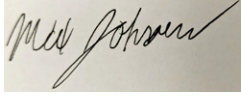



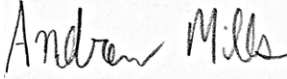


Steven Meis

Andrew Mills

Nathan Sunnarborg



Team Members

Team Member	AIAA Number	Signature
Max Johnson Co-Author	1069044	
Jacob Gorman Co-Author	998671	
Justin Matt Co-Author	985135	
Steven Meis Co-Author	985214	
Andrew Mills Co-Author	980191	
Nathan Sunnarborg Co-Author	1069091	
Dr. R. Barrett-Gonzalez Adviser	022393	

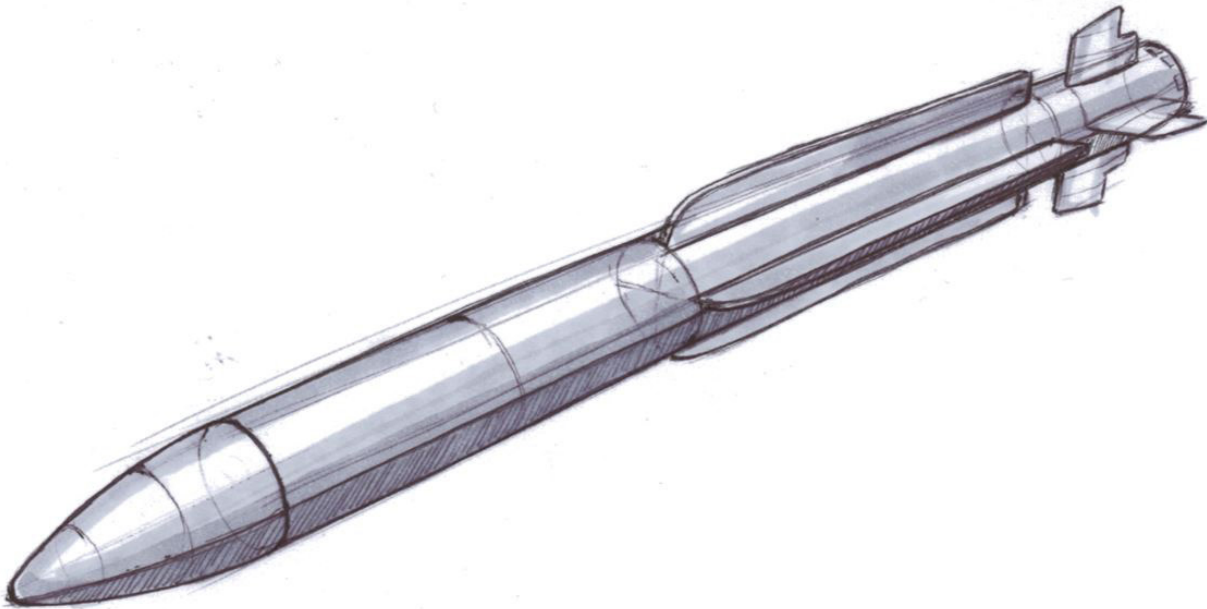


Table of Contents

1. Introduction.....	1
1.1 Mission Specifications & Profile	1
1.2 Mission Profile.....	1
1.3 Design Methods and Process.....	2
1.4 Conclusions and Recommendations.....	3
2. Historical Target Drone Relevant Designs.....	3
2.1 Orbital Sciences GQM-163 Coyote.....	3
2.2 Lockheed Q-5/AQM-60 Kingfisher	3
2.3 Beechcraft AQM-37 Jayhawk	4
2.4 Nord CT41 Narwhal	4
2.5 BrahMos Supersonic Cruise Missile	4
2.6 MBDA Meteor Air-to-Air Missile	5
2.7 Rim-67 Standard ER.....	5
2.8 Conclusions and Recommendations.....	6
3. Design Vector and Weights Establishment	6
3.1 Objective Function	6
3.2 Weighting Survey	7
3.3 Conclusions and Recommendations.....	7
4. STAMPED Analysis	7
4.1 STAMPED Analysis Technique	8
4.2 STAMPED for Major Design Drivers.....	9
4.3 Conclusions and Recommendations.....	10
5. Weight Sizing.....	10
5.1 Tentative Selection of Preliminary Design Weights.....	10
5.2 Iterative Design of Preliminary Design Weights using Fuel Fractions	11
5.3 Conclusions and Recommendations.....	11
6. Wing and Powerplant Sizing.....	11
6.1 Performance Constraints	12
6.2 Preliminary Drag Polar.....	12
6.3 Sizing Chart Analysis	12

6.4 Conclusions and Recommendations.....	13
7. Class I Configuration Matrix and Initial Downselections.....	15
7.1 Major Impacts on Configuration Design	15
7.2 Concept of Operations.....	15
7.3 Configuration Matrix	16
7.4 Conclusions and Recommendations.....	17
8. Class I Cockpit and Fuselage Layout Designs.....	18
8.1 Conclusions and Recommendations.....	18
8.2 Fuselage Summary and Recommendations.....	19
9. Class I Engine Installations.....	20
9.1 Fuselage Summary and Recommendations.....	20
9.2 Propulsion Design, Mounting, and CG Location	20
9.3 Propulsion Conclusion and Recommendations	22
10. Class I Wing Layout Designs.....	23
10.1 Wing Design Layout.....	23
10.2 Wing Design Layout.....	24
11. Class I High Lift Device Sizing.....	25
11.1 Design of High Maneuverability Devices	25
11.2 Conclusions and Recommendations	25
12. Class I Empennage Sizing.....	25
12.1 Design Process.....	25
12.2 Design of the Empennage.....	26
12.3 Design of the Empennage.....	26
13. Class I Launcher Design	27
13.1 Surveying Launchers of Similar Systems.....	27
13.2 Constraints and Considerations	28
13.3 Layout of Launcher	29
13.4 Conclusions and Recommendations.....	29
14. Class I Weight and Balance Analysis.....	30
14.1 Class I Weights Breakdowns	30
14.2 Class I Weight and Balance Calculation.....	31
14.3 CG Excursion	32
14.4 Weight and Balance Conclusions and Recommendations.....	32



15.	V-n Diagram.....	33
15.1	Presentation of the V-n Diagram	33
15.2	Gust Spectrum Analysis, Dynamic Loading and Flight Path Deviations.....	34
15.3	Conclusions and Recommendations	34
16.	Class I Stability and Control Analysis	35
16.1	Required Fin Deflection and Thrust Vectoring Angles.....	35
16.2	Conclusions and Recommendations	37
17.	Class I Drag Polar and Analysis.....	37
17.1	Drag Polar Analysis with Wetted Area Breakdown.....	37
17.2	Conclusions and Recommendations	38
18.	Analysis of Weight and Balance, Stability and Control.....	39
18.1	Impact of Weight and Balance and Stability and Control	39
18.2	Analysis of L/D Results.....	39
18.3	Design Iterations Performed.....	39
18.4	Conclusions and Recommendations	40
19.	Class I Aircraft Characteristics.....	42
19.1	Table of Class I Aircraft Characteristics.....	42
19.2	Class I Aircraft Description	43
20.	Description of Major Systems.....	43
20.1	List of Major Systems	43
20.2	Description of the Flight Control System.....	43
20.3	Description of the Fuel System	44
20.4	Environmental and Human Impact.....	48
20.5	Description of the Electrical System	48
20.6	Description of the Hydraulic System	50
20.7	Staging.....	51
20.8	Conflict Analysis	51
20.9	Conclusions and Recommendations	51
21.	Recovery System.....	52
21.1	Nap of the Earth Recovery	52
21.2	High Diver Recovery.....	52
21.3	Water Recovery	53
21.4	Conclusions and Recommendations.....	53

22.	Initial Structural Arrangement.....	54
	22.1 Nose Cone	54
	22.2 Fuselage Body and Internal Structure	54
	22.3 Propulsion System	55
	22.4 Strakes and Fins.....	55
	22.5 Assembly Procedure	56
	22.6 Conclusions and Recommendations	57
23.	Class II Weight and Balance	57
	23.1 Weight and Balance Calculations	57
	23.2 CG Position and Excursion	58
	23.3 Conclusions and Recommendations.....	60
24.	Class II Weight and Balance Analysis.....	60
	24.1 Weight and Balance Analysis	61
	24.2 Conclusions and Recommendations.....	61
25.	Updated 3-View & Aircraft Family Summary	61
26.	Advanced Technologies	64
	26.1 Hybrid Rockets.....	64
	26.2 Conclusions and Recommendations.....	64
27.	Risk Mitigation.....	64
	27.1 Risk Mitigation and Implications	65
	27.2 Conclusions and Recommendations.....	65
28.	Manufacturing Plan.....	66
	28.1 Bill of Materials.....	66
	28.2 Material Processing	66
29.	Cost Analysis.....	69
	29.1 Conclusions and Recommendations.....	71
30.	Class II Stability and Control.....	71
	30.1 Dynamic Longitudinal Stability	71
	30.2 Dynamic Lateral-Directional Stability and Dynamic Coupling.....	72
	30.3 Conclusions and Recommendations.....	72
31.	Advanced Performance	72
	31.1 Takeoff and Stall.....	72
	31.2 Climb	72



31.3 Cruise, Range, and Payload Range.....	73
31.4 Endurance and Loiter	74
31.5 Dive	74
31.6 Maneuver.....	75
31.7 Landing.....	75
31.8 Conclusions and Recommendations.....	75
32. Specification Compliance.....	75
33. Marketing Plan and Path Forward.....	76
References.....	77



<u>Symbol</u>	Description	Units
a.....	Acceleration.....	ft/s ²
AR.....	Aspect Ratio.....	(~)
b.....	Wingspan.....	ft
c.....	Chord.....	ft
C _D	Drag Coefficient.....	(~)
C _{D,0}	Parasite Drag Coefficient.....	(~)
C _L	Lift Coefficient.....	(~)
D.....	Drag.....	lbf
e.....	Oswald Efficiency Factor.....	(~)
ft.....	feet.....	ft
g.....	Acceleration of Gravity.....	ft/s ²
in.....	inch.....	in
lbs.....	pounds.....	lbs
L.....	Lift.....	lbf
M.....	Mach Number.....	(~)
n.....	Load Factor.....	(~)
nmi.....	Nautical Miles.....	nmi
q̄.....	Dynamic Pressure.....	psf
R.....	Rankine.....	degrees
S.....	Wing Area.....	ft ²
T.....	Thrust.....	lbf
T/W.....	Thrust Loading.....	(~)
W.....	Weight.....	lbf
W/S.....	Wing Loading.....	lb/ft ²
<u>Greek Symbol</u>		
Description		
α.....	Angle of Attack.....	(rad)
β.....	Sideslip Angle.....	(rad)
ρ.....	Air Density.....	(slug/ft ³)
σ.....	Standard Deviation.....	(~)
<u>Subscripts</u>		
Description		
D.....	Drag.....	(~)



D,0	Parasite Drag	(~)
e.....	empty	(~)
L.....	Lift	(~)
oe.....	operational-empty	(~)
to	Take-off	(~)

Acronyms..... Description Units

AIAA.....	American Institute of Aeronautics and Astronautics	(~)
AMROC.....	American Rocket Company.....	(~)
BVRAAM.....	Beyond Visual Range Air to Air Missile	(~)
CEP	Circular Error Probable	(~)
CG.....	Center of Gravity.....	(~)
GNC	Guidance, Navigation, and Control.....	(~)
HTPB	Hydroxy-Terminated Polybutadiene	(~)
IOC	Initial Operational Capability	(~)
KNEAS	Knots Equivalent Air Speed.....	(~)
LOx	Liquid Oxygen.....	(~)
RDTE.....	Research, Development, Testing, and Evaluation	(~)
RFP	Request for Proposal	(~)
SCFS	Slip-Cast Fused Silica	(~)
STAMPED.....	Statistical Time and Market Predictive Engineering Design.....	(~)
TDRS	Target Drone Recovery System.....	(~)
TSFC.....	Thrust Specific Fuel Consumption	(~)



1. Introduction

This report covers the summary of the aircraft design created by the University of Kansas Design Team for the American Institute of Aeronautics and Astronautics (AIAA) Graduate Team Missile Systems Design Competition. Teams were tasked with designing a supersonic aerial target drone capable of representing a variety of supersonic airborne cruise missile threats that is deployable from a fixed ground site. For the competition, teams have to design and analyze an aircraft that meet the specifications outlined in the 2019-2020 Graduate Team Missile Systems Design Competition Rules (Ref. 1).

1.1 Mission Specifications & Profile

For the 2019-2020 AIAA Graduate Team Missile Systems design competition, the Supersonic Aerial Target must be adaptable to different flight profiles and payload packages as well as the following requirements. It must be launched from a ground site, reach the desired cruise altitude and speed. It also must perform end game maneuvers including a terminal or a series of high g maneuvers. The initial operational capability (IOC) for this missile system is December of 2026.

1.2 Mission Profile

The Supersonic Aerial Target must be capable of two main flight profiles. A high altitude profile as well as a low altitude profile. Figure 1.1 shows visually outlines the high altitude mission profile and Figure 1.2 shows the low altitude mission profile.

The high altitude mission profile must meet the following requirements:

- A threshold range of 60 nmi and an objective range of 150 nmi at the end of the terminal phase;
- Cruise at an altitude between 5,000 and 65,000 ft;
- Cruise at a speed between Mach 2.0 and 4.5;

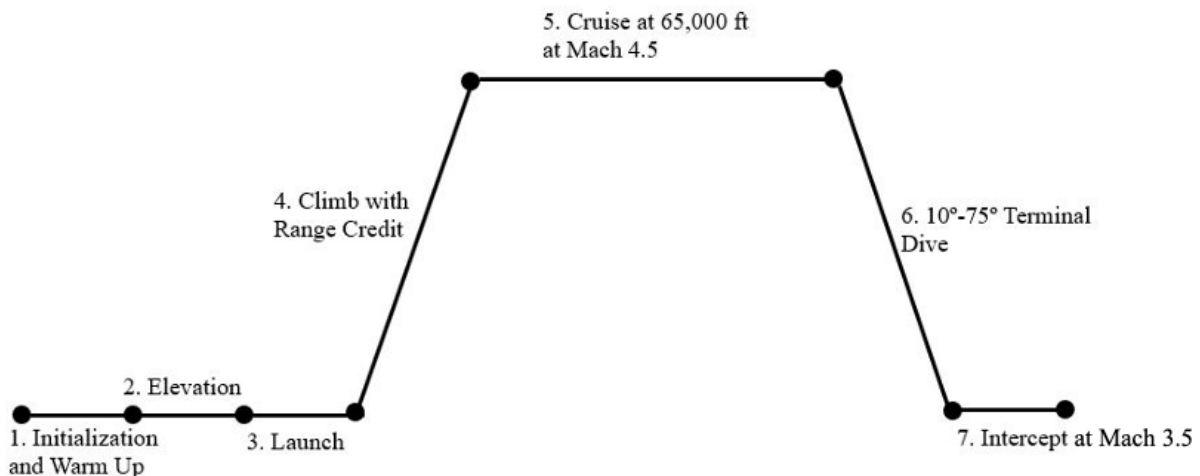


Figure 1.1: High Diver Altitude Mission Profile

- Perform a terminal dive between 10° and 75°;
- Terminal impact speed between Mach 0.9 and 3.5.

The low altitude mission profile must meet the following requirements:

- Meet the same range requirements as the high altitude mission profile;
- Cruise at an altitude between 15 and 200 ft;
- Cruise at a speed between Mach 2.0 and 3.5;
- Perform terminal high-g maneuvers during the final 20 nmi of the trajectory;
- Terminal impact speed between Mach 2.0 and 3.5.

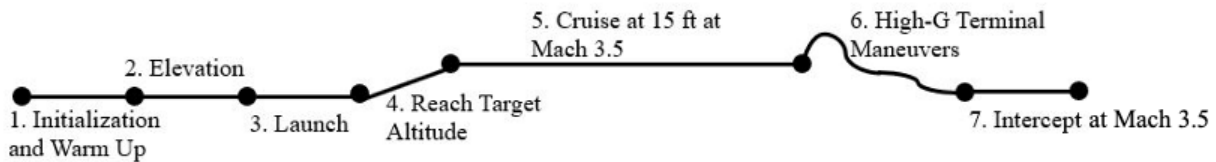


Figure 1.2: Low Altitude Altitude Mission Profile

The two designs must be capable of maintaining a course within ± 1500 ft of the programmed mid-course cruise phase and achieving a 50 ft Circular Error Probable (CEP) at the end of the terminal phase. The target system shall be compatible with modular payloads. The equipment bay to carry payload modules must provide a cylinder at least 3.5 ft long by 10 inch diameter and the total payload weight shall not exceed 500 lb (Ref. 1).

Due to International Traffic in Arms Regulations (ITAR), this target drone cannot be exported without the consent of the State department in its current state. The 500 lb payload allows for this target drone to be weaponized. A different version of the target drone can be designed without the payload bay to allow for international sales.

1.3 Design Methods and Process

Dr. Jan Roskam’s Aircraft Design Series (Ref. 2) combined with Statistical Time and Market Predictive Engineering Design (STAMPED) analysis was the basis for the design of a target drone that will be competitive in 2026. Table 1.1 outlines the design process.

Table 1.1 Design Process

Design Step	Summary
Mission Specifications	The RFP was used to identify the main objectives of the mission
Historical Overview	Similar target drones and weapons systems the drone was designed to imitate are analyzed
STAMPED Analysis	Historical data was used to establish trends in technological advancement to determine available technologies at date of IOC
Class I Designs and Down Selection	Configurations were created and compared to identify which one best met RFP requirements

1.4 Conclusions and Recommendations

The authors conclude the RFP requirements summarized in Table 1.2.

Table 1.2 RFP Restrictions

High Altitude		Low Altitude	
Altitude	65,000 ft	Altitude	15 ft
Mach Cruise	4.5	Mach Cruise	3.5
Lateral Maneuvers	N/A	Lateral Maneuvers	15 g
Vertical Maneuvers	N/A	Vertical Maneuvers	7 g

2. Historical Target Drone Relevant Designs

This chapter provides historical information from other target drones and missiles similar to what is required by the RFP.

2.1 Orbital Sciences GQM-163 Coyote

The GQM-163 Coyote is a target drone designed by Orbital Sciences that has a near-identical mission profile to the specified mission profile. It is designed for both a high diver and sea-skimming mission and is used as a training target for ship defense systems.

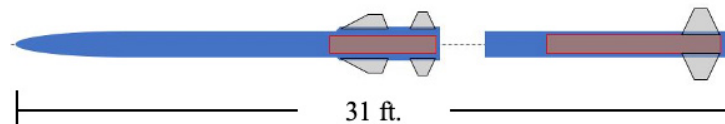


Figure 2.1: GQM 163 Coyote

The two power plants for the GQM-163 are a Hercules MK 70 solid-fueled rocket for the detachable booster stage, and an Aerojet MARC-R-282 solid-fueled ducted rocket/ramjet engine. These engines paired with the fin configurations create maximum lateral maneuvers for the Coyote that are rated for 12G, and vertical maneuvers that are rated at 5G (Ref. 3). This is slightly less than what is required for this design. However, it sets a good starting point for the design of the project in both the propulsion system design, and aerodynamic control design. It is important to note



Figure 2.2: Coyote in Flight
Courtesy of Orbital Sciences

that the Coyote is a single-use, non-recoverable design.

2.2 Lockheed Q-5/AQM-60 Kingfisher

The Lockheed Q-5/AQM-60 Kingfisher was a modification of the United States Airforce's (USAF) unmanned experimental aircraft, the X-7. In 1951, small modifications changed the X-7 into the AQM-60 Kingfisher missile defense target drone. The Kingfisher performed so well at avoiding missile defense systems that the project was shut down due to substantial political recoil.

A tapered wing is located just aft of the center of the target drone, while a conventional tail design is located just in front of the ramjet nozzle. The conventional tail adds weight and high load points compared to conventional

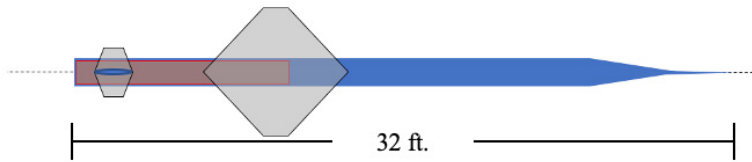


Figure 2.3: Q-5/AQM-60 Kingfisher

nose down, where the large front spike pierces the ground, absorbing the brunt of the impact and protecting the rest of the target drone (Ref. 4).

missile design fins. It does boast, however, an innovative land recovery feature unique to most target drones. Once out of fuel, it deploys parachutes that guide the Kingfisher

2.3 Beechcraft AQM-37 Jayhawk

The AQM-37 Jayhawk is an aerial launched, expendable target drone designed for the USAF in 1959. The Jayhawk was launched from a fighter aircraft and had only a five-minute flight time and a range of 100 nmi before it would self-destruct. Since production began, a total of over 5,000 AQM-37 target drones have been produced and used.

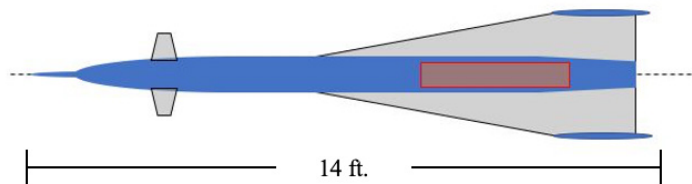


Figure 2.4: Beechcraft AQM-37 Jayhawk

Unique to the Jayhawk is a 3 ft 4 in wing-

span tapered wing with large wingtips extending above and below the wings (Ref. 5). Canards are also located near the nose cone of the Jayhawk to help with aerodynamic control and maneuvers. The Jayhawk has no vertical tail or lateral control surfaces. This design will cause high drag which needs to be minimized elsewhere.

2.4 Nord CT41 Narwhal

The CT41 Narwhal was a supersonic target drone built by the French company Nord that was designed in 1959 for use from the French Air Force. A total of 62 target drones were produced and they faced early retirement due to being too fast for interceptor pilots to practically train on.

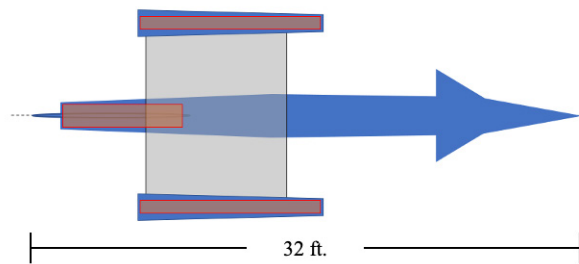


Figure 2.5: Nord CT41 Narwhal

The Narwhal launched from an elevated ramp using two solid-fueled rocket engines attached just aft of the front canards and sustained flight through two Type 625 ramjet engines mounted on its wingtips. For aerodynamic control, the Narwhal had two frontal canards, a large rectangular wing, and a large tail

extending above and below the fuselage. These surfaces would cause large drag and weight compared to target drones and missiles of today. Unlike some other designs, it was made recoverable using a parachute after the flight mission was over (Ref. 6).

2.5 BrahMos Supersonic Cruise Missile

Like the GQM-163 Coyote, the BrahMos cruise missile flies at similar specifications to the desired mission profile. It is a universal cruise missile that has been designed to launch from ships, submarines, aircraft, and land-based mobile launchers. It is a joint effort project from India's Defense Research and Development Organization and

the Russian NPO Mashinostroyenia who provided the base design with the P-800 Oniks cruise missile.

The ramjet design, unlike many missiles, requires no added inlets on top

of the missile. This is due to the forward placement of the ramjet, allowing the nose cone to act as the inlet. Also different from other missiles and target drones, the BrahMos had very little in the way of aerodynamic control surfaces. It has four large fins located just aft of midway for control and four even smaller fins just forward of the nozzle. Unlike most configurations, these fins appear to just be able to guide the missile but offer little in performing highly loaded maneuvers.

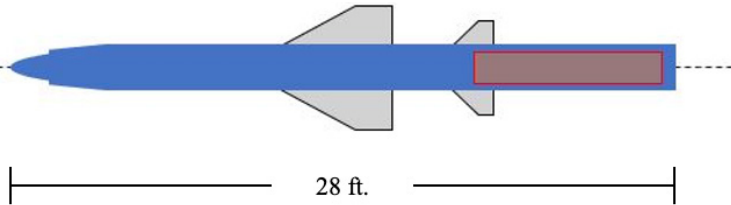


Figure 2.6: BrahMos Supersonic Cruise Missile

2.6 MBDA Meteor Air-to-Air Missile

The MBDA Missile is classified as a beyond-visual-range air-to-air missile (BVRAAM). This missile was heavily adopted for use in Europe after its introduction in 2016 and is becoming increasingly popular across

the world. It is an active radar guided missile that showcases the largest no escape zone for all air-to-air missiles to date at 53 nmi and a total range of 162 nmi.

A key feature of the missile is its throttleable ducted rocket ramjet engine, or air augmented rocket. This type of engine has been incorporated into experimental aircraft prior to the Meteor but had never before been successfully mass produced. The advantages of this design are a very high specific impulse, improved ramjet efficiency, and performance at zero forward velocity. Disadvantages for the design largely revolve around its complexity. Inlets for proper and efficient airflow into the engine largely are the driving design factor for this propulsion system and require most design choices be made around it (Ref. 7).

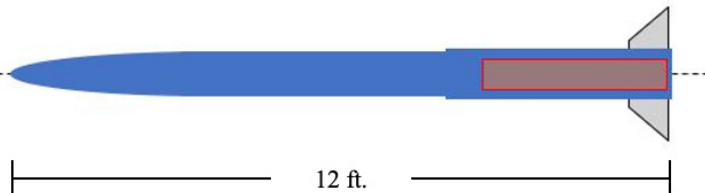


Figure 2.7: MBDA Meteor Air-to-Air Missile



Figure 2.8: MBDA Meteor
Courtesy of MBDA

2.7 Rim-67 Standard ER

The RIM-67 Standard ER is a dual role missile designed for the United States Navy by Raytheon in 1981. It was created to replace the dated RIM-8 Talos and RIM-2 Terrier. The RIM-67 was launched from the deck of a

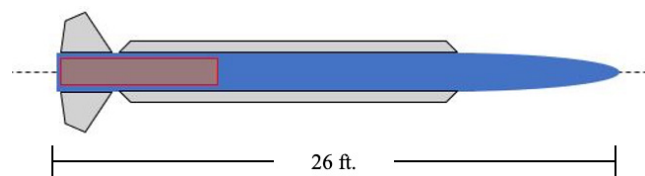


Figure 2.9: Rim-67 Standard ER

naval vessel and could be used for both anti-ship and surface-to-air mission profiles. Uniquely, the RIM-67 uses two solid fuel rockets for all its propulsion. Over time through tried and true performance, it has become the

standard missile for the navy (Ref. 8).

2.8 Conclusions and Recommendations

The authors conclude the following information in Table 2.1.

The authors recommend that:

- A higher fidelity search of similar aircraft be conducted for more design possibilities.

Table 2.1: Historical Data Tabulation

	Cruise Speed (Mach)	Max Service Ceiling (ft)	Target Range (nmi)	Maneuver Loading (g)	Length (ft)	Weight (lb)
GQM-163 Coyote	2.6-4.0	55,000	45	5-12	31	3,260
AQM-60 Kingfisher	4.3	98,000	113	-	32	8,000
AQM-37 Jayhawk	4.0	100,000	100	-	14	620
CT41 Narwhal	3.1	65,000	-	-	32	2,860
PJ-10 BrahMos	3.0	49,000	270	-	28	6,600
MBDA Meteor	4.0	-	53-262	-	12	420
RIM-67 Standard	2.5	80,000	601-00	-	26	2,960
F-22 Raptor	2.3	65,000	1600+	-	62	85,000
RFP Requirements	2.0-4.5	65,000	60-150	7-15	-	-

3. Design Vector and Weights Establishment

To hone the design of the target drone, two objective functions were created based on the requirements from the RFP. To maximize the functions, the modular design must not only meet all RFP requirements for both mission profiles, but also optimize the design components such as the engine and recovery systems. Using historical data along with STAMPED analysis, the two objective functions were created in Section 3.1.

3.1 Objective Function

The *Engine** factor was broken into four sections with the goal of minimizing the complexity of each section, shown in Table 3.1. *Engine** will be equal to four minus the sum of all sections. The process of formulating this objective function is discussed in Section 3.2.

The authors' goal is to design a missile that is capable of emulating current missile designs in addition to being cost effective and reliable. After the initial design, iterations of variants can be designed to increase performance to overmatch the market and emulate future missile systems.

$$\begin{aligned}
 OF = & \text{(Meets All RFP Requirements)} \\
 & * \left[\left(\text{Engine}^* \right)^2 + \left(\frac{5300 \text{ }^\circ\text{R}}{\text{Actual Engine Temperature}} \right)^2 \right. \\
 & + \left(\frac{10 \text{ ft}^2}{\text{Actual Radar Cross Section}} \right)^2 + \left(\frac{\text{Actual \% of Cost Recovered}}{50 \% \text{ of Cost Recovered}} \right)^2 \\
 & \left. + \left(\frac{\$ 2.6 \text{ Million}}{\text{Actual Total Cost}} \right)^2 + \left(\frac{3}{\text{Total Parts Count}} \right)^2 \right]
 \end{aligned}$$

Figure 3.1: Objective Function

Table 3.1 Engine Factors for Objective Function

Section	Value
Total Engine Count	1 per Engine
Complexity of Moving Parts	1 for Turbomachinery & Variable Nozzle 0.5 for Turbomachinery or Variable Nozzle 0 for Neither
Fuel Storage	1 for Liquid Rocket Fuel 0.5 for Solid Rocket Fuel and/or Jet Fuel 0 for Solid Rocket Fuel
Inlet Complexity	1 for Variable Inlet 0.5 for Inlet 0 for No Inlet

3.2 Weighting Survey

When creating the objective functions, a weighting system was introduced to help guide the design decisions. The most important criterion for the design was meeting the RFP requirements; if requirements were not met, the design could not be submitted for the competition. Dr. Saeed Farohki, a Propulsion Engineer and Professor at the University of Kansas was interviewed to discuss the weighting of external design factors not stated in the RFP (Ref. 10). Among these were propulsion system selection, recoverability, total cost, and design simplicity. Dr. Farohki emphasized that the design can be optimized for any of these sections; however, the best design lies within coupling all of these factors to choose the final design. RFP's for similar designs provided insight into important design factors throughout the industry. This information allowed for sizing based on the most common industry trends for vehicles of similar design.

3.3 Conclusions and Recommendations

The authors conclude that:

- Historical data shows the expected length to be 25 feet, and expected weight is 3600 lb;
- Most researched designs require booster rockets for ground launch;
- Large fins and wings will create too much drag for this mission profile.

The authors recommend that:

- A higher fidelity search of more aircraft and more technical data be performed.

4. STAMPED Analysis

The Statistical Time and Market Predictive Engineering Design, known as STAMPED, utilizes market trends to predict future values for critical preliminary design variables. STAMPED eliminates the use of acceptable ranges for variables by predicting more precise and exact values.

4.1 STAMPED Analysis Technique

Aerospace design engineers gather and document wide varieties of aircraft variables and characteristics for comparing with other aircraft families and models. Trends can be made when observing these specific variables when paired with time, to predict sizing and performance criteria for future aircraft designs. One method of determining this information is an aircraft sizing chart is shown in Figure 4.1, found in (Ref. 2). Such charts can be used for providing some of the required design parameters, but others are frequently chosen from

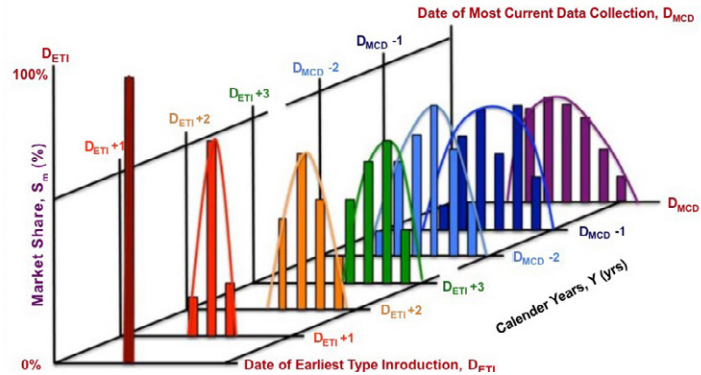


Figure 4.1: Aerospace Market Maturation Example (Ref. 12)

“‘logical choices’ to be guided by rough ‘acceptable’ ranges” (Ref. 12). A technique known as Statistical Time and Market Predictive Engineering Design (STAMPED) demonstrates the vector movement as a function of time for a variable, thus eliminating the need for choosing acceptable ranges.

The STAMPED method revolves around market analysis that ranges from the birth of an aircraft to a planned future date of optimization. The distance into the future of this optimization date has no importance due to the predictiveness of the technique. Trending can be studied for a single or group of variables, and anywhere from entrance into the market to an entirely developed market. The evolution of a variable in a market through time can be presented in a fashion such as Figure 4.1. The shape of a statistical distribution for a certain variable in a market allows for the determination of the ideal value. Following the peak through the years of the market can predict what will dominate the market at a future date.

The STAMPED technique can be extended by tracking two variables in the same market over the same time period, an example is presented in Figure 4.2. It can be seen that the peak value of the two variables are not correlated,

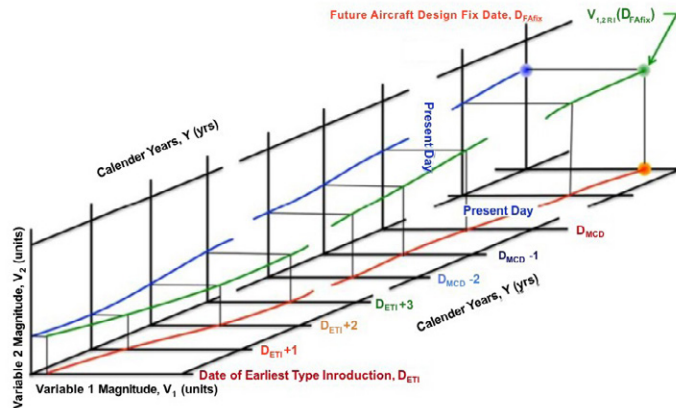


Figure 4.2: Multivariable Trending with Time

and vary independently through time. By looking at an aircraft sizing chart, a trend line over time is modified into a two-dimensional plot shown in Figure 4.3. This additional presentation of information from Figure 4.2 shows both direction and speed of a variable, in this case wing and power loading. The use of plots such as Figure 4.3 arrive at exact final design values. Using STAMPED vector analysis and following dominating market trends provides

the most accurate prediction of future design parameters.

4.2 STAMPED for Major Design Drivers

A sample of 39 different aircraft was collected to predict the direction the market is heading. This collection spans 60 years. Due to the confidential nature of munitions, data available is sparse, and many different types of aircraft were collected for analysis including target drones, air-to-air and surface-to-air missiles.

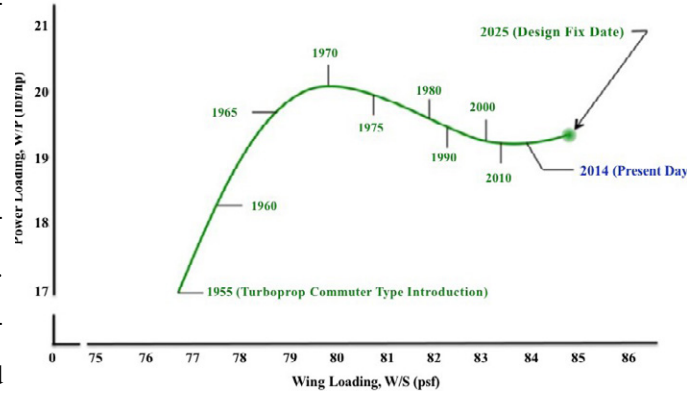


Figure 4.3: Design Point Trend with Time (Ref 12)

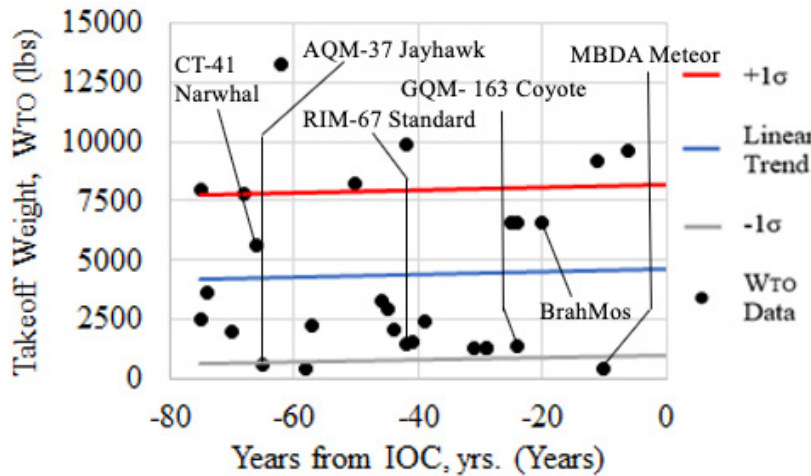


Figure 4.4: Historical Takeoff Weight

Gross takeoff weight was graphed as shown in Figure 4.4. As noted, the sparse information available for target drones and similar aircraft results in a large scatter of data and high standard deviation. Using an aggressive design approach at 25% standard deviation, the linear trend predicts a design point of 5,200 lbs.

In addition to takeoff weight, the empty to takeoff weight and thrust to weight ratios were graphed in Figure 4.5 and Figure 4.6. For aircraft with both sustaining powerplants and rocket boosters, thrust to weight data is for just the sustaining powerplant. The

Linear trends in the market were found for takeoff weight, empty weight to takeoff weight ratio, and thrust to weight ratio of the main powerplant of the aircraft. These trends were projected to initial operational capability. By calculating one standard deviation above and below the linear trendline, aggressive and conservative design points can be found.

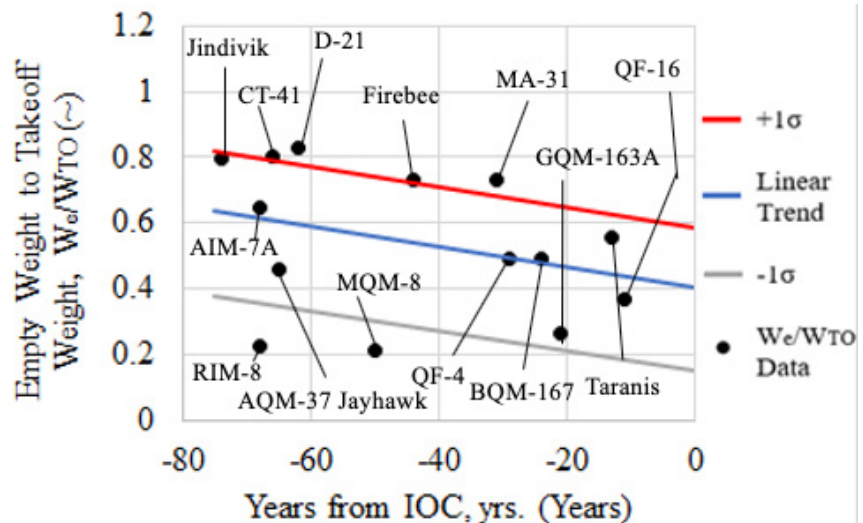


Figure 4.5: Historical Empty to Takeoff Weight

sample size of this data is even smaller, so predictions are less accurate. The aggressive design point is 0.34 for empty weight to takeoff weight and 0.58 for thrust to weight.

4.3 Conclusions and Recommendations

The authors conclude an initial estimate of takeoff weight of 5200 lbs, an initial empty-to-takeoff weight ratio of

Figure 4.6: Historical Thrust to Weight

0.34, and an initial empty weight of 1768 lbs. Due to the military aspect and application of the aerial target, information on similar existing designs is scarce and often classified outside of basic fuselage dimensions and overall weight.

The authors recommend spending more time researching military papers or contacting companies in an attempt to gather more details.

5. Weight Sizing

The weight sizing initially comes from STAMPED analysis empty to takeoff weight ratio. An iterative process is performed to determine the final take-off weight, empty weight, and fuel weight following the methods similar to those outlined in Dr. Roskam’s Airplane Design Part 1 (Ref 2). The exact step-by-step process laid out by Dr. Roskam was for airplane design and required modification by STAMPED methods to be compatible with a missile design.

5.1 Tentative Selection of Preliminary Design Weights

The iterative process began with an estimate of takeoff weight and design point for empty to takeoff weight which came from STAMPED analysis. With these known, a tentative value for the operating empty weight could be calculated. Note that because there is no crew, and unusable fuel and oil is neglected during this preliminary design stage, empty weight and operating empty weight will be equal.

Table 5.1: Initial Design Weight Estimates

W_{to} (lbs)	W_c/W_{to} (~)	W_{oe} tent (lbs)
5200	0.34	1768



5.2 Iterative Design of Preliminary Design Weights using Fuel Fractions

The objective of the iterative process is to determine the takeoff weight using Equation 2.4 from Airplane Design Part 1 (Ref. 2), while keeping the empty weight to takeoff weight within 0.5% of 0.34. To do this, the fuel weight must be determined. Since the target drone’s mission shall terminate with impact, the fuel used is designed to be 100% of the total fuel.

Fuel weight estimation is performing using the fuel fraction method. Fuel fractions were determined for each stage of the two mission profiles, with separate calculations for a ten degree and 75 degree dive during the high altitude profile. The ten degree dive was the constraining profile for fuel weight estimation. Fuel fractions are obtained from the Breguet range and endurance equations (Equations 2.8 and 2.10) from (Ref. 2). Fuel fractions are a function of lift-to-drag ratio, velocity, thrust specific fuel consumption (TSFC), and endurance or range. Lift-to-drag ratio is calculated using equations from Tactical Missile Design (Ref. 13) on page 26, and preliminary TSFC was estimated by an expert in the field (Ref. 14).

After calculating fuel fractions for each stage of the mission profile, the mission fuel fraction and fuel weight are determined. This process is repeated with different takeoff weights until the final empty to takeoff weight is within 0.5% of the design point. Different mission profiles require different amounts of fuel. The missile can be loaded with just as much fuel as required to improve efficiency and minimize pollution after impact. The mission profile that requires the most amount of fuel is the 70° high diver. The values shown in Table 5.2 account for that mission profile. The spreadsheet used to generate these values are shown in Figure 5.1.

5.3 Conclusions and Recommendations

The authors conclude that:

- The final preliminary design weights can be seen in Table 5.2;
- The initial weight changes less than 1%.

Figure 5.1: Hand Calculations

Table 5.2 Final Preliminary Design Weights

W_{to} (lbs)	W_e/W_{to} (~)	W_{oc} tent (lbs)	W_{fuel} tent (lbs)	$W_{payload}$ tent (lbs)
5150	0.34	1750	2900	500

The authors recommend a higher fidelity STAMPED analysis for better initial estimates, as well as obtaining TSFC estimates from STAMPED analysis. This was not performed due to too sparse of data, but could be collected with more time and research.

6. Wing and Powerplant Sizing

Airplane Design Part 1 by Dr. Jan Roskam (Ref. 2) was used to size the wing and powerplant of the Road Runner. This is a slightly modified version of the Roskam method since his design series is for airplanes and a missile is being designed in this scenario. The first iteration of hand calculations can be found in Figure 6.2.

6.1 Performance Constraints

The RFP for the Road Runner has restrictions for the take-off, cruise and terminal maneuvers. For the takeoff, the Road Runner will be launched from a rail, requiring no takeoff sizing requirements. Since the Road Runner is a target drone and is expected to be shot down, no landing sizing is necessary. The RFP restrictions are depicted in Table 6.1.

Table 6.1 RFP Restrictions

High Altitude		Low Altitude	
Altitude	65,000 ft	Altitude	15 ft
Mach Cruise	4.5	Mach Cruise	3.5
Lateral Maneuvers	N/A	Lateral Maneuvers	15 g
Vertical Maneuvers	N/A	Vertical Maneuvers	7 g

6.2 Preliminary Drag Polar

The S_{wet} was found by extrapolating from Figure 3.22d on pg 126 of Roskam 1 (Ref. 2). The coefficient of friction was assumed to be 0.0025 because of the smooth outer skin.

Oswald's Efficiency Factor was assumed to be 0.8. The $C_{D,o}$ was calculated using Equation 3.20 from Roskam 1 (Ref. 2). A subsonic, transonic, and supersonic drag polar was then plotted alongside each other in Figure 6.1 to illustrate the L/D values through each region. Since the Road Runner is being powered by an integrated hybrid rocket, no booster rocket will be needed and only a clean drag polar is necessary for Class I sizing.

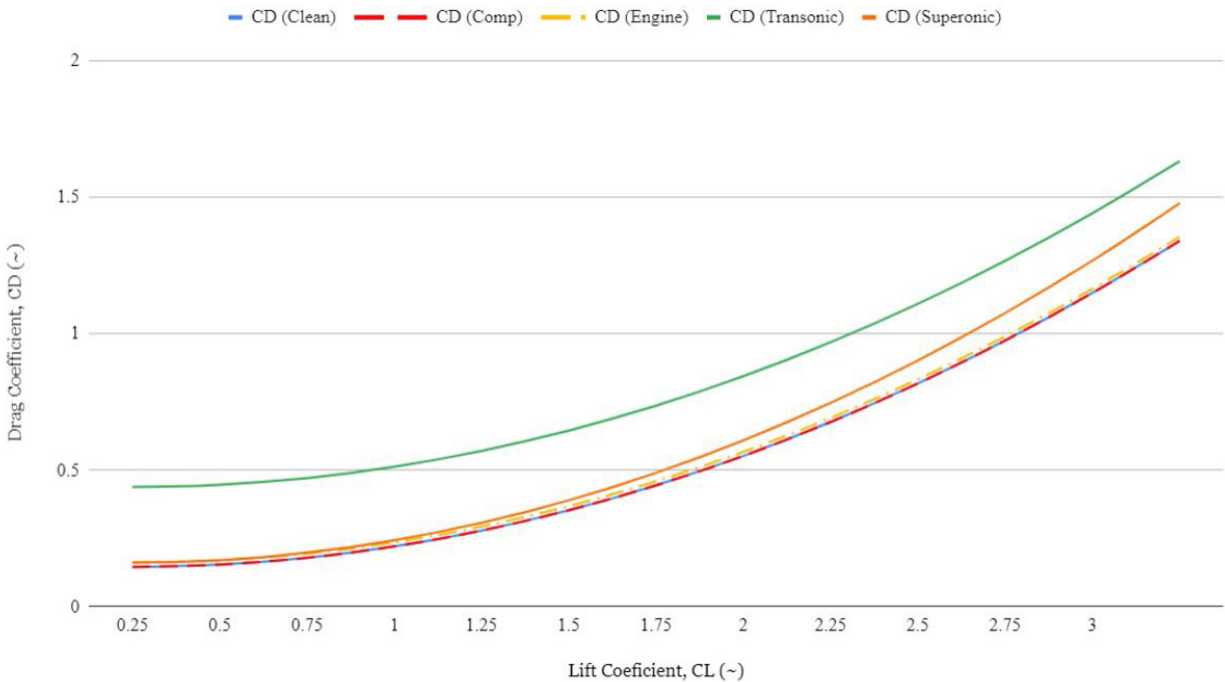


Figure 6.1: Drag Polar

6.3 Sizing Chart Analysis

The sizing was done following the linear method outlined in Chapter 3 of Roskam 1 (Ref. 2). $C_{L,max}$ values



were assumed using Table 3.1 from (Ref. 2). $C_{L,max,TO}$ isn't necessary since the roadrunner will be utilizing rocket power to take off. Using the sizing chart the salient characteristics of Class I wing and powerplant sizing were found. The values can be observed in Table 6.2. A sizing chart was created with bounds coming from the restrictions of the RFP. The design point was selected because it allows for the smallest engine and the smallest wings. This is desirable to keep costs low, reduce drag, and keep low observability.

Table 6.2 Salient Sizing Characteristics

Wing Loading, W/S (psf)	660
Thrust-to-Weight, T/W (~)	1.45
Wing Reference Area, S (ft ²)	7.6
Take-Off Thrust, T _{to} (lbf)	7510
Aspect Ratio, AR (~)	3
$C_{L,max}$ (~)	1.2
$C_{L,max,TO}$ (~)	N/A
$C_{L,max,Terminal}$ (~)	1.8

6.4 Conclusions and Recommendations

The authors conclude that:

- The aircraft will have adequate thrust to be able to take-off vertically from $V_0 = 0$ kts;
- The wing loading of the Roadrunner is 660 psf;
- The MQM-1A has an adequate thrust to weight ratio to achieve steady-state cruise at high altitudes.

The author recommends that:

- a higher fidelity of STAMPED data will create more accurate estimates for values like wing reference area or aspect ratio;
- The authors recommend adding strakes to help achieve 15 G lateral maneuvers.

Figure 6.2: Hand Calculations



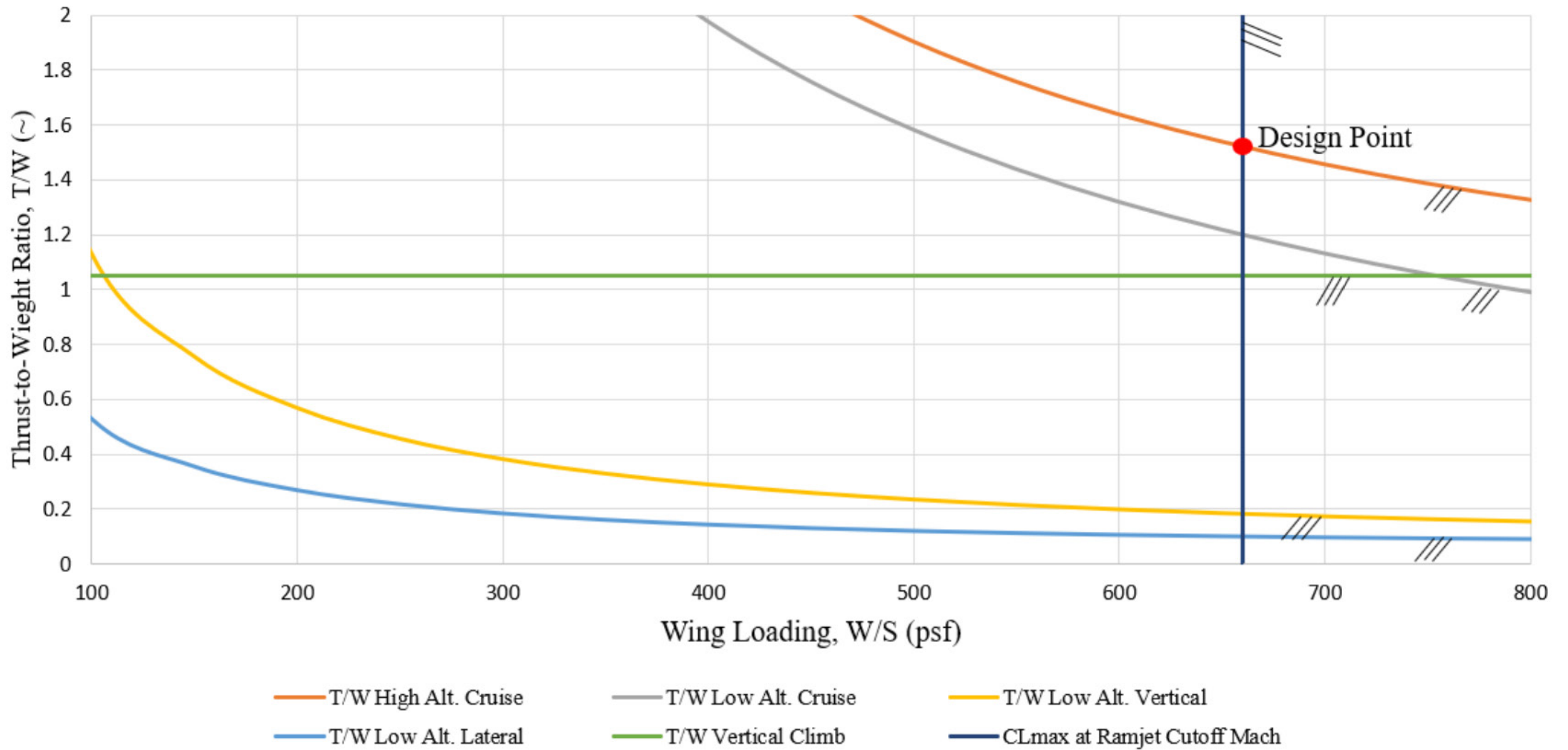


Figure 6.3: Sizing Chart

7. Class I Configuration Matrix and Initial Downselections

The methods outlined in Airplane Design Part 2 by Dr. Jan Roskam (Ref. 20) were used for preliminary configuration design selection for supersonic cruise aircraft configurations. This process requires determining the mission specifications most impactful on the configuration design and comparing historical configurations to these specifications. A design decision is then made based on the configuration the authors believe best fulfill the mission specifications.

7.1 Major Impacts on Configuration Design

Referring to the RFP and the objective function defined in Section 3, the authors have determined the following specifications have a major impact on configuration selection:

- Capable of cruise at Mach 2.0 at 65,000 ft.
- Capable of cruise at Mach 3.5 at 15 ft.
- Capable of pulling 15 g lateral maneuvers at 15 ft.
- Drag
- Total Cost

7.2 Concept of Operations

As stated by the RFP, the target drone must be able to carry out both the high altitude and low altitude mission profile. The mission will begin by loading the target drone onto the launch system. Next, if required, the target drone will be elevated to prepare for launch. After launch the missile will traverse to the desired altitude depending on the mission profile. For the high-altitude profile, the target drone must be able to produce enough lift to cruise at 65,000 ft at Mach 2.0. The low dynamic pressure at this flight condition must be considered when choosing a configuration. The high altitude mission profile ends with a terminal dive before interception of the target

During the low-altitude profile, the target drone will climb shortly to gain speed before descending to about sea level. The target drone will then cruise at Mach 3.5 at just above sea level for up to 150 nautical miles. After cruise, the low altitude profile terminates with 15-g lateral maneuvers and 7-g vertical maneuvers before interception. The control surfaces chosen must have

enough control authority to perform these 15-g maneuvers.

After terminal maneuvers, if the target has been missed, the target will perform recovery maneuvers to gain altitude and then deploy the recovery system. Figure 7.1 displays the concept of operations for the high and low altitude profiles.

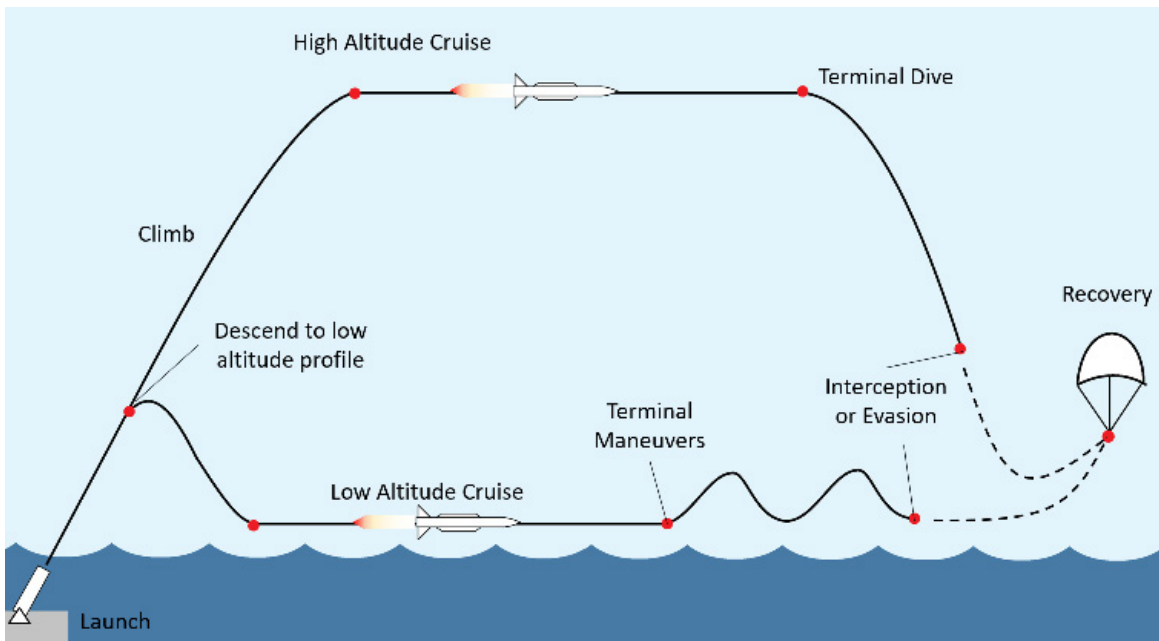


Figure 7.1: Concept of Operations

7.3 Configuration Matrix

Comparing historical configurations with similar mission specifications assists in selecting a final configuration. Table 7.1 shows the aircraft derivatives of many of the configurations shown in Figure 7.2. Refer back to Section 2 for a review of some of the historical aircraft in this table.

Table 7.1: Configuration Comparisons

Configuration	Historical Comparison	Aircraft Type
1	GQM-163 Coyote	Target Drone
2	RIM-67 Standard ER	Surface-to-air missile
3	R-77	Air-to-air missile
4	RIM-8 Talos	Surface-to-air missile
5	AQM-60 Kingfisher	Target Drone
6	Python-5	Air-to-air missile
7	AIM-9 Sidewinder	Air-to-air missile

The objective function was used to determine the optimal configuration for the target drone. Due to the limitations of physics, many aspects of the configuration are fixed such as the fuselage is required to be long and slender. The remaining work was to determine the type, size, and shape of different lifting surfaces. Figure 7.2 illustrates the performed configuration sweep. The target drones shown have varying combinations of canards, wings, strakes, and tail fins.

Many aspects of the objective function cannot be accurately estimated until later in the design stage. The primary focus was to determine the ability for the target drone to meet RFP requirements. Those that met the requirements

were compared and the most viable option was chosen.

Characteristics of the configurations such as a movable nozzle or a nose cone spike are not standalone designs, but can be added to any other design if needed to improve its performance. A decision on these features can be made later in the design process.

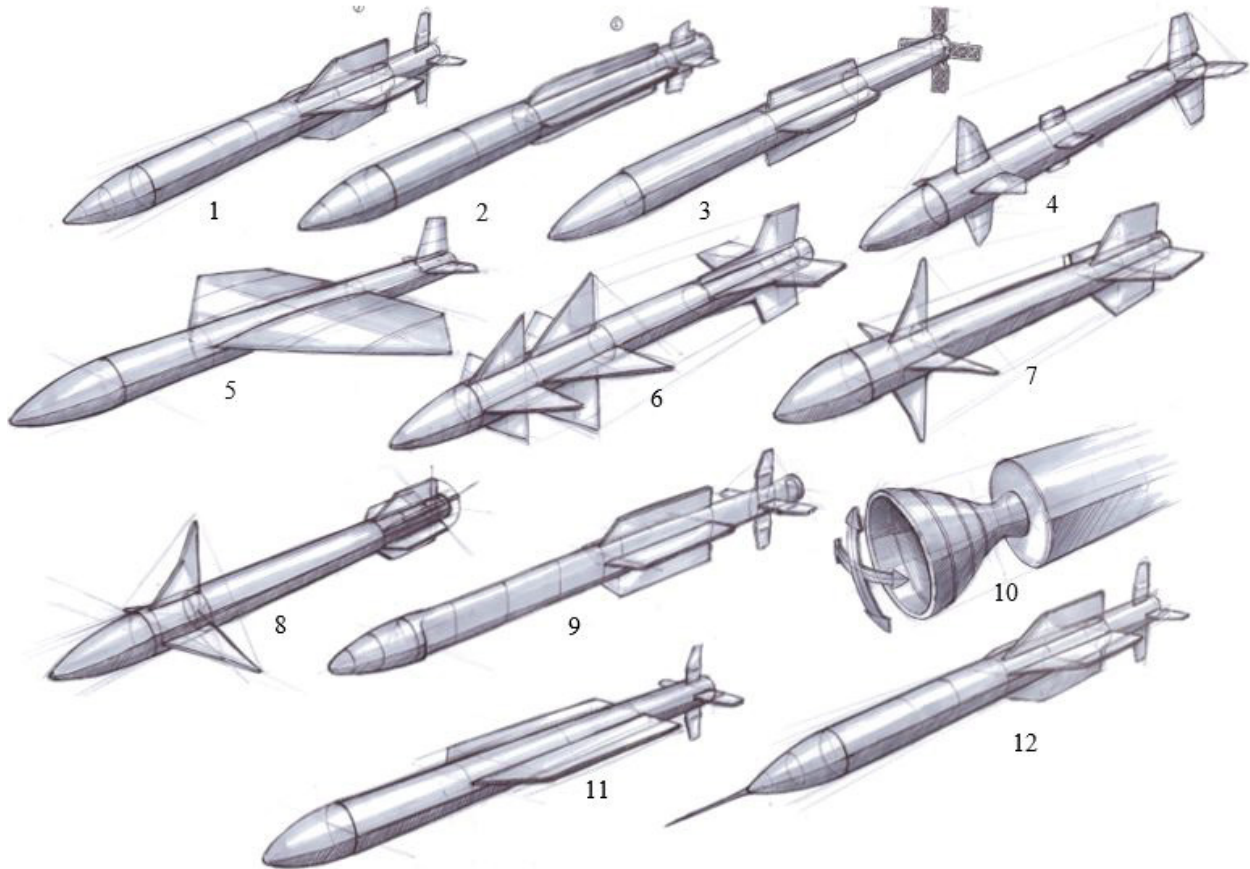


Figure 7.2: Configuration Sweep (Ref. 9)

7.4 Conclusions and Recommendations

This author concludes that configuration 2 was chosen for the following reasons:

- Strakes provide increased fin control authority to enable higher G maneuvers;
- Strakes provide the additional lift required at low dynamic pressure;
- The smaller strakes provide the advantages above while reducing wetted area, hence reducing drag;
- Tail control is more effective at high angles of attack compared to canard control
- Tail control provides low induced rolling moment.

This author recommends:

- More time to dive deeper into objective function components to get an accurate OF score;
- Or simplify the OF for a Class I design.

Table 7.2: Configuration Objective Function Comparison

Design Description	Design #	OF Highlights	OF Score (0-1)	
Higher aspect ratio strakes, cruciform fins	1	Low S_{wet} , strakes provide increased maneuverability	> 0	✓
Lower aspect ratio strakes, cruciform fins	2	Lower S_{wet} , strakes provide increased maneuverability	> 0	✓
Large strakes, grid fin	3	Grid fins create a lot of drag at low supersonic Mach #	0	✗
Canards, strakes, X-fins	4	Large S_{wet} , large drag	0	✗
Large wings, conventional tail	5	Large S_{wet} , large drag, bank to turn not ideal	0	✗
Split canards, cruciform fins	6	Large S_{wet} , canard control less desirable than tail control	0	✗
Canards, X-fins	7	Canard control less desirable than tail control, more maneuverability with cruciform tail	0	✗
3 canards, 6 fins	8	Large S_{wet} , large drag	0	✗
Elliptical lifting body, cruciform fins	9	More expensive to manufacture, smaller L/D at low angle of attack	0	✗
Movable nozzle	10	Increases maneuverability	N/A	N/A
2 large wings, cruciform tail	11	Bank to turn not ideal	0	✗
Nose cone spike	12	Increases recoverability	N/A	N/A

8. Class I Cockpit and Fuselage Layout Designs

The layout of the fuselage is critical for meeting the requirements of the RFP. Namely, the fuselage must accommodate the 500 lb. payload specified. The target drone will have no cockpit. Successfully designing the layout of internal fuselage elements is paramount for the performance of the aircraft. This design of the fuselage follows the steps outlined in Airplane Design Part 2 Chapter 4 (Ref 20).

8.1 Conclusions and Recommendations

The fuselage contains the following internal components: payload, powerplant, power supply, guidance, control systems, recovery system, and flight control actuators. Figure 8.1 shows the layout of the internal components of the fuselage. The payload is a 10 in. diameter cylinder centered with respect to the fuselage cross section.

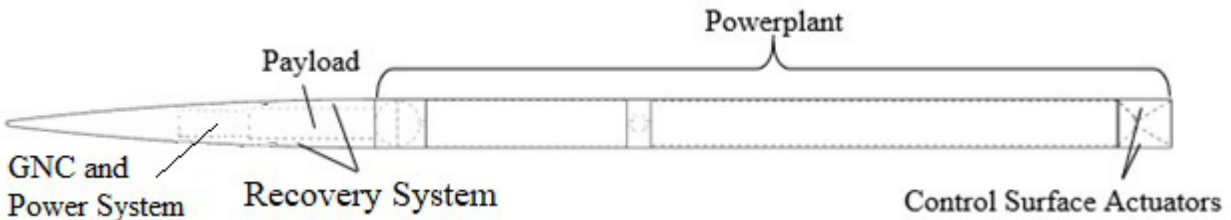


Figure 8.1: Fuselage Internal Layout

The fuselage nose is a tangent ogive extending until the beginning of the powerplant. It is blunted to a radius of 10% of the base diameter to reduce aerothermal heating and prevent imperfections in the tip that may come from mishandling of the aircraft. The remaining body is a 16 in. diameter cylinder, which was required to accommodate

the powerplant. The long nose design was chosen to attempt to emulate the Sears Haack profile, which represents the minimum wave drag coefficient a supersonic body can achieve, as seen in (Ref. 15). Figure 8.2 shows the cross-sectional area of the fuselage compared to that of the sears haack profile. The cross-section and fuselage stations are also shown in Figure 8.3.

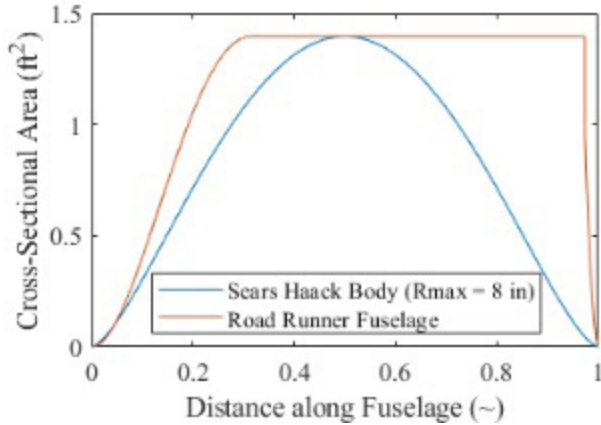


Figure 8.2: Cross Sectional Area of Fuselage

8.2 Fuselage Summary and Recommendations

Table 8.1 lists the salient characteristics of the fuselage.

Table 8.1: Fuselage Characteristics

Diameter (in.)	Length (in.)	Nose Cone Length (in.)
16	418.5	129

The author recommends further exploring powerplant solutions with a smaller nozzle. This would allow for “boat tailing” of the fuselage to further reduce drag by getting closer to the Sears Haack profile.

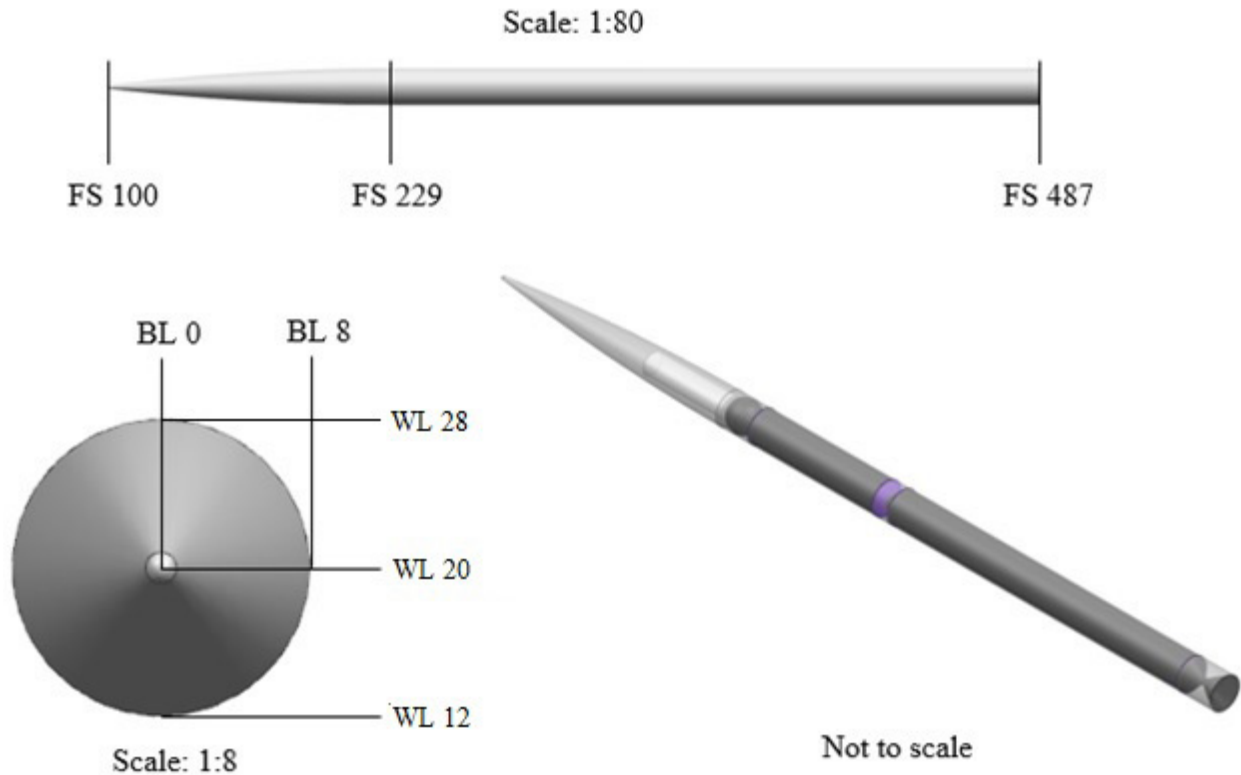


Figure 8.3: Fuselage Layout (All Dimensions in Inches)

9. Class I Engine Installations

The initial design for the Road Runner has three viable options for the propulsion selection; including ramjets, solid rockets, or liquid rockets. Between these options, there are mixtures of designs such as ram rockets and hybrid rockets. All designs mentioned above have been tested and flown prior to the design year of 2021 and are capable for operation in 2026. The iterative design process below was created from the books “Fundamentals of Hybrid Rocket Combustion and Propulsion” by George Story (Ref. 17) and “Rocket Propulsion Elements” by George Sutton (Ref. 18).

9.1 Fuselage Summary and Recommendations

The propulsion system selected for this mission needed to meet the requirements for both mission profiles as well as the sizing selections created in Chapters 5 and 6. The current generation of missiles and target drones are equipped with solid fueled rockets, ramjets, or ram-rockets. While these designs include great benefits such as low cost, low maintenance, and simplicity, the propulsion system chosen for this design is a single hybrid rocket. Below in Table 9.1, is a table listing the main advantages and disadvantages to hybrid propulsion rockets. The advantages listed below, along with requiring only one single propulsion system became the main deciding factors for selecting a hybrid rocket.

9.2 Propulsion Design, Mounting, and CG Location

Hybrid rockets have been tested throughout the years for many applications, from target drones, missiles, and low-earth orbit systems. Although it has not been widely tested like other systems, two main projects have been tested that acted as the basis for design of the Road Runner propulsion system.

The first project in the 1960’s was a joint effort between United Technologies Center and Beech Aircraft.

A target drone dubbed the sandpiper used a 12-inch, MON-25 and polymethacrylate, hybrid engine that propelled the drone to an altitude of 86 nmi with a flight time of over 300 seconds (Ref. 16). However, historical data and specifications of the rocket are too scarce to completely create

Table 9.1: Hybrid Rocket Advantages and Disadvantages (Ref 16, 17, 18)

Advantages	Disadvantages
Increased Safety regarding fires, inadvertent droppings, and explosions	Mixture ratio and specific impulse may vary during steady flow operations
HTPB and LOX are cheap, easily storable, simple processing, and high performance.	
Stop-Start-Reset Capabilities	Complicated fuel grains create unavoidable fuel slivers reducing mass fraction
Simplicity and low cost compared to liquid rockets	
Better performance than ramjets and solid rockets	Prone to low frequency pressure fluctuations
Low fuel regression rate increases endurance	
Can smoothly throttle over a wide range	Present day descriptions are currently incomplete
Environmentally clean	
Low temperature sensibility	O/F shift during flight can also cause unpredictability

a design around. Later on, in the 1980-1990's, the largest hybrid rockets ever tested were designed by American Rocket Company (AMROC). Many rockets were tested, ranging from 10 to 250,000 pounds of thrust, that were comprised of hydroxyl-terminated polybutadiene (HTPB)/ liquid oxygen (LOx) propellant (Ref. 17). Due to the availability of the

Table 9.2: Preliminary Design Variables (Ref. 16, 18)

Thrust to Weight Ratio Minimum (~)	1.60
Initial Estimated Fuel Weight (lb)	2900
Force Thrust (lb)	12,000
Chamber Pressure (psi)	1000
Chamber Temperature (K)	6160
Atmospheric Pressure (psi)	0.83
Oxidizer/Fuel Ratio (~)	3.00
Specific Heat Ratio (~)	1.13

engine specifications, the hybrid rocket sized for the Road Runner is primarily based from the research done by AMROC and their tested rocket repertoire.

From the designs in Chapter 5 and 6 came two important design criteria, the total fuel weight allowed, as well as the minimum thrust to weight ratio allowed. This data, paired with the fuel data, atmospheric data, and the AMROC engine data created the preliminary design information listed in Table 9.2. Since the engine design was based from the AMROC engines, the initial design also uses the HTPB/LOx propellant combination. The initial design was tested using the atmospheric data at

Table 9.3: Hybrid Rocket Design Specifications

both altitudes; but the high-flight mission profile conditions were the final driving conditions for the design.

Thrust to Weight Ratio Actual (~)	2.2
Propellant Weight (lb)	2900
Total System Weight (lb)	3000
Force Thrust (lb)	12,000
Total System Length (ft)	21.50
System Diameter (ft)	1.33
Exit Mach at Sea-Level (~)	3.11
Exit Mach at High Altitude (~)	4.42

To size the information, a MATLAB code was written to properly size the nozzle, length, diameter, and volume of the fuel chambers, and total weight of the entire system. The nozzle design process was formulated from George Suttons "Rocket Propulsion Elements," along with

Figure 9.1 Hand Calculations

the propellant mass flow rates, propellant mass, and propellant volume. To solve for the fuel regression rates and total system weight, design steps were formulated from Ronald Humbles book "Space Propulsion Analysis and

Design.” From this design process, a hybrid rocket with the following parameters was created.

The final design of the hybrid rocket includes a blowdown tank, LOx tank, a solid fuel combustion chamber, and a Rao nozzle with thrust vectoring capabilities. The nozzle has the ability to deflect the flow 15 degrees in both the vertical and horizontal direction. This nozzle will allow for better flight control. The blowdown tank is filled with a high-pressure gas to ensure a proper LOx flowrate through the combustion chamber during flight.



Figure 9.3: Hybrid Rocket CG Position Scale 1:40 (Units in Inches)

To mount the rocket engine assembly, ring frames will be located around the solid rocket fuel casing, as well as the LOx tank. These ring frames will bolt onto the outer shell of the missile skin all the way around the engine casings. The frontal pressurization blowdown tank will be attached in place through the design of the dual-purpose bulkhead-firewall. The design of the mounting section can be found in Figure 9.2.

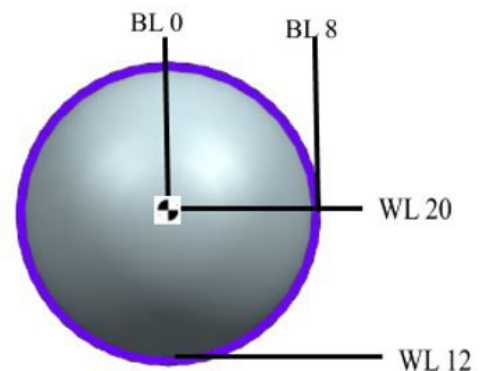


Figure 9.4: CG Position Scale 1:8 (Units in Inches)

From the design process, the individual weights for each section of the hybrid rocket components were calculated. This information, along with the length dimension created for each section of the engine, then defined the CG location for the engine. The final CG location of the engine is shown below in Figure 9.3; it is located 7.10 feet from the start of the blowdown pressurization tank.

9.3 Propulsion Conclusion and Recommendations

The author concludes that the findings from the design process are:

- A single hybrid engine will produce 12,000 lb of thrust, reaching both Mach requirements set by the mission profile;
- The engine is 16 in in diameter, 258 in long, and weighs 3210 lbs;
- The CG location is 7.1 ft from the start of the blowdown tank.

The author recommends:

- Locating more specifications and design data on previously tested engines;
- Locate more information about other oxidizers to test find the ideal propellant mixture.

10. Class I Wing Layout Designs

Preliminary design for the wing layout followed Chapter 2 of (Ref. 13), “Tactical Missile Design” by Eugene Fleeman. An iterative process was applied until the wing characteristics generated enough lift for the constraining flight conditions.

10.1 Wing Design Layout

As mentioned in Section 5.2, the 10° high altitude dive flight profile was the constraining mission in terms of fuel consumption. This same flight profile is constraining for lift generation. The worst-case scenario that needed to be designed for was cruise at 65,000 ft and Mach 2. This is the minimum cruise speed given in (Ref. 1) and the most difficult altitude to generate lift at due to extremely low air density. Table 10.1 shows the flight conditions for this scenario.

Table 10.1: Constraining Flight Profile Characteristics

Flight Characteristic	Value
Density, ρ , (slug/ft ³)	1.83*10 ⁻⁴
Specific Heat Ratio, γ , (~)	1.40
Gas Constant, R, ($\frac{ft \cdot lb_f}{slug \cdot ^\circ R}$)	1716
Temperature, T, (°R)	391.11
Mach Number, M, (~)	2
Speed of Sound, a, (ft/s)	969.33
Velocity, V, (ft/s)	1.94*10 ³
Dynamic Pressure, q, (psf)	342.96

With the flight conditions set, the geometry of the wings could be plugged in and iterations could begin.

Based on the configuration down selection discussed in Section 7, it had been determined that an X-tail of delta fins were to be used for tail control. Placeholder values in Table 10.2 were input for the fin geometry to allow for wing sizing until the empennage dimensions are designed in Section 12.

Iterations for the wing sizing could now begin, with the final goal of generating enough lift at 65,000 ft and

Table 10.2: X-Tail Placeholder Geometry to Allow for Wing Sizing

Root Chord, c_{rf} , (ft)	Tip Chord, c_{tf} , (ft)	Leading Edge Sweep, Λ_{LEf} , (deg)	Span, b_f , (ft)
3	0	60	4.8

Mach 2 to counteract the total take-off weight of

5,150 lb. When the Road Runner successfully generates more than 5,150 lb of lift at these conditions, it was assured that it would also create enough during the other aspects of the high and low altitude profiles. After numerous

Table 10.3: Final Wing Configuration Characteristics

Strake Characteristic	Value
Configuration, Strake Shape	X, trapezoids
Root Chord, c_{rw} , (ft)	15
Tip Chord, c_{tw} , (ft)	10.67
Taper Ratio, λ_w , (~)	0.71
Leading Edge Sweep, Λ_{LEw} , (deg)	60
Trailing Edge Sweep, Λ_{TEw} , (deg)	-60
Span, b_w , (ft)	3.83
Area, S_w , (ft ²)	45.38
Aspect Ratio, AR_w , (~)	0.32

iterations of differing wing geometry, an X-configuration of trapezoidal strakes with the dimensions in Table 10.3 was chosen.



Multiple views of the final strake design with relevant fuselage stations are shown in Figure 10.1 through Figure 10.3. Detailed hand calculations of optimized values are also included for verification of results.

10.2 Wing Design Layout

The major results of the wing/strake layout and sizing include:

- Angle of attack of 9° is required at 65,000 ft and Mach 2 to sustain flight, will be decreased as Mach increases;
- Sufficient normal force is generated from the body, strakes, and placeholder fins to counteract drag;
- Total lift of 5,369 lb;
- Lift to drag ratio of 2.97;
- Lift to take-off weight ratio of 1.04.

The authors recommend the following for improvement:

- Optimize the tail fins later for better tail control which could decrease strake area and drag;
- Run more iterations to get total lift closer to take-off weight, removing excess area;
- Test other strake shapes that could change results;
- Run flow simulation for calculating exact induced drag instead of estimating it.

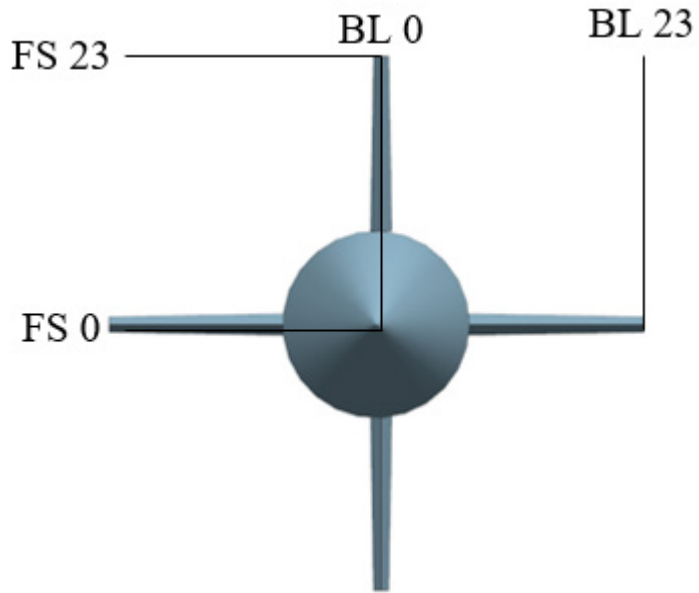


Figure 10.1: Top View of Strakes (1:10 Scale)
(Units in Inches)

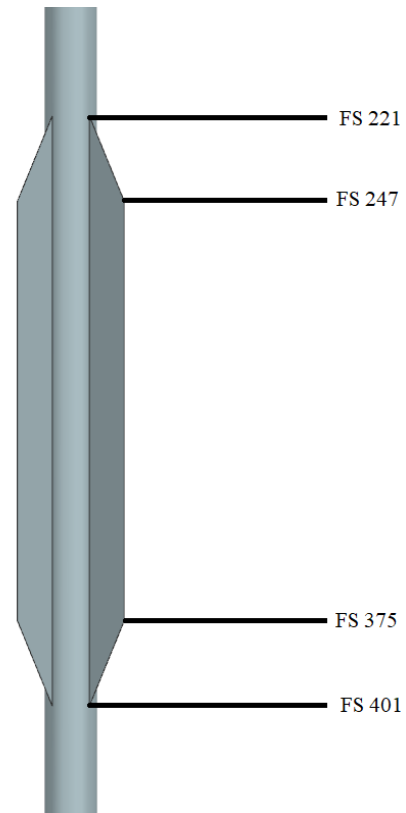


Figure 10.2: Relevant Strake Fuselage Stations
(1:40 Scale) (Units in Inches)

Figure 10.3: Hand Calculations

11. Class I High Lift Device Sizing

Conventional high lift devices are not necessary for the Road Runner since this aircraft is a rocket powered missile. However, the MQM-1A will need to be sized for the 15 G lateral maneuvers in the terminal phase of the sea skimming flight profile.

11.1 Design of High Maneuverability Devices

Techniques from (Ref. 13) were used to determine the necessary normal force per angle of attack ($C_{N\alpha}$). The aircraft needs to be able to accelerate up to 15 G's in the lateral plane. The Road Runner has three lifting surfaces: body, strakes, and tail fins. The component build up method can be used to calculate the amount $C_{N\alpha}$ for the given configuration. If the calculated normal force is greater than the required normal force to maneuver, then no extra maneuver device will be needed. The sample calculations can be seen in Figure 11.1.

Figure 11.1 Hand Calculations

11.2 Conclusions and Recommendations

A table of all the salient characteristics can be seen in Table 11.1. The authors conclude that:

- The Road Runner is capable of creating enough normal force to accelerate at 15 G's in the lateral plane at the critical condition of Mach 2.0 and at 15 ft above sea level;
- The strakes create the largest value of normal force;
- The aircraft must fly at an angle of attack of 9.5 degrees to be able to laterally accelerate at 15 G's.

The authors recommend that:

- The Road Runner should fly at mach 3.5 to give the aircraft greater maneuverability;
- The area of the lifting surfaces could be decreased if the flight envelope of the road runner became specialized to specific configurations.

Table 11.1: Salient High Lift Device Characteristics

$C_{N\alpha, \text{Need}}$ (Rad ⁻¹)	$C_{N\alpha, \text{Body}}$ (Rad ⁻¹)	$C_{N\alpha, \text{Tail}}$ (Rad ⁻¹)	$C_{N\alpha, \text{Strake}}$ (Rad ⁻¹)	$C_{N\alpha}$ (Rad ⁻¹)
27.7	2.0	12.1	16.5	30.6

12. Class I Empennage Sizing

The authors utilized methods from Ref. 20 to determine if the tail fins sized in chapter 11 are adequate when compared to other similar missiles.

12.1 Design Process

The Road Runner, like many other missiles, is symmetric along both the Y and Z body axes. Therefore, the horizontal and vertical tails will be the same. The volumetric coefficient is used to determine the size of tail compared to the size of the missile. The volumetric coefficient of five similar missiles were calculated and then tabulated in Table 12.1 below.



Table 12.1: Tail Volumetric Coefficients of similar Missiles

Missile	$\bar{V}_t (\sim)$
RIM-66 Standard	2.23
RIM-67 Standard	1.10
AGM-78B	1.23
AIM-9 Sidewinder	2.65
AIM-54 Phoenix	1.23
<i>Average</i>	<i>1.69</i>

The calculated tail volume coefficients were then averaged to create a design point for the Road Runner. Since the road runner has a fixed length of 32.9 ft and a fixed A_{max} of 1.4 ft² the value for X_n and S_t must come out to be 77.8 ft³.

12.2 Design of the Empennage

The empennage was designed to have four tail fins in an X-pattern. This was done to increase their $C_{N,\alpha}$ for high G maneuvering in Chapter 11. The tail fins were designed to be delta fins with high sweep. This was done to increase the structural integrity of the fins at high Mach numbers in dense air. Due to this the fins have a leading-edge sweep angle

and chord that are higher than the range the was set by the other five missiles. Other than these two factors the Road Runner empennage fits in the range, as seen in Table 12.2.

Since the MQM-1A is symmetric along two axes only a top view, back view, and isometric view is needed to see every angle of the aircraft. These views can be seen in Figure 12.1 through Figure 12.3.

Table 12.2: Tail Fin Design Geometric Characteristics Based on Similar Missiles

Characteristic	Acceptable Range from Similar Missiles	Design Value for MQM-1A Road Runner
Aspect Ratio, $AR_t (\sim)$	1.54 – 6.01	4.43
Span, b_t (ft)	1.25 – 5.17	4.80
Chord, \bar{c}_t (ft)	0.75 – 1.54	2.00
Area, S_t (ft ²)	1.02 – 8.06	5.20
Sweep, Λ_t (°)	0 – 45	60
Taper Ratio, $\lambda_t (\sim)$	0 - 1	0
Airfoil (\sim)	N/A	Flat Plate

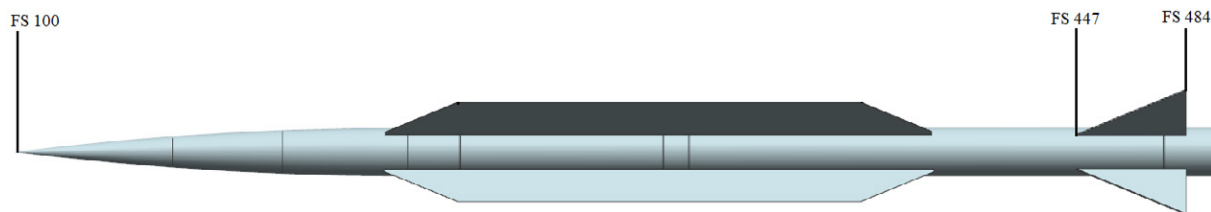


Figure 12.1: Roadrunner Side View (1:50 Scale) (Units in Inches)

12.3 Design of the Empennage

The authors conclude that

- The Road Runner has a volumetric coefficient of 1.69, which is average of the other missiles;
- The Road Runner have increased structural integrity of the tail fins due to delta wing configuration;
- A flat plate or supercritical airfoil will be adequate for the tail fins.

The authors recommend that

- The chord length be decreased by half a foot, so the chord can be within range of similar missiles;

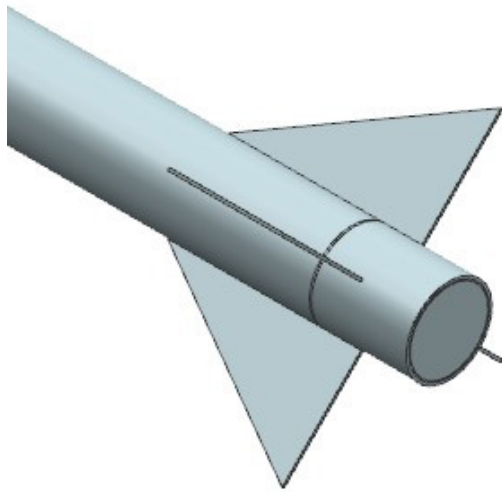


Figure 12.2: Isometric View of Empennage (Not to Scale)

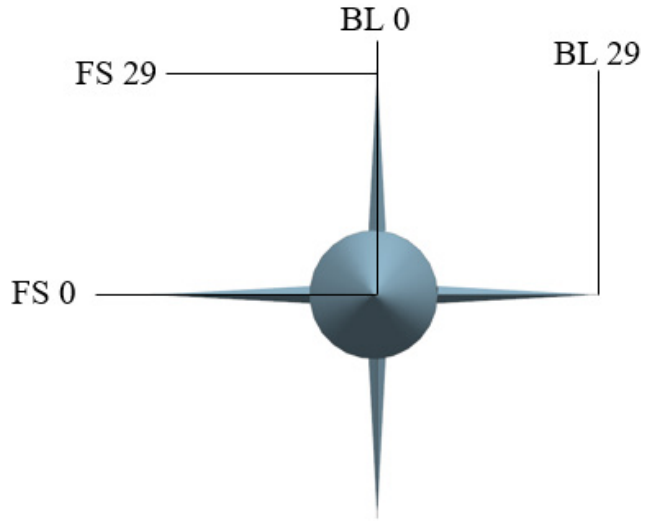


Figure 12.3: Roadrunner Back View (1:20) (Units in Inches)

- The sweep angle be decreased by at least 15° , so the sweep angle will be within range of similar missiles.

13. Class I Launcher Design

This section will detail a brief design of the Wile E. Coyote (WEC) launch system for the supersonic aerial target. This will include rough dimensions and a configuration of the launcher design and how it will be transported.

A 3-view and trimetric angle of the launcher is shown in Figure 13.1.

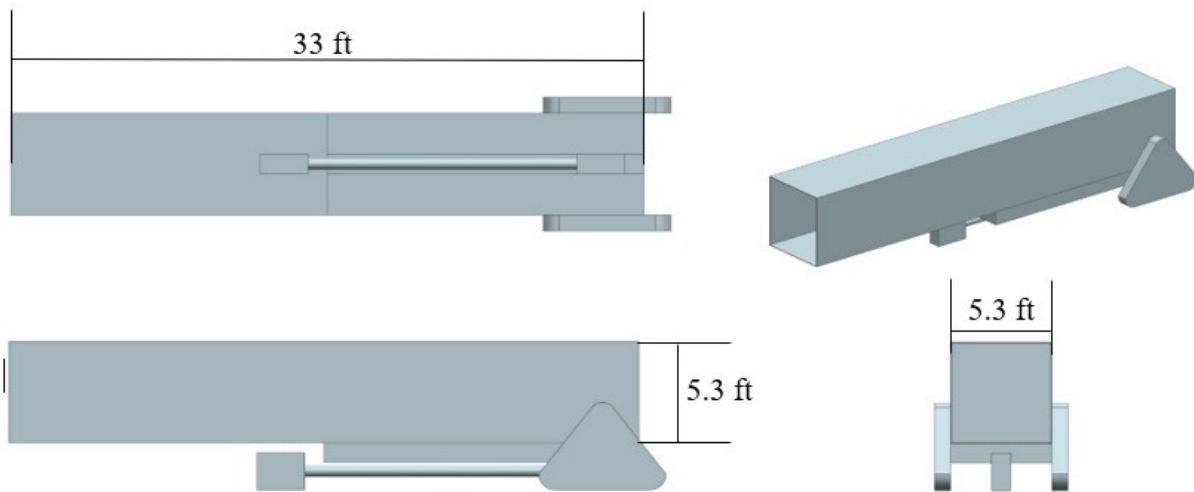


Figure 13.1: Launcher (1:100 Scale)

13.1 Surveying Launchers of Similar Systems

To formulate a design for the launcher, historical missiles similar to the Road Runner were studied to find an array of launchers to be considered. Table 13.1 lists the Road Runner and the missiles chosen, their characteristics, and their respective launcher characteristics.

13.2 Constraints and Considerations

Since the desired configuration for the launch vehicle is a tractor trailer, constraints to ensure a safe and reliable system are needed. The maximum weight allowed for a semi-trailer is 80,000 lbs in the United States. Since the tractors themselves weigh about 35,000 lbs, about 40,000 lbs are left for the payload. The Road Runner's width only allows for one missile to feasibly be placed on the truck bed, as the max allowed width of a semi-trailer is about 8.5 ft, and the Road Runner will easily fit on a truck bed that is 48ft in length.

Table 13.1: Historical Missile and Launcher Characteristics

	Road Runner	RIM-66 SM2MR BLKII	RIM-67 SM2ER BLKII	MIM-104 Patriot PAC-2	MGM-140 ATACMS SSM
Missile Length (ft)	32.25	15.50	26.20	17.40	13.00
Missile Max. Width (ft)	7.33	3.50	5.16	3	4.58
Missile Weight (lbs)	5150	1561	3284	2200	3690
Launcher Name	WEC Launcher	Mark 26 Mod 0	Mark 10	M901	M270
Launcher Length (ft)	33	16.6 (Max length of missile)	27 (Max length of missile)	20.01	22.5
Launcher Weight (lbs)	-	170,158	(Unknown)	1750 (per launcher box)	54,578 (loaded)
Launcher Missile Capacity	1	24, rear loading magazine	40, rear loading magazine	2-4	2
Launcher Cost	~\$2-3 million	(Included with Navy ship)	(Included with Navy ship)	\$2 million	\$2.3 million
Launcher Type	Truck Bed	Ship Based	Ship Based	Truck Bed	Armored Vehicle

The Road Runner will be housed in a box launcher with a width and height of 5.3ft. This creates a 7.5ft diagonal that will fit the wingspan of the Road Runner. The length of the box launcher will be 33ft so that it will fit the Road Runner with some extra room. These dimensions give a volume of 927 ft³ for the box launcher. The launcher

will be brought to a 45 degree angle at launch. While the missile and launch vehicle are not in use, the missile will be based in the box launcher which is in the truck container at a storage facility that can easily load the container onto any available standard tractor trailer bed. Since the missile can be safely stored when not in use it will have a long service life. The truck and trailer will cost approximately \$150,000 and the box launcher will cost about \$2-3 million.

13.3 Layout of Launcher

The WEC Launch System will comprise of a 5.3 x 5.3 x 33 cubic foot box launcher which houses the Road Runner missile until use. This launcher, the mechanism for creating the desired launch attitude, and the stabilizing legs will be stored and transported within a modified tractor trailer shipping container with a height of 8.5ft, width of 8ft, and a length of 40ft. This container will be unfolded upon launch and set up as the truck drives to a safe location for launch. The truck can return and the container can be reclosed to transport the trailer back to a site to load another missile. Figure 13.2 shows how the container will be unfolded to reveal the box launcher.

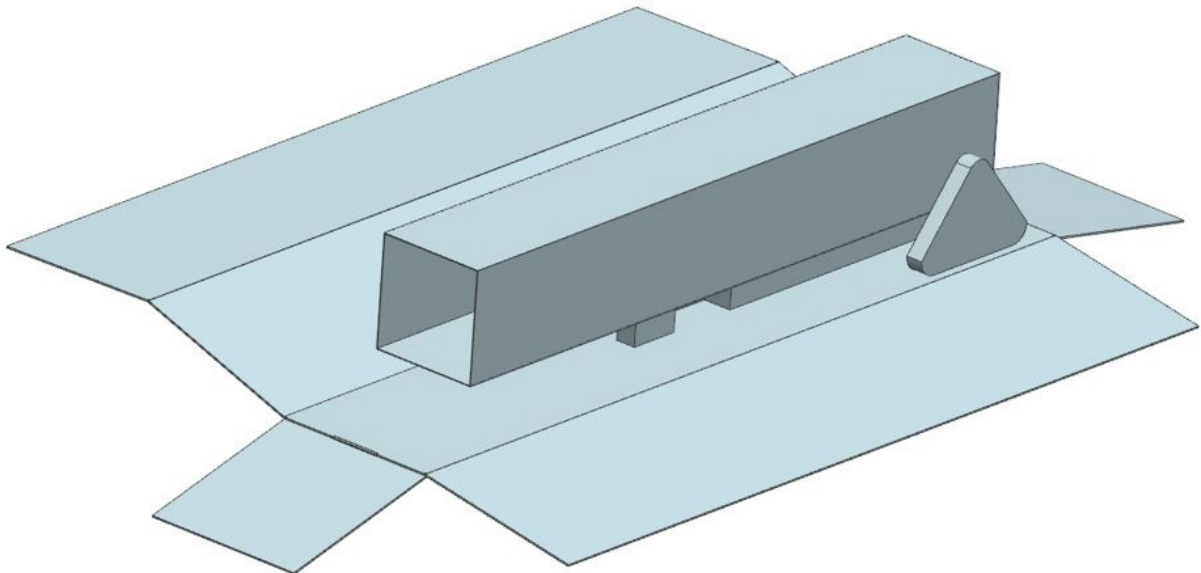


Figure 13.2: Unfolded Container Showing Box Launcher

13.4 Conclusions and Recommendations

The authors conclude:

- A 33 ft. long square box launcher will be used to launch the Road Runner;
- The box launcher is capable of launch azimuth angles ranging from 0°-90°;
- The target and launcher will be stored in a 40 x 8.5 x 8 ft³ foldable shipping container that is easily transportable by tractor trailer.

The authors recommend further research in launch constraint conditions and manufacturing feasibility of the launcher.

14. Class I Weight and Balance Analysis

This section follows the weight and balance methods presented in Airplane Design Part II (Ref. 20) and Part V (Ref. 22) for calculating preliminary subsystem weights and center of gravity locations (CG). A preliminary two-view of the target drone is shown in Figure 14.1. Note that the missile is completely symmetric in the front-view.

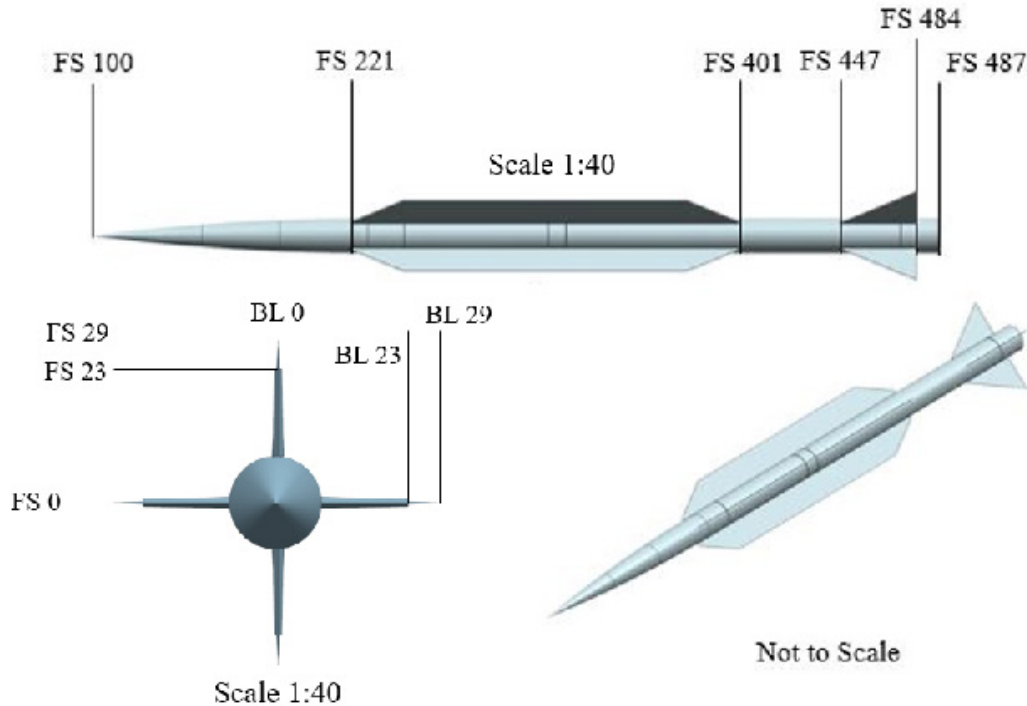


Figure 14.1: Preliminary 2-View (Units in Inches)

14.1 Class I Weights Breakdowns

Each component of the target drone is integral towards the balance of the aircraft. Thus, individual subsystem weights must be calculated in order to perform proper weight and balance calculations. To design the component weights, historical missiles with similar specifications to the Road Runner were analyzed. Table 14.1 shows the missiles chosen and their characteristics compared to the Road Runner. The data in this table and the missiles' component weights and weight fractions, shown in Figure 14.4, were taken from (Ref. 21).

The component weights for these missiles were split into five categories: propulsion, warhead, guidance, navigation, and control (GNC), wing/fin, and structural. These same categories were used for initial weight component design of the component weights. Some preliminary weights are already designed; these weights are shown in Table 14.2. Fuel fractions will be defined as a percentage of the gross weight, which was chosen to be equal to the takeoff weight.

Table 14.1: Historical Missile Comparison (Ref. 21)

Aircraft	Type	Range (nmi)	Mach	Length (ft)	Diameter (ft)	Weight (lbs)
Road Runner	Target Drone	150	2.5-4.5	32.25	1.33	5150
RIM-66 SM2MR BLKII	SAM	80	3.0	15.50	1.13	1561
RIM-67 SM2ER BLKII	SAM	90	2.5	26.20	1.13	3284
MIM-104 Patriot PAC-2	SAM	62	3.4	17.40	1.33	2200
AIM-54 Phoenix	AAM	100	5.0	13.00	1.25	1030
AIM-9 Sidewinder	AAM	22	2.5+	9.92	0.42	188
Standard Arm AGM-78	ASM	56	1.9	15.00	1.13	1370

Table 14.2: Known Component Weights

Takeoff Weight (lbs)	Gross Weight (lbs)	Fuel Weight (lbs)	Powerplant Weight (lbs)	Payload Weight (lbs)
5150	5150	2900	3210	500

Table 14.3: Component Weights and Weight Fractions

Component Weight Sizing		
	Weight (lbs)	Weight Fraction
Gross Weight	5150	-
Lifting Surfaces		
Wing Fins	41	0.008
Tail Fins	26	0.005
TOTAL	67	0.013
Structure		
Body	311	0.060
Nose Cone	153	0.030
TOTAL	464	0.09
Powerplant		
Propellant	2900	0.56
Casing	310	0.060
TOTAL	3210	0.62
Equipment		
GNC	773	0.15
Recovery System	155	0.030
Payload	500	0.097
TOTAL	1427	0.28

The component weights were designed using weight fractions, defined as the component weight divided by the gross weight. Weight fractions from the historical dataset were averaged, and these values were used in coordination with the known component weights to design the coordinate weight fractions. Table 14.3 shows the component weights and weight fractions selected.

14.2 Class I Weight and Balance Calculation

Table 14.4 provides a weight and balance breakdown of all components within the missile. Each component is listed denoting their weight, locations of component CG with respect to fuselage stations and water lines, and the moment created. The moment listed in the table was calculated around fuselage station zero. This breakdown allows for the computation of the takeoff weight CG position for the missile. The final missile CG position is at fuselage station 277. This is shown in Figure 14.2.



Table 14.4: Location of Component CG

	Component	CG Fuselage Station	Weight (lb)	Moment (lb*ft)	CG Water Line	Moment (lb*ft)
1	GNC & Power	169	773	130000	20	14000
2	Payload	208	0	0	20	0
3	Recovery System	208	155	32000	20	2780
4	Powerplant	350	310	109000	20	5580
5	Strake Surfaces	310	40.8	13000	20	734
6	Tail Surfaces	475	26.2	12000	20	472
7	Nose Cone	186	153	28000	20	2750
8	Fuselage Body	358	311	111000	20	5590

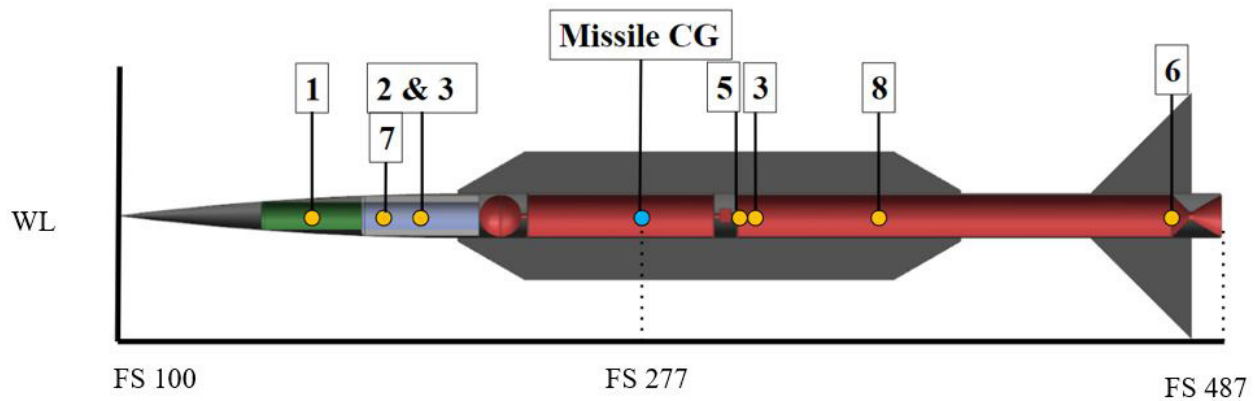


Figure 14.2: Missile CG Locations (1:50 Scale) (Units in Inches)

14.3 CG Excursion

The Road Runner missile will have four primary loading stages throughout its life cycle. The CG location of the missile will change depending on how it is loaded and with the drone’s flight condition. The four determining weights for the target drone are the empty weight, empty weight plus the payload, empty weight with full fuel, and the final takeoff weight. The furthest forward CG is at FS station 238, while the furthest aft CG position is at FS station 285. The largest shift occurs during flight, in which the CG shifts forward 47 in. Figure 14.3 shows the CG location for different flight conditions.

14.4 Weight and Balance Conclusions and Recommendations

The weight and balance analysis outlined in this section concludes that the takeoff weight CG is at FS 277. The CG shifts forward by a maximum of 16% when flying with a full payload and empty fuel. The CG shifts aft wards by a maximum of 3% when flying with full fuel and no payload. The author recommends doing a complex study of the fuel burned over time to create a high-fidelity model of the CG shift during the flight.

Figure 14.4: Historical Missile Component Weights

Figure 14.3: CG Excursion Chart

15. V-n Diagram

The V-n diagram for the missile was constructed using equations and processes from Jan Roskam’s Airplane Design Part V (Ref. 22). V-n diagrams determine what g-loads the aircraft will experience and constrain the structural design.

15.1 Presentation of the V-n Diagram

The RFP outlines terminal maneuver g-load requirements of positive and negative 15 g’s. The one-g stall speed (V_{S1}) is 265 KNEAS and the design cruise speed (V_C) is set by the RFP at Mach 3.5. The gust lines are the

dotted blue lines in Figure 15.1 while the black curved lines show the maneuver loads. Gusts begin to affect the maneuver g-loads before the cruise speed but all this is a moot point since the transportation loads are the largest g-loads the

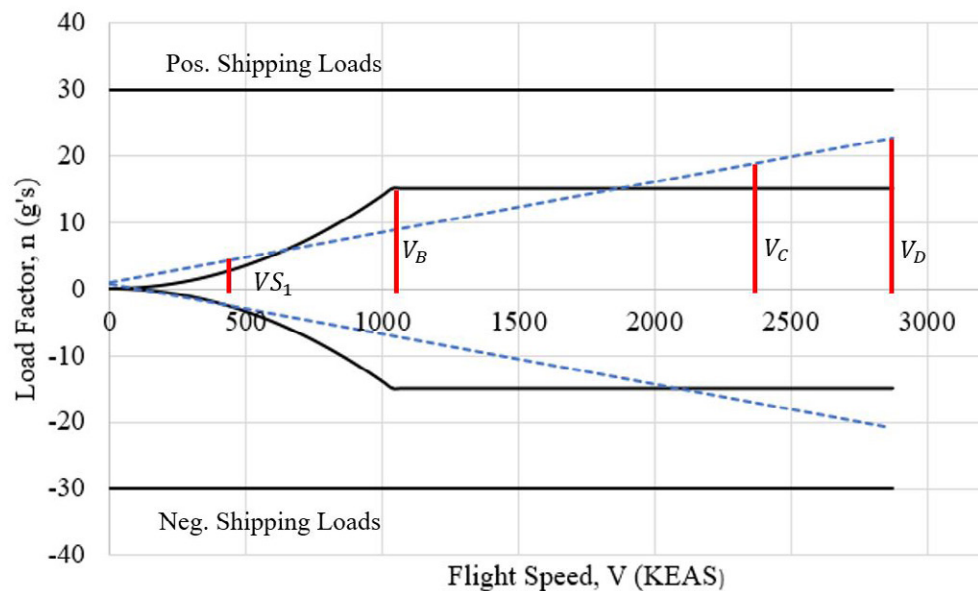


Figure 15.1: V-n Diagram

missile will encounter. Hand calculations are provided in Figure 15.2.

15.2 Gust Spectrum Analysis, Dynamic Loading and Flight Path Deviations

Gust spectrum analysis was performed using steps outlined in Jan Roskam's Flight Dynamics Part II (Ref. 23). Using the Von Karman spectrum, different intensities of RMS gust velocities at 100 ft were used to find the worst-case gust scenario that the Roadrunner will encounter. The max increases in angle of attack, side slip, normal force, side force, acceleration, and total flight path deviation. The flight path deviations are plotted in Figures 15.2 and 15.3.

15.3 Conclusions and Recommendations

The authors conclude the following information in Table 15.1 and Figures 15.2 and 15.3.

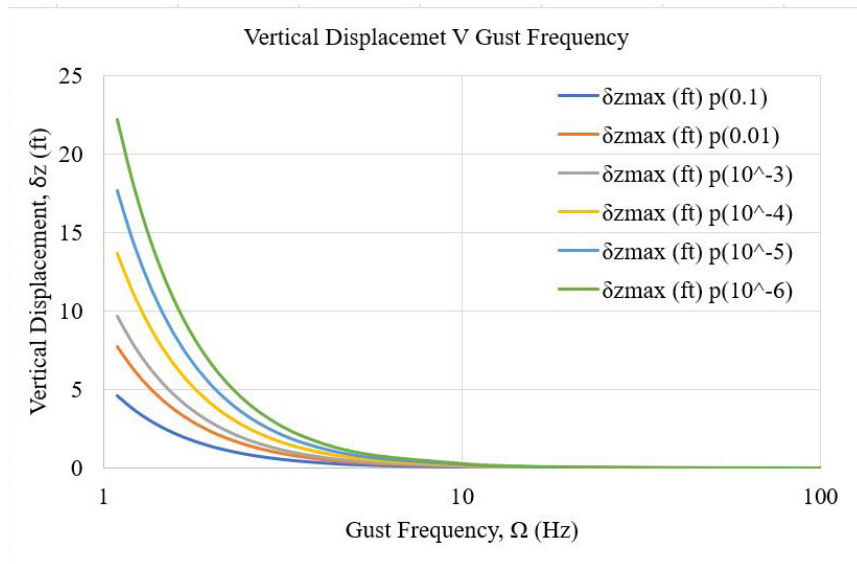


Figure 15.2: Vertical Displacement

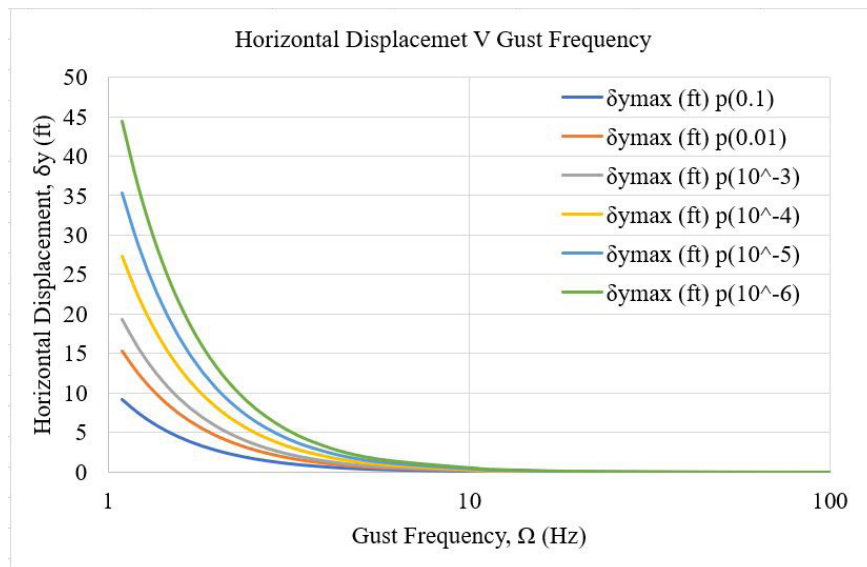


Figure 15.3: Horizontal Displacement

Table 15.1: Salient V-n Diagram Information

$N_{lim,pos}$ (g)	V_{S1} (KNEAS)	V_B (KNEAS)	V_C (KNEAS)	V_D (KNEAS)	Shipping loads (g)
15	265	1030	2300	2900	30

The authors recommend;

- Size the missile’s structure to the 30-g shipping loads;
- Use supersonic information when generating the V-n diagram.

16. Class I Stability and Control Analysis

Figure 15.4: Hand Calculations

The Class I Stability and Control design process follows the Roskam method in the book Airplane Design Part II. It is also heavily influenced from two technical documents, NASA TN D-7228 (Ref. 25) and NOTLR 73-225 (Ref. 26). From these three resources, calculations for the required fin deflection and thrust vectoring angles were calculated.

16.1 Required Fin Deflection and Thrust Vectoring Angles

The mission design for the Road Runner missile requires that it can handle a 15 G lateral maneuver, as well as have a fine point handling accuracy of 50 feet within its target. To design to these specifications, the fins and thrust vectoring needs to be able to handle the worst-case scenario of forces being acted upon the missile during flight; for both the takeoff weight and empty weight. Missiles endure large CG excursions during flight, which make them inherently unstable in their design. Therefore, the controllers have to be tested for multiple configurations.

The aerodynamic center for the missile had to first be calculated. To do so, by solving for the coefficient of lift at each maneuver, as well as similar missile data in, NASA TN D-7228, the aerodynamic center as a function of length could be solved for. This also determined the angle of attack required for each maneuver. The aerodynamic center allows for the location of the aerodynamic moments to be calculated. Below in Figure 16.1, locates both the full weight and empty weight locations of the aerodynamic centers.

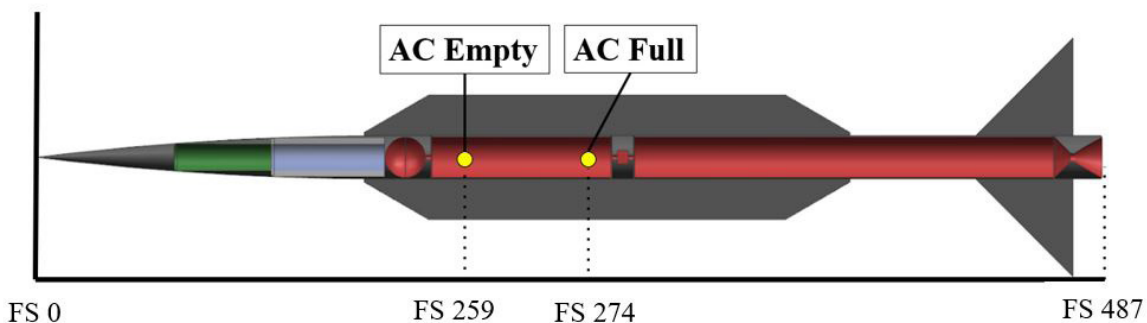


Figure 16.1: Aerodynamic Center Locations

With the aerodynamic centers, calculation the moments for the gusts, maneuvers, thrust, and fins needed to be solved. From these values, the deflection angles for both the fins and thrust vectoring can be solved. All moments are used at the worst-case scenario, including the largest gust forces acting upon the missile, as well as the full 15 G maneuver. Figure 16.2 below depicts how the forces act upon the roadrunner missile.

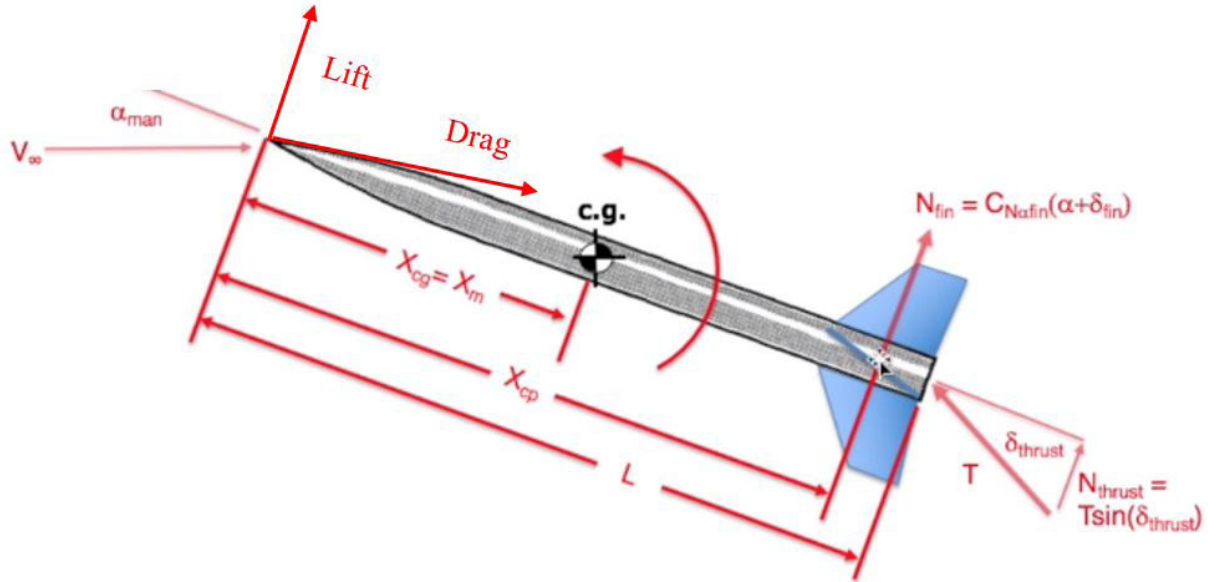


Figure 16.2: Moments Acting on the Road Runner (Ref. 24)

The moments calculated were then compared to solve for the maximum angles required for both the fin deflection and thrust vectoring angle. The worst-case scenario for the Road Runner was found at seal level flying Mach 3.5. Below in Table 16.1, depicts the values calculated. The largest thrust vectoring angle required is 5.45° which falls within the designed values of 15°. This allows for the engine to increase the flow angle if the engine is not running at full throttle, maintaining the ability to control the Road Runner. The tail fins are required to turn 13° when used in unison with the thrust vectoring. The design of the actuators turning the tail fins will cover a range up to 60° to ensure conditions where an error could occur with thrust vectoring, or the missile is cruising with the engine off.

Table 16.1: Stability and Control Calculation Results

Full Takeoff Weight		Empty Takeoff Weight	
$CL_{Maneuver}$ (rad)	3.04	$CL_{Maneuver}$ (rad)	1.37
$\alpha_{Maneuver}$ (degree)	25	$\alpha_{Maneuver}$ (degree)	12
X_{AC} (FS)	274	X_{AC} (FS)	257
$Cn\alpha_{Fins}$ (rad)	6.5	$Cn\alpha_{Fins}$ (rad)	6.5
M_{Gust} (lb.*in)	21301	M_{Gust} (lb.*in)	14624
$M_{Maneuver}$ (lb.*in)	402.8	$M_{Maneuver}$ (lb.*in)	-301.1
δ_{Thrust} (degree)	5.45	δ_{Thrust} (degree)	2.78
δ_{Fins} (degree)	10	δ_{Fins} (degree)	13

16.2 Conclusions and Recommendations

The authors conclude that:

- The worst-case scenario requires a fin deflection angle of 13° and thrust vectoring angle of 5.45° . These angles are both achievable through this current design.
- The design is driven through the nap of the earth mission profile forces.

The authors recommend that:

- That future iterations should rely more heavily on control through aerodynamic controls, due to the possibility of engine failure.

Figure 16.3: Hand Calculations

17. Class I Drag Polar and Analysis

With most preliminary geometry designed, the actual wetted area of the aircraft can be calculated and used to find drag polars. The methods used to predict the drag coefficient come from Jan Roskam’s Airplane Design Part VI (Ref. 27). The drag polars calculated will be used in Section 18 to find new lift to drag ratios.

17.1 Drag Polar Analysis with Wetted Area Breakdown

Most of the components’ wetted areas were calculated using CAD models. These numbers were verified with hand calculations of similar, simplified geometry to ensure the CAD software was calculating the areas properly. The wetted area of the fuselage was a simple hand calculation of the surface area of a cylinder without the sections where the lifting surfaces meet the fuselage. The wetted area breakdown is shown in Table 17.1.

Table 17.1: Wetted Area of Components

Component	Wetted Area (ft ²)
Nose Cone	30.1
Fuselage	36.5
Strakes	142.8
Tail Fins	21.4
TOTAL	230.8

Figure 17.1 shows the perimeter plot of the fuselage to provide an

understanding of the change in wetted area along the length of the fuselage. The plot was created from the section

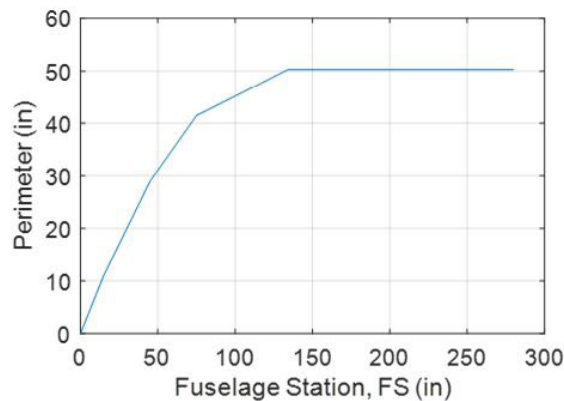


Figure 17.1: Fuselage Perimeter Plot

views shown in Figure 17.2.

The wetted area is used to calculate a new drag polar. The drag coefficients for the fuselage, wings, and tail fins are calculated independently using the methods outlined in Chapter 4 of (Ref. 27) (Roskam Part 6). The individual drag coefficients are summed to find the overall drag relationships.

Figure 17.3 shows the relationships of lift and drag with angle of attack. Then, the drag polar and L/D is calculated, shown in Figure 17.4. The critical drag condition is flying at Mach 4.5 for the high-altitude profile and Mach 3.5 for the

low-altitude profile. Hand calculations for this analysis are found in Figure 17.5.

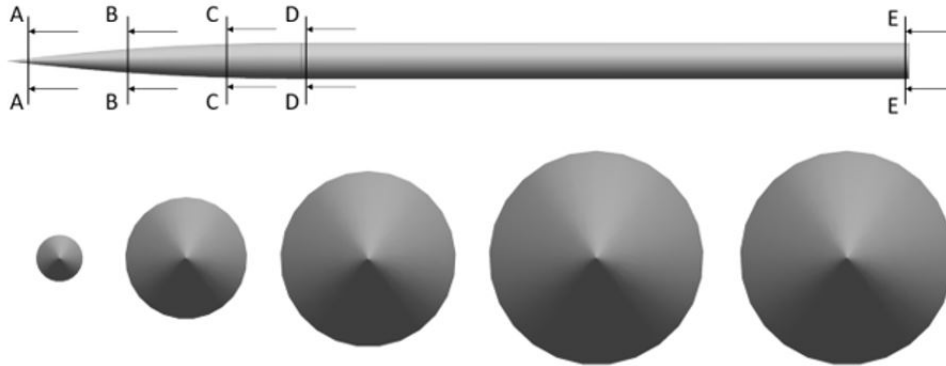


Figure 17.2: Fuselage Cross Sections

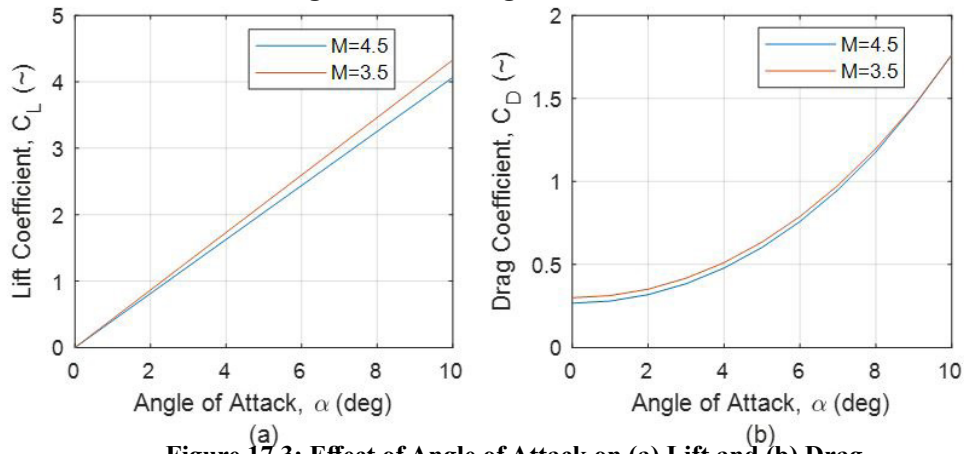


Figure 17.3: Effect of Angle of Attack on (a) Lift and (b) Drag

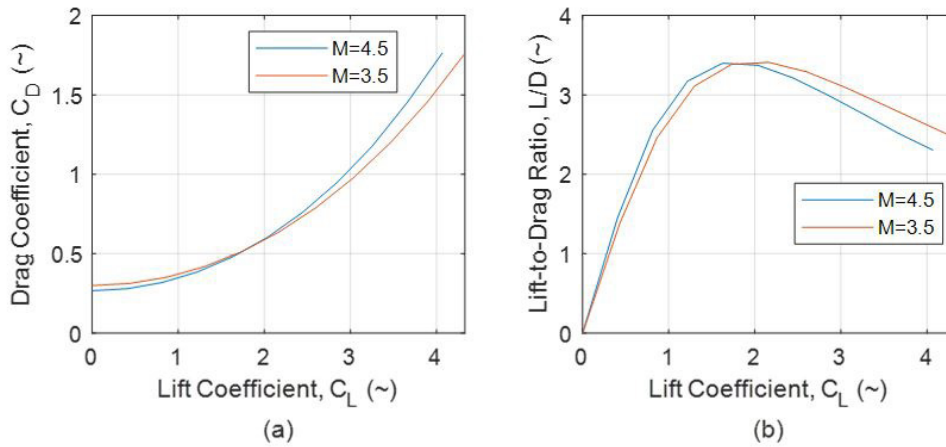


Figure 17.4: (a) Updated Drag Polar and (b) Lift-to-Drag Ratio

17.2 Conclusions and Recommendations

The major conclusions from this chapter are:

Table 17.2: Drag Polar Conclusions

Mach, M	Zero-lift drag coefficient, C_{D0}	Lift-to-drag ratio, L/D
3.5	0.300	3.41
4.5	0.267	3.40

18. Analysis of Weight and Balance, Stability and Control

This section will discuss the current state of the design and what may change moving forward. Design iterations will be implemented if necessary to ensure the design will meet all mission requirements for the RFP.

18.1 Impact of Weight and Balance and Stability and Control

The weight and balance of the design are focused all along the centerline of the missile, which allows for ease of control during the flight due to symmetry throughout the design. The CG along the length of the missile greatly changes during flight; by 47 inches. This is caused by the burning of fuel through the propulsion system. This, however, is the case for all missile designs. To rectify this, the control system that is designed must be able to react quickly and be able to easily adjust for any instability in the flight path. To counteract this, the fin deflection angle and the thrust vectoring work in unison to control the Road Runner. The worst-case scenario flight conditions required a fin deflection angle of at least 13° and a thrust vectoring angle up to 6°. Both of these cases are easily achieved with the design. In fact, both systems have been designed so that these angles are less than half of the allowable range of motion. Allowing for a measure of safety in case of component failure.

18.2 Analysis of L/D Results

Lift to drag ratios of the road runner were calculated to depict the aerodynamic efficiency of the aerial target. The original L/D was sized using sizing charts with STAMPED data from other similar missiles. The new L/D was calculated using equations from (Ref. 27). The current weight of the aircraft is within 1% of the original value, therefore no new calculations will need to be done as deemed in (Ref. 20). Supersonic aerial targets are generally not environmentally friendly. This is due to the nature of the mission which is test defense systems that are tasked to shoot down the target. However, the Roadrunner uses the most efficient rocket propellant HTPB to try to lower the environmental impact of during the lifespan of each MQM-1A. Also, the higher L/D means the aircraft will be more efficient which will lead to less burned rocket fuel.

Table 18.1: Lift to Drag Iterations

Original Weight (lbf)	Current Weight (lbf)	Original L/D (~)	Current L/D (~)
5200	5150	3.37	3.4

18.3 Design Iterations Performed

The first design iteration performed was on the propulsion sizing. It was required to have a maximum thrust while minimizing weight and overall size. The initial design of the propulsion system doubled our final weight, was 10 feet longer, and 8 inches in diameter larger. This was not acceptable, as the diameter design point was 10 inches. After multiple iterations optimizing the nozzle epsilon ratio and fuel weight. The design reached its final iteration values shown in Table 18.1 below. This final design meets the requirements specified by the RFP and other selected design criteria.

Table 18.2: Propulsion System Initial and Final Design

	Initial Design	Final Design
Weight (lb)	5300	3210
Length (feet)	32.2	21.5
Diameter (inches)	27	16
Meets RFP Requirements	Yes	Yes

The second design iteration performed was on the strakes. The primary concern was sizing the geometry to generate enough lift to counteract weight at the constraining flight condition, which as Mach 2 at an altitude of 65,000 ft. In the initial design, all the lift was generated by the nose, body, strakes, and fins so large surface area was required for the strakes in order to maintain an L/W greater than one at such high altitude. In the final design, strake area was drastically decreased due to the addition of thrust vectoring capabilities. This created additional lift that allowed for reductions in the strake span. Table 18.2 provides the geometric characteristics of the strakes for the initial design without thrust vectoring and the final design with thrust vectoring, both of which fulfilled all RFP requirements.

Table 18.3: Strake Geometric Characteristic Changes

Characteristic	Initial Design	Final Design
Span (ft)	3.83	2.17
Area (ft^2)	45.38	16.83
Aspect Ratio	0.33	0.28
Meets RFP Requirements	Yes	Yes

The third design iteration came to the missile launcher. As a result of the strake area decrease, the maximum span of the missile became 4.8 ft at the tip of the tail fins. This led to the single launcher box having a smaller front facing area, featuring a 3.54 ft width and height. The length of the launcher remained at 33 ft. This sizing change allowed for 4 box launchers to be included on the truck bed in a 2 x 2 orientation with a width and height of 7.07 ft. The total volume of these 4 launchers is 1654 ft. Since the capacity of the truck increases, transport of the missiles becomes cheaper when multiple missiles are required to be launched. This change also allows for more launches to be made without having to restock the truck, which can benefit missions that require 2-4 missiles instead of 1 by reducing firing time between missiles. The new launcher also includes an updated hydraulic system setup. Figure 18.1 provides a 3 view of the new launcher with dimensions. The figure shows the launcher set upon the truck bed.

18.4 Conclusions and Recommendations

The authors conclude that:

- The weight and balance are acceptable for missiles, and can be controlled with reasonable tail fin deflection and thrust vectoring angles;
- The L/D of the Roadrunner is 3.4;

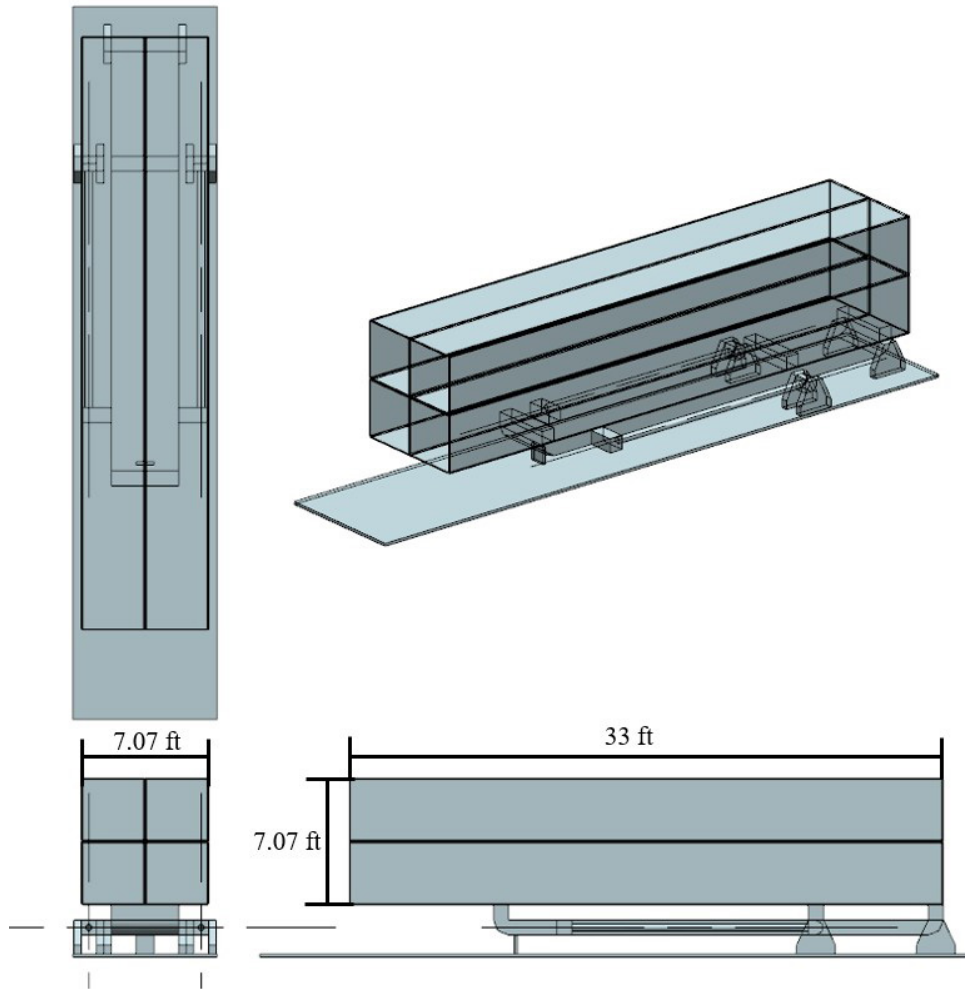


Figure 18.1: 3-View and Trimetric View of Updated Launcher (Scale 1:100)

- Design iterations changed the engine size from 32.2 feet to 21.5, the diameter from 27 inches to 16, and the weight from 5300 lb to 3210;
- A final lift force of 4164 lb. is generated during high altitude cruise at Mach 2 with an L/W of 1.01;
- The addition of thrust vectoring capabilities caused:
 - Strake span to be reduced from 3.83 ft to 2.17 ft;
 - Strake area to decrease from 43.38 ft² to 16.83 ft².
- For the low altitude 15g maneuver, the following are required depending on if there is remaining fuel or not.

Table 18.4: Required Deflection Angle for 15g Terminal Maneuver

Fuel Condition	$C_{Lmaneuver}$	$\alpha_{maneuver}$	δ_{thrust}	δ_{fins}
Fuel Remaining	1.58	13°	6.5°	6.5°
Fuel Empty	1.34	11°	-	5.5°

The authors recommend that:

- Further analysis in the weight and balance of the missile be conducted to optimize the CG excursion throughout the length of the mission profile;
- Make the Roadrunner elusive enough to evade the defense system and then be reused, which will lower the environmental impact.

19. Class I Aircraft Characteristics

Completion of Class I design results in the determination of many salient characteristics of the aircraft. This chapter outlines the major aircraft characteristics of the target drone.

19.1 Table of Class I Aircraft Characteristics

Table 19.1 shows a summary of the major characteristics at this stage in the design process. At the end of the chapter, a two-view with major aircraft geometry is shown in Figure 19.1.

Table 19.1: Summary of Class I Design Characteristics

	Wings	Tail Fins		
Number of Surfaces	4	4	Nose Cone Length (ft)	10.75
Area (ft ²)	25.12	5.2	Total Length (ft)	33.33
Span (ft)	2.16	4.8	Diameter (ft)	1.33
Mean Geometric Chord (ft)	12.95	2	Propellant	HTPB
Leading Edge Sweep Angle (deg)	60	60	Oxidizer	LOx
Trailing Edge Sweep Angle (deg)	-60	0	Takeoff Weight (lbs)	5150
Taper Ratio (~)	0.71	0	Empty Weight (lbs)	1750

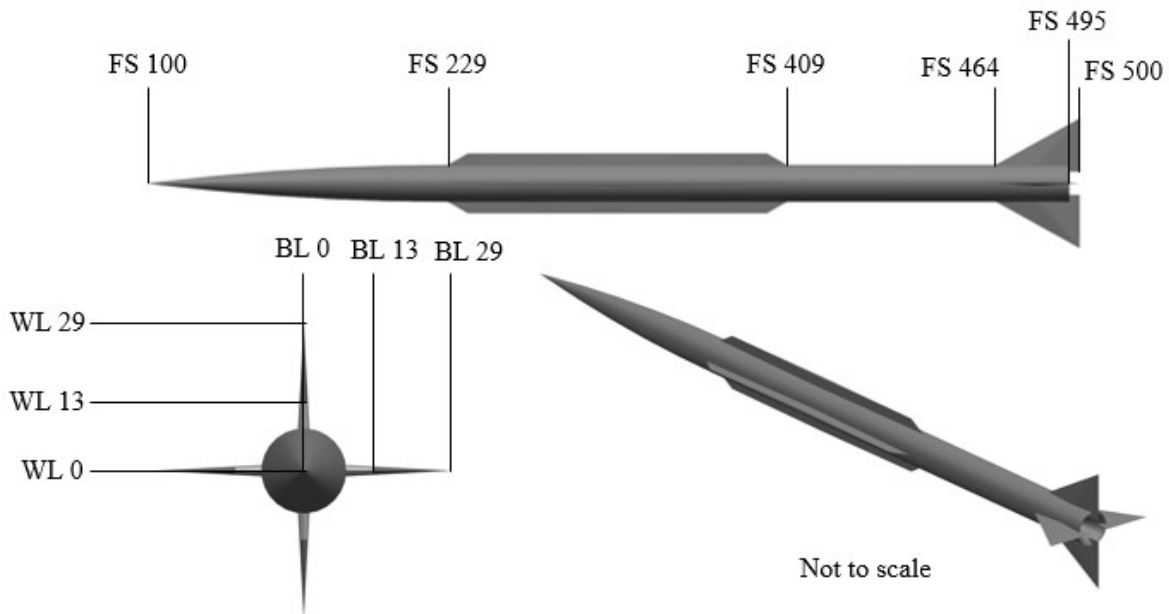


Figure 19.1: Overall Class I Design (Scale 1:40) (All Dimensions in Inches)

19.2 Class I Aircraft Description

The Road Runner weighs 5150 lbs. at takeoff, 2900 lbs. of which is fuel. Designed to perform two different mission profiles, the drone is capable of both extremely high-altitude flight and rapid, high-g maneuvers. The hybrid rocket engine allows the Road Runner to meet the desired range without need for additional stages. This rocket easily propels the aircraft to the maximum desired speeds even at the extremely high dynamic pressures of the sea skimming profile. The combination of wings and tail fins provides enough lift to fly at 65,000 ft. in addition to providing the agility for 15-g maneuvers on the deck. With these capabilities, it is likely Road Runner will evade its pursuers, which is why the target drone is also equipped with a recovery system that will save costs.

20. Description of Major Systems

The description and layout of the Roadrunner's major systems were done following the methods prescribed by Jan Roskam's Airplane Design Part IV. (Ref. 34).

20.1 List of Major Systems

The Roadrunner's major systems include:

- Flight control system;
- Fuel system;
- Electrical system.

The launcher also contains a hydraulic system. In depth descriptions and layouts of these systems are included in the sections below.

20.2 Description of the Flight Control System

Irreversible flight control systems will be used as there are no physical controls of the tail fins, only electronic controls. The systems requiring control are the tail fins and jet vanes used for thrust vectoring. In order to save costs and increase simplicity, the jet vanes are integrated into the tail fins. The tail fins extend around the rocket nozzle so they may direct the thrust. This is shown in Figure 20.1.

The actuators were sized by finding the stall torque and corner frequency required in order to meet the CEP specified by the RFP. The stall torque required is sized for 15 g maneuvers, and the corner frequency required is determined from the frequency of a gust with a 10^{-4} chance of displacing the aircraft by 45 ft. With these requirements, the actuators specifications were then scaled up from common aircraft servomotors. Hand calculations for finding the actuator specifications are shown in Figure 20.3. The actuator specifications

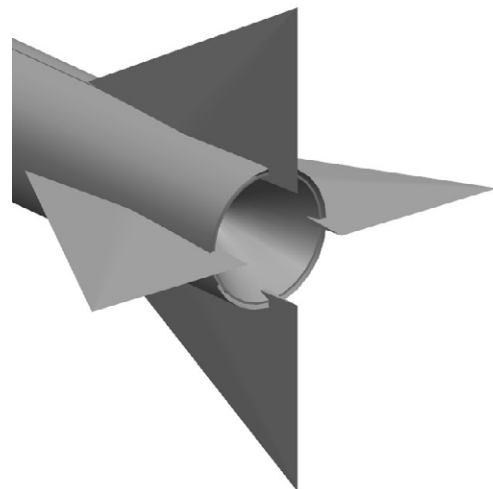


Figure 20.1: Jet Vanes (Not to Scale)

designed are shown in Table 20.1.

Table 20.1: Actuator Specifications

Weight (lbs)	Volume (in ³)	Corner Frequency (Hz)	Power (kW)	Stall Torque (ft·lbs)
24.1	429	1.62	18.1	983

The normal force acting on the tail fin is assumed to act at 35% of the mean geometric chord, per (Ref. 28). Thus, the actuators will connect to the tail fins at this location. The actuators are powered by the electrical system, with wires running from the power system to each of the four actuators. Figure 20.2 shows the layout of the flight control system.

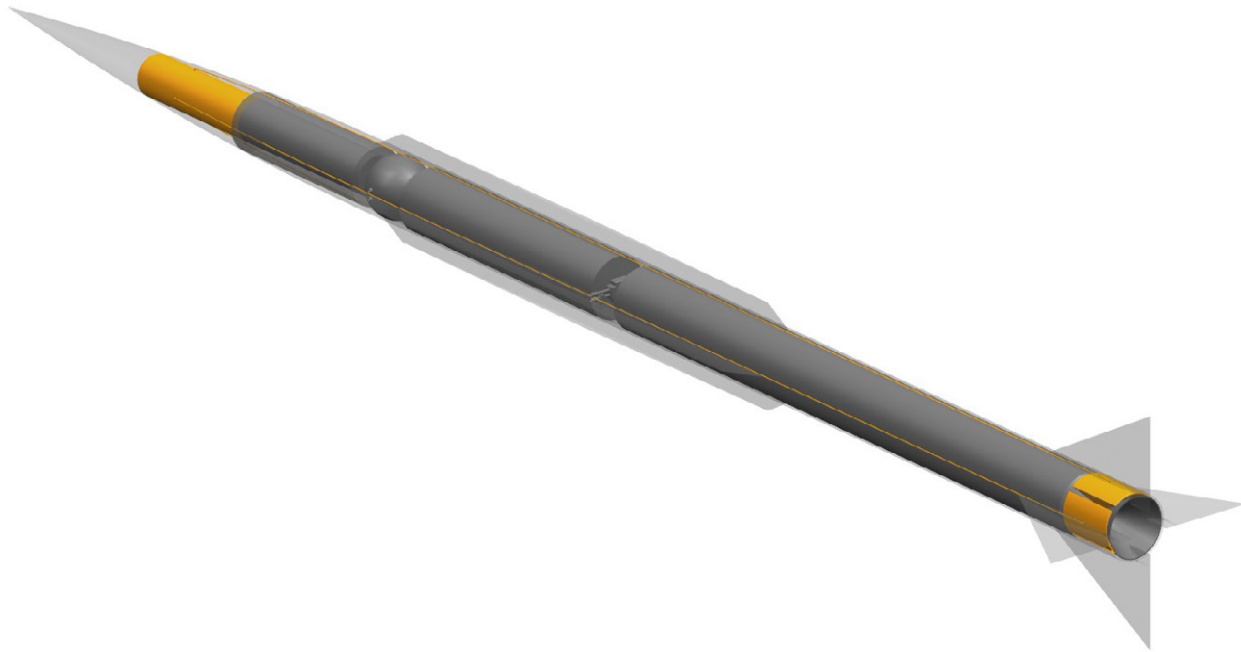


Figure 20.2: Flight Control Systems Layout (Not to Scale)

20.3 Description of the Fuel System

The fuel system is constrained heavily by standard propulsion designs that have held true over the last few decades. A hybrid rocket system of this caliber is required to follow some specific designs, with the only minor liberties in design choices. The selections that were made for the fuel system included the solid fuel type, grain pattern, liquid oxidizer, and some minor system choices.

The fuel system uses a solid propellant named HTPB.

This solid fuel is a staple in hybrid propellant design due to its low cost, ease of manufacturability, and its ability to not self-deflagrate under any known conditions. It has been used in almost all hybrid rockets conducted so far and is currently the solid fuel for SpaceShipOne (Ref. 18). Hybrid rockets require high liquid oxidizer flow rate through the combustion chamber.

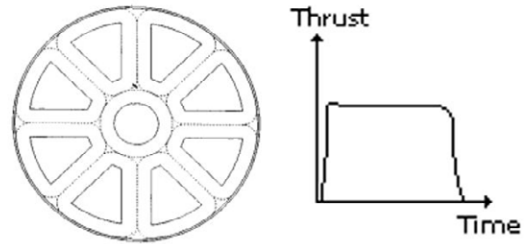


Figure 20.4: Solid Fuel Grain Pattern (Ref. 18)

This limits the solid fuel grain pattern of the HTPB fuel. The standard grain pattern that is used for all hybrid rockets, including this system, is shown below in Figure 20.4.

This pattern offers a neutral burn, which is not the perfect pattern for a missile such as this, which would ideally use a huge boost off the pad with a delay before using a constant burn. However, hybrid propulsion systems offer the ability to throttle, stop, and restart. Allowing for much more flexibility than other systems despite a constant fuel grain pattern.

The liquid oxidizer the original design was sized to was Liquid Oxygen. It is a common propellant, specifically in larger hybrid rockets, that is low cost, high performance, and relatively safe. The main downside of this propellant is that it needs to be stored cryogenically. For the application of this design, this will significantly drive up cost of storage and handling of the oxidizer. Figure 20.5 shows theoretical specific impulse values using HTPB solid fuel within a constrained test system. This shows that with a mixture ratio around 2.3, liquid oxygen has a theoretical specific impulse of around 330.

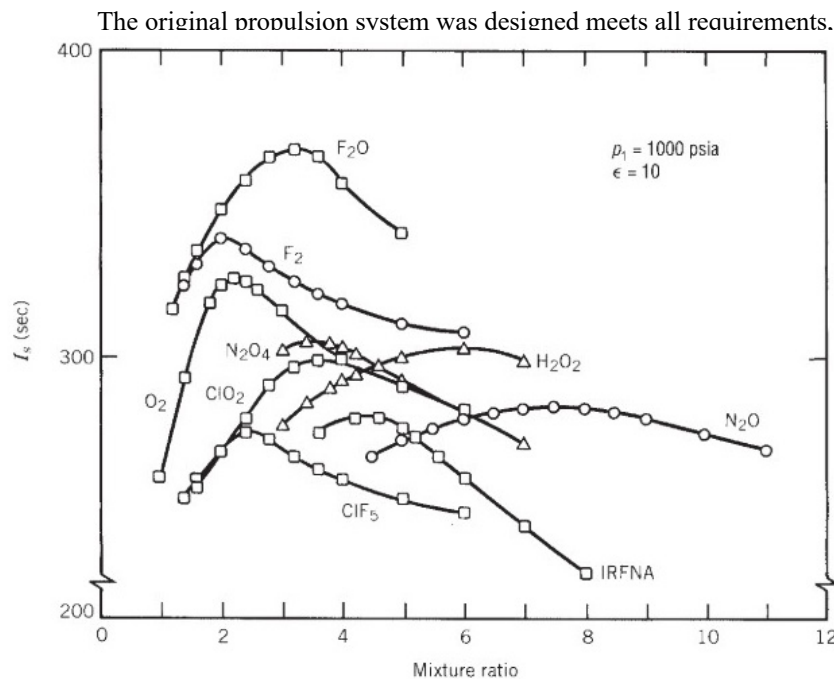


Figure 20.5: Theoretical Oxidizer Specific Impulse Values

The original propulsion system was designed to meet all requirements, but is drastically impaired due to the storage of liquid oxygen. To remedy this issue, a possible switch to a hydrogen peroxide (H_2O_2) liquid oxidizer and a hydroxyl ammonium nitrate (HTP) solid fuel. According to George Sutton, this combination has desirable thermodynamic characteristics, non-toxic exhausts, very attractive density-specific impulses, regression rates and combustion efficiencies comparable to liquid oxygen, and has great advantages in storability of the liquid oxidizer. Due

to lack of chemical composition information, a proper sizing calculation is currently unavailable.

The liquid oxygen in hybrid rockets, specifically in high speed applications require a system to ensure consistent oxidizer flow rate into the combustion chamber. Many systems have been used to remedy this problem, but in this specific application, one design is heavily used. A sealed piston system paired with a blowdown tank will be used to ensure proper oxidizer flow rate. The basic design of this system can be viewed in Figure 20.6.

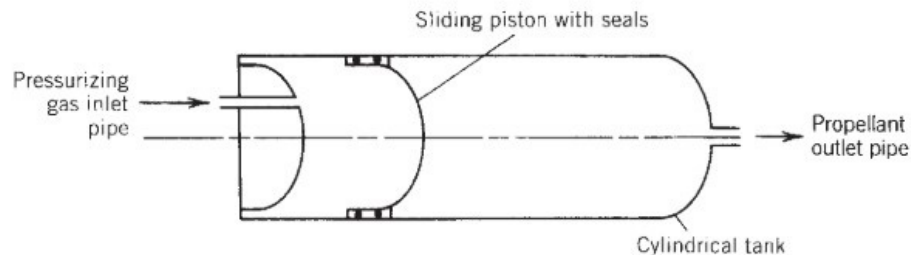


Figure 20.6: Piston Blowdown System (Ref. 18)

This piston system has many advantages over traditional bladder or diaphragm systems. It handles extremely well at high acceleration applications; both vertically and laterally. It offers the best expulsion efficiency of all blowdown systems as well as the best center of gravity control. Both features are key components required for the Road Runner design. Lastly, it boasts a long service life over other designs. The only disadvantages it has its possible leaks from the seals around the piston head and it is slightly heavier than other designs.

The material for both tanks in this system will follow tradition design for hybrid rockets. Due the liquid oxygen, the solid fuel tank requires a different material than most solid rocket booster casings. The design process sized and used the same material as the AMROC test rockets mentioned in Chapter 9. An A588 Steel case will be used to house the solid propellant HTPB. It will not add any weight to the design already as this was used for the weight estimate prior. Both liquid oxygen and hydrogen peroxide require high grade steels or aluminums for safe storage. As with the solid rocket tank, the oxidizer tank has already been sized using the heavier steel.

Between the oxidizer tank and solid fuel tank is a system for filling-defueling the oxidizer tank, as well as the valve control system for the oxidizer, and the removable hypergolic ignition system. In Figure 20.7, a detailed view of all components can be found.

There is also a system to ensure proper control of the blowdown tank that pressurizes the oxidizer tank. This system has a filling-defueling system for the blowdown tank, as well as a control valve between the blowdown tank and oxidizer tank. This system can be found in Figure 20.8.

This fuel system in the current state only controls a single redundancy of protection. All rocket systems when carrying passengers or precious cargo require a double redundancy on all ports, valves, tubing systems, and controls to ensure safety. However, missiles and target drones due to their mission profiles do not require this level of safety. Therefore, this design follows the standard practice of missiles and target drone systems.

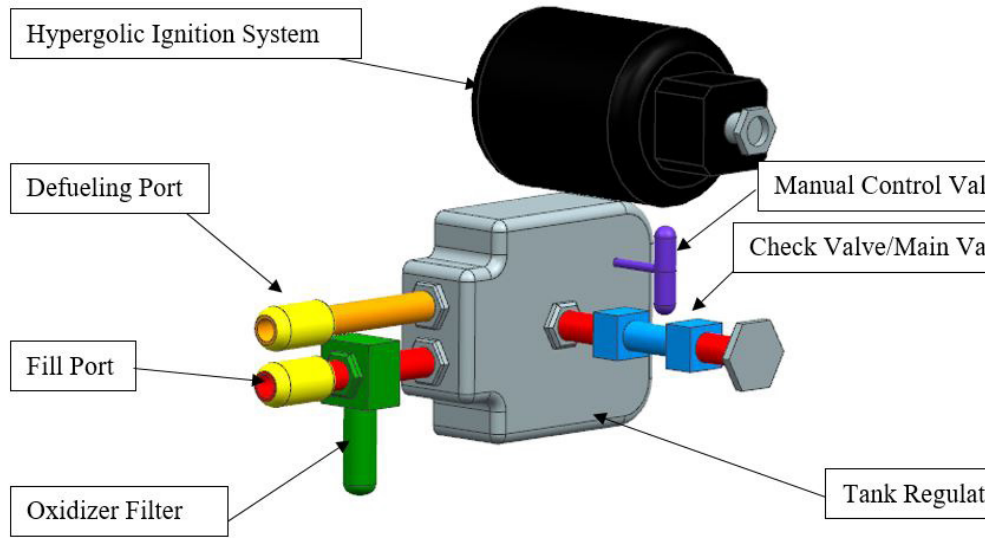


Figure 20.7: Oxidizer Fuel System (Not to Scale)

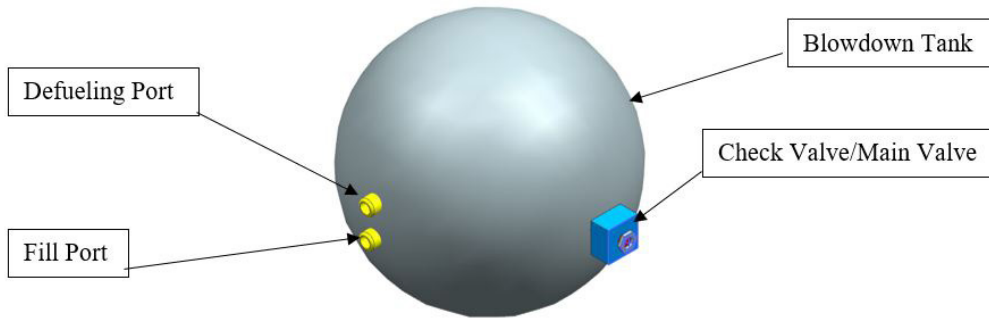


Figure 20.8: Blowdown Fuel System (Not to Scale)

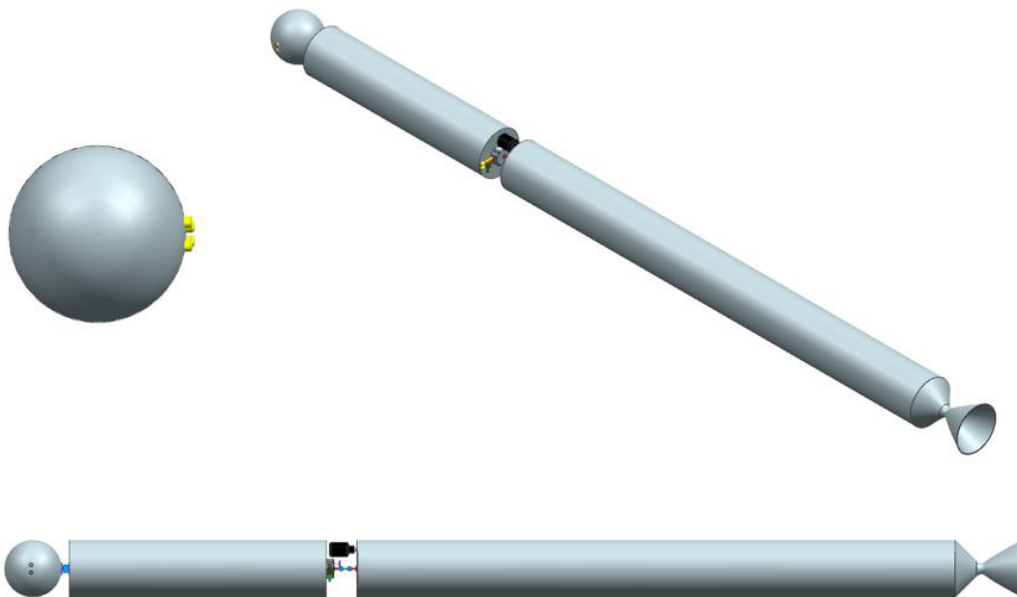


Figure 20.9: Full Fuel System Layout (Not to Scale)

20.4 Environmental and Human Impact

Fuel for the hybrid propulsion system is split into two components, the solid HTPB fuel and the LOx oxidizer. In rockets current state, there are so few flights that the environmental impact of our fuel in a program this size would have little to no impact compared to other environmental factors. However, due to the combustion efficiency of the hybrid rockets, they do produce more emissions than liquid fueled rockets. Also, HTPB fuel when run does produce a larger emissions footprint than a standard propeller driven engine. HTPB does have a larger environmental impact than most standard aircraft, but in this scale, it will not have a large impact on the environment. The LOx has a much better environmental impact than the solid fuel. In fact, it is used because it produces a nontoxic, and fairly smoke-free exhaust.

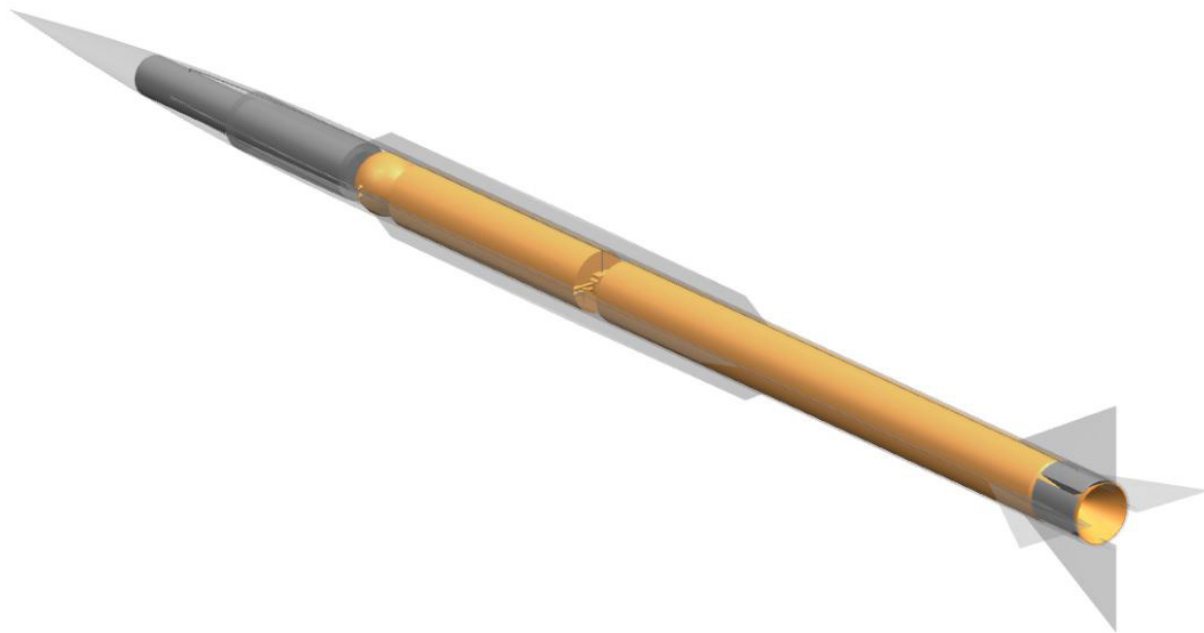


Figure 20.10: Ghost View of Propulsion System (Not to Scale)

20.5 Description of the Electrical System

The amount of power required for pre-flight operations, takeoff and climb, cruise, terminal maneuvers, and the recovery sequence of the Roadrunner was estimated. The values were found using the known power required for the missile's actuators, then using the average percentage of power usage by systems in missiles in (Ref. 30) to back out rough estimations for the power required for the GNC system, transponder, motor, and telemetry module. The terminal maneuver flight sequence is expected to require the most power while pre-flight operations are expected to use the least. A breakdown of the power usage of each system at each flight sequence is shown below in Figure 20.11. A wiring diagram of the missile's electrical system is shown in Figure 20.12. And the battery location and wire routing are shown in Figure 20.13.

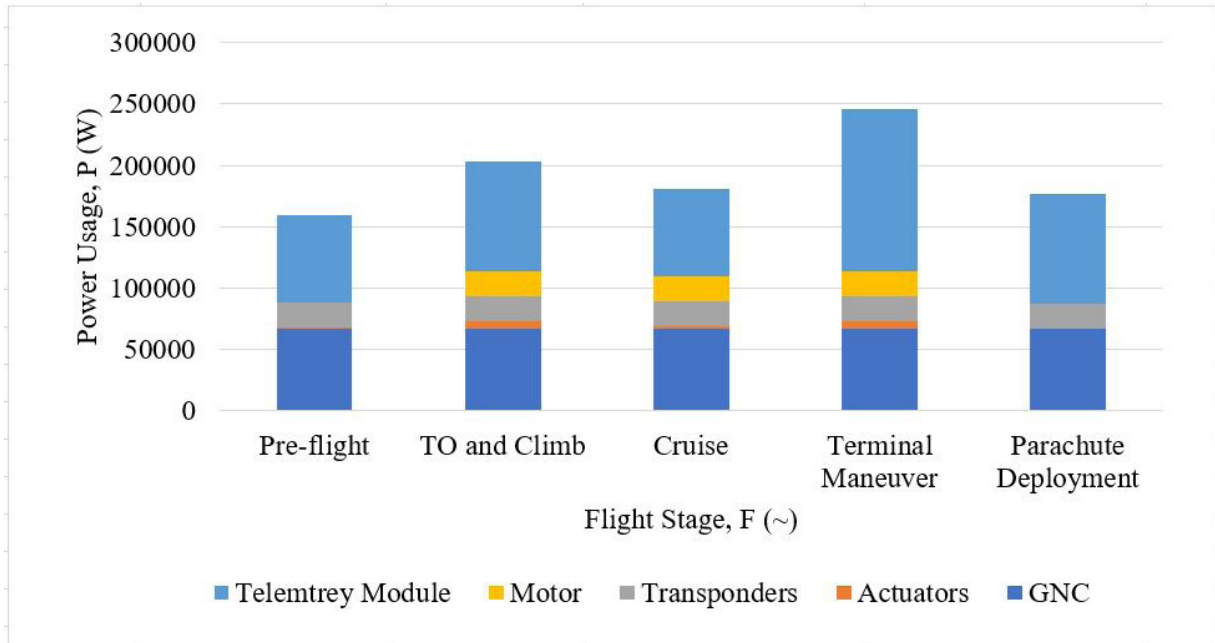


Figure 20.11: Power Breakdown

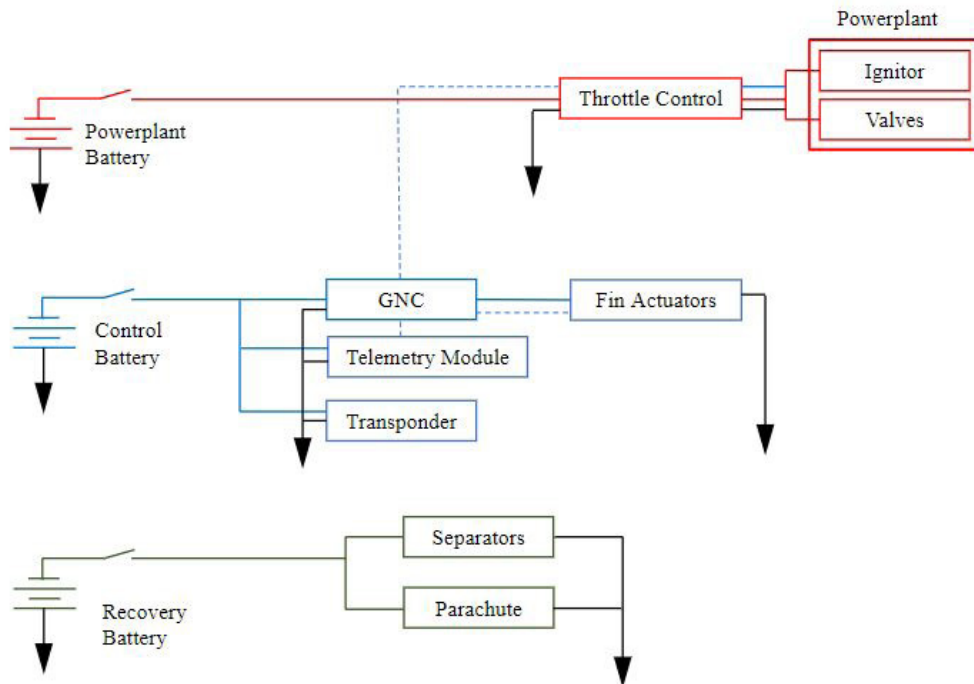


Figure 20.12: Wiring Diagram

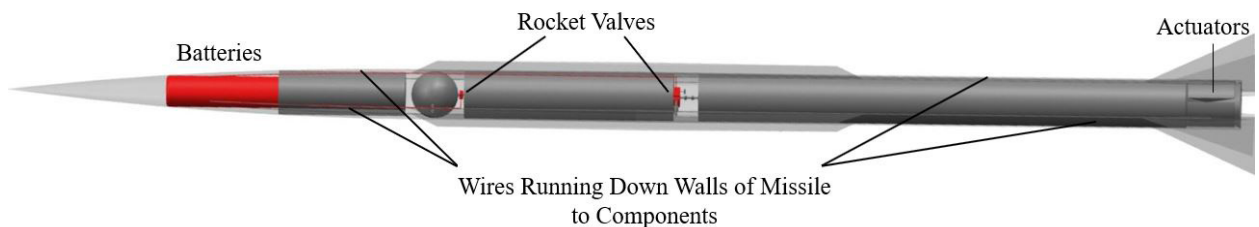


Figure 20.13: Battery and Wire Layout (Scale 1:80)

20.6 Description of the Hydraulic System

To achieve the correct launch attitude, the launcher includes two double acting hydraulic cylinder arms that lift the launcher to a 45° angle. Figure 20.14 shows a similar system in which two hydraulic arms are lifting a launcher. The hydraulics cylinders rotate about each end. As the hydraulic extends, the rotating ends allow for the launcher to pitch upwards. The hydraulic serves to raise and support the launch attitude angle.



Figure 20.14: Active Hydraulics on Japanese Missile Launcher

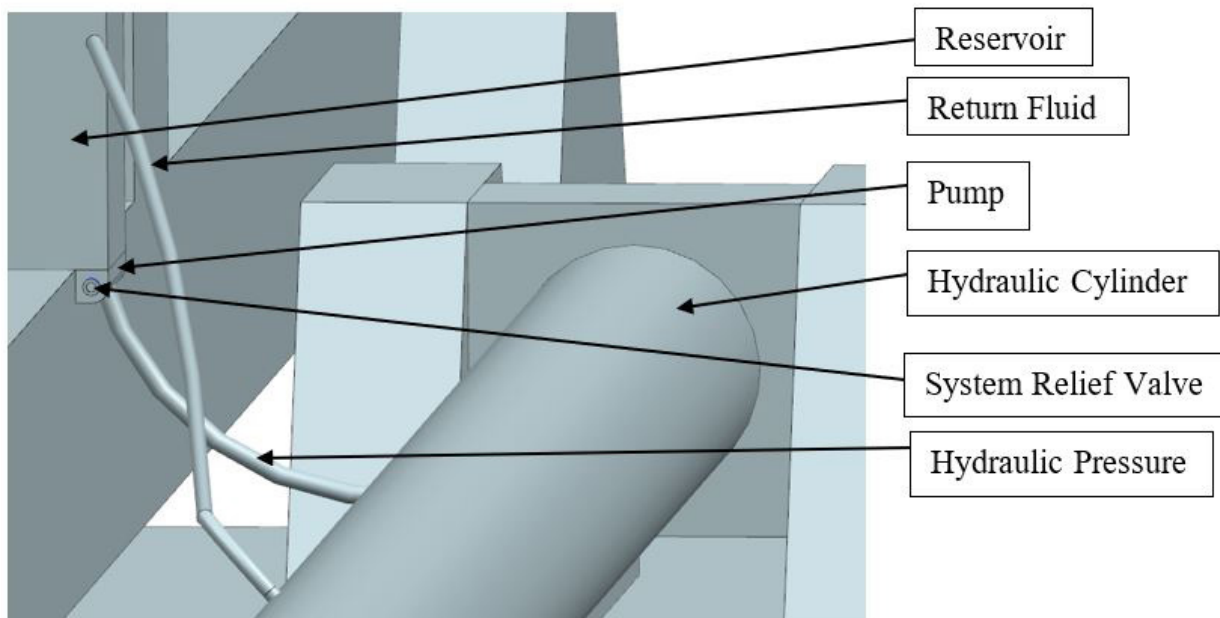


Figure 20.15: Launcher Hydraulic System Model

The double acting hydraulic cylinder is part of the hydraulic system that mostly rests underneath the launcher. The reservoir feeds into each cylinder on each side of the launcher. The pump takes fluid from the reservoir and feeds it into the cylinder. Return fluid that is housed on the other side of the piston will feed back into the reservoir as the volume of the hydraulic fluid increases and extends the piston forward. Figure 20.15 labels the compo-

nents of this system as they appear on the launcher model.

20.7 Staging

The Roadrunner features no booster system in the initial design. It boasts a large scale, single stage design using a hybrid propellant system. By using a single stage hybrid rocket, it allows for a more powerful, efficient, and throterablle engine compared to standard solid rocket-ramjet configurations.

Since staged designs dispose of the booster, the design is able to separate between the propellant bay and the front aft of the target drone, allowing for a disposable system for recovery. When over land, the propellant section of the missile will remain attached and be used as a cushion for the Roadrunner to land on. While overseas, the propellant bay will detach to allow for ease of recovery of the front section of the target drone. The reason the roadrunner has ability to choose the landing configuration is because it maximizes the recovery efficiency over multiple types of terrain.

20.8 Conflict Analysis

The design in its current state has a few areas for concern. The first is the level of redundancy in the propulsion system. It was designed to only have a single level of redundancy, since it is not carrying any human life. This will save on cost and complexity during manufacturing, however, will run the chance of propulsion system failure that has no option for recoverability.

Another area of concern is the integration of the jet vanes into the aerodynamic control fins. Not only will the coupled control be very complex to control, but another added element will be a changing thrust level from the propulsion system. Due to the structural integration, a large increase in structural rigidity and actuator sizing for the control surfaces is required. Due to the small spaces within the design, concerns need to be raised when sizing the structures in this area.

The last area of concern is the region of the missle where stage separation will occur. The technology used behind stage separation is either controlled explosive bolts or actuating hinges. In such a small scale, explosives have the possibility to damage important components in the front end of the Roadrunner. Actuators will increase the complexity and possibly overall length or diameter of the design.

20.9 Conclusions and Recommendations

The authors conclude:

Table 20.2: Actuator Specifications

Weight (lbs)	Volume (in ³)	Corner Frequency (Hz)	Power (kW)	Stall Torque (ft·lbs)
37.2	661	1.51	30.0	1750

- The fuel system utilizes a standard hybrid rocket grain pattern, liquid oxygen, and a piston blowdown system;
- The electrical system requires a total of 250 kW of power and has wires running linearly down the walls of

the missile;

- Hydraulics are utilized in the launcher to achieve the desired launch angle.

The authors recommend searching the market for readily available actuators that meet these requirements to reduce costs.

21. Recovery System

After an interceptor misses the MQM-1A, a vertical pull up will be made to activate the target drone recovery system (TDRS).

21.1 Nap of the Earth Recovery

The speed of the Road Runner will be decrease by transferring kinetic energy to potential energy and thermal energy due to drag. A 15G vertical pull will be initiated to create a 90° pitch angle propelling the craft straight into the air. After the desired pitch is reached the rocket engine will be shut off and the road runner will cruise until the vertical velocity (V_z) reaches 0 ft/s. The change of kinetic energy and velocity with correlation to altitude is depicted in Figure 21.1 and Figure 21.2. As the drone begins

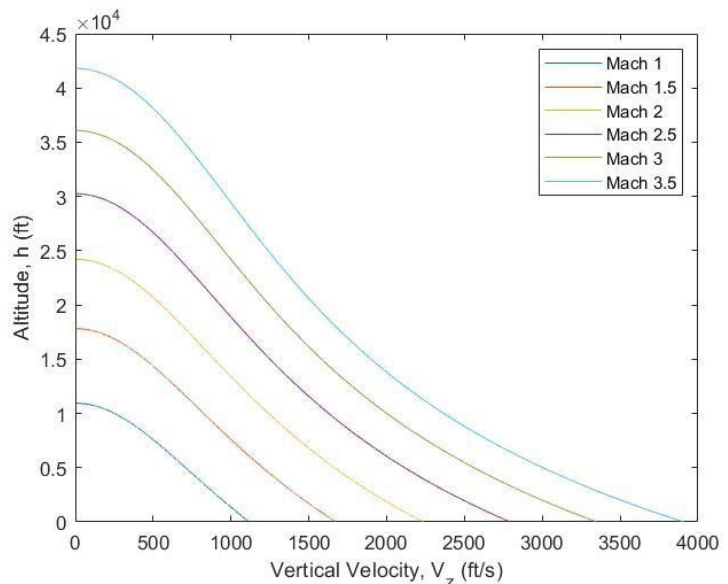


Figure 21.1: Vertical Velocity During 90° Pitch Climb

descent toward the earth the nose cone will detach releasing a G-12 cargo parachute. The G12 is a military used para-

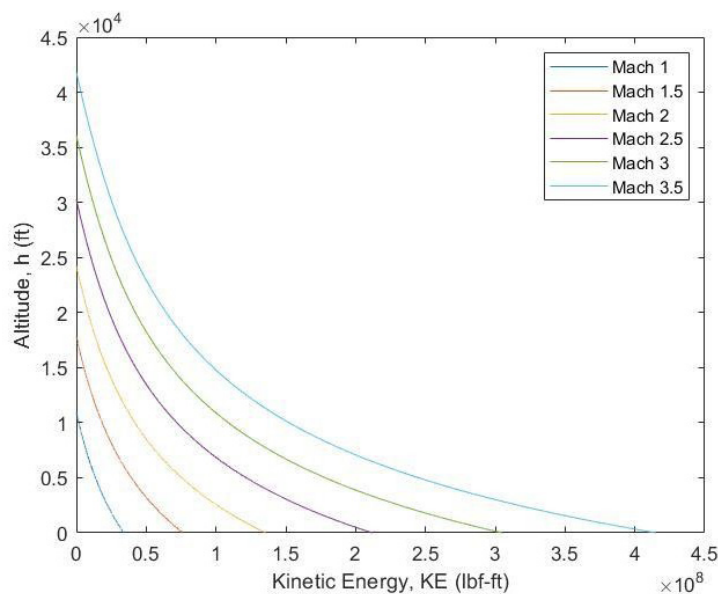


Figure 21.2: Kinetic Energy During Energy Burn Off

chute which is designed for aircraft between 500 and 2,200 pounds (Ref. 31). This will allow for a safe landing back on the surface below Wempty is 1750 lbf. A transponder will be continuously sending out the location of the drone to reduce the risk of losing it on descent.

21.2 High Diver Recovery

To ensure the craft will not crash into the ground a 30 G vertical pull up will be made until a pitch angle of 90° is reached. Even with the 30 G pull the road runner is still limited in its ability to pull out of the dive.

The minimum altitude where a successful pull up can happen is illustrated in Figure 21.3. To be conservative, drag was not considered because it would help slow the vertical descent of the aircraft. After the pull up the high diver recovery will follow the same process as the nap of the earth recovery. Hand Calculations documenting the physics of both the energy burn off and vertical pull up can be seen below in Figure 21.4.

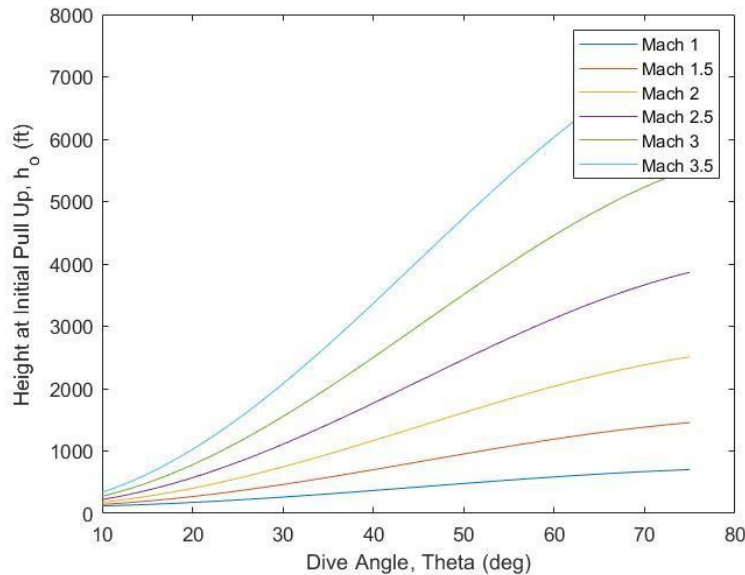


Figure 21.3: Minimum Initial Height to Perform Successful Pull Up Maneuver

21.3 Water Recovery

Both flight profiles may have a desired target over water. The buoyant force of the drone is great enough to keep over 35% of the missile afloat as seen in Figure 21.5. The transponder will also play a crucial role in finding the partially submerged drone, since over half of it will be under water.

21.4 Conclusions and Recommendations

The authors conclude that:

- it will take approximately 21 seconds for the Road Runner to reach a V_z of 0 ft/s at Mach 3.5;
- the pull up maneuver must be initiated at or before 7500 ft on the high diver at Mach 3.5 to avoid ground contact;
- the buoyant force of the fully submerged drone (2810 lbf) is enough to make the empty drone float with a factor of safety of 1.6.
- From Chapter 16, a 30 G maneuver requires 4° fin deflection and 4° thrust deflection to complete.

The authors recommend that:

- a backup parachute be installed in case of failed deployment;



- the impact speed of the high diver be designed at Mach 2, decrease the minimum height for successful pull up;
- the Road Runner should be shipped with the transponder installed to ensure the drone won't be lost if shipping malfunctions occur.

22. Initial Structural Arrangement

Figure 21.4: Hand Calculations

The structural layout of Road Runner follows the methods laid out in Roskam Airplane Design Part II (Ref. 20) and Part III (Ref. 32). The sections below detail the material selection, manufacturing process, and assembly pattern for Road Runner.

22.1 Nose Cone

Selecting the material for the nose cone requires meeting a multitude of conditions, such as high melting temperatures, high strength, low coefficient of thermal expansion, and a low dielectric constant for radio frequencies. Materials that fit these characteristics are slim but do exist. The market for these materials tends to be cornered by two to three main manufacturers.

The material chosen for the nose cone is Slip-Cast Fused Silica (SCFS) made by Brunswick and Ceradyne (Ref. 33). As denoted by the name, this material can be easily cast into the desired shape of the nose cone; adding to ease of manufacturing. It is a reliable material that has been used for many years on the Patriot missile line. It has many beneficial characteristics, specifically the best radar transmission qualities compared to other materials. Table 22.1 below shows the SFCS qualities compared to other materials.

22.2 Fuselage Body and Internal Structure

The fuselage and internal structures, while experiencing high temperatures, do not require the same resistances that the nose cone and aerodynamic controls do. The most important conditions for these materials to meet



are high strength, lightweight, and easy manufacturability. For these structures, Aluminum 7075 was chosen. This aluminum alloy has zinc as the main alloying agent. It boasts high strength, low density, good thermal properties, and can be highly polished to reduce drag.

The body panels for the Road Runner will be made from rolled sheets of this aluminum alloy. The sheets will be curved to match half of the outer diameter of the Road Runner. Rivets and bolts will be used to attach the semi-circle aluminum sheets to the ring frames and bulkheads located throughout the structure.

Internal structure for systems similar to the Road Runner are very tight and compact. Therefore, ring frames and bulkheads that follow the form of the outer mold line are used extensively to hold the components in place.

Rigidity of the ring frames and bulkheads is very important to keep the center of gravity of the missile in a locked position. It also prevents damage of moving components. The front bulkhead attached the nose cone to the aft assembly, as well as protecting the GNC and payload from extreme temperatures. The aft

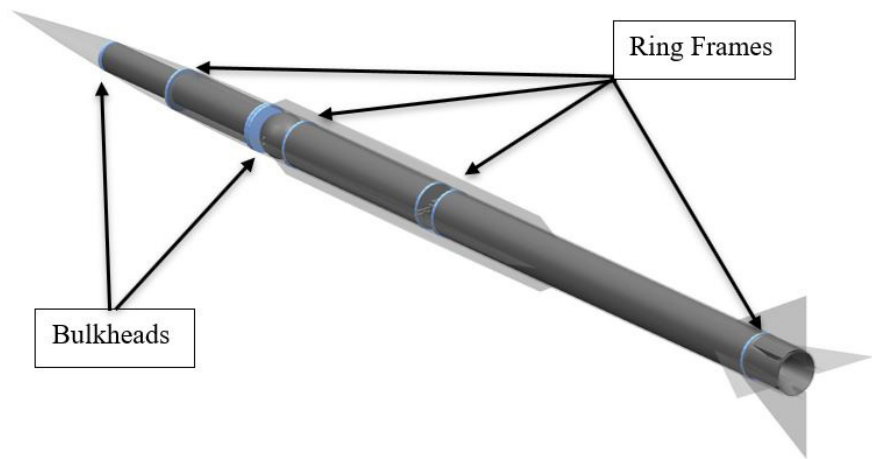


Figure 22.1: Internal Structure Locations (Not to Scale)

bulkhead protects the front assembly from catastrophic damage that could occur due to engine failure. The ring frames are in place to secure components along the missile's centerline. The positions of the bulkheads and ring frames are shown in Figure 22.1. All aluminum parts will be chromated to prevent corrosion in long term storage.

22.3 Propulsion System

As mentioned in Chapter 20, the tanks for both the liquid oxygen tank and the solid fuel case will be made from A588 Steel. It was used specifically during the AMROC testing of large-scale hybrid rocket tests with great success. The liquid oxygen tank will be made similarly to all high-pressure gas tanks. This process involves extruding the steel through various dies to properly form the shape of the tank. The solid fuel tank requires being cast due to having the solid fuel HTPB inside of the casing.

The throat of the nozzle will be made from Carbon-Carbon material. It is excellent in temperature resistance with low thermal expansion, despite being quite expensive. Due to this, the rest of the nozzle will be fitted niobium alloy refractory metal (Ref. 18). The metal for the exit nozzle can be manufactured easily using a process called metal spinning.

22.4 Strakes and Fins

Strakes and fins are prone to high temperatures as well as intense loading. The material chosen for the fins

and strakes is 309 Stainless Steel. This is an austenitic chromium-nickel alloy that has high strength, creep strength, and good corrosion resistance at high temperatures. Allowing for heating of the aerodynamic surfaces, while maintaining their strength and performance at high Mach numbers.

This form of stainless steel comes in many forms but for the manufacturing of the Road Runner will be bought in flat sheets or small squares; depending on the thickness required. These can then be cold-formed, machined, and finished into the desired shape.

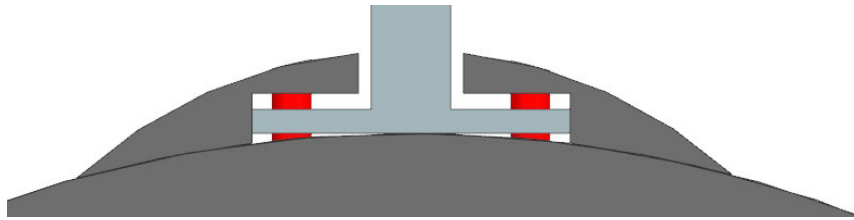


Figure 22.2: Strake and Body Integration (Scale 1:8)

Strakes for the Road Runner will be able to be removed to reduce the shipping volume. This requires a simple yet sturdy solution to attaching the strakes to the outer mold line of the Road Runner. A simple channel system was selected that will allow the strakes to be bolted in place into the body ring frames and bulkheads.

Fin attachments for this design follow very similarly to the AIM-9. A ball and hitch design protruding from the tail fins will enter the body and be locked in place into the actuator. This allows for rotation of the entire tail fin, as well as a sturdy connection point for attachments. The location of the connection is at the 35 percent location of the root chord. This prevents flutter in the tail fins by creating a moment around the connection point.

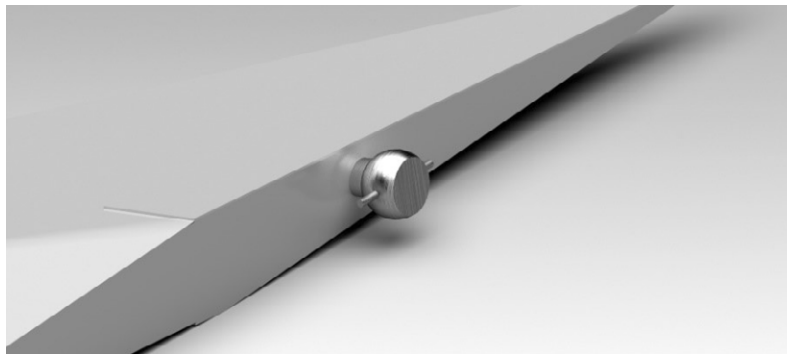


Figure 22.3: Tail Fin Integration (Not to Scale)

22.5 Assembly Procedure

The assembly of the Road Runner follows a specific pattern to not only ensure the components can be easily inserted into the frame but to maintain quality control of the missile.

The assembly steps are listed and shown in Figure 22.4 below.

- Step 1: Attach the nose cone to the front bulkhead.
- Step 2: Fasten nose cone assembly to front ring frame and center bulkhead using the bottom half of the body skin.
- Step 3: Insert GNC, payload, and electrical system into the front-end assembly.

- Step 4: Fasten the front assembly with the final ring frames and bulkhead using the bottom half of the body's skin.
- Step 5: Insert the propulsion system and fasten it into the assembly.
- Step 6: Closeout assembly by attaching the upper skin across the entire assembly.
- Step 7: Attach strakes and fins when preparing for flight.

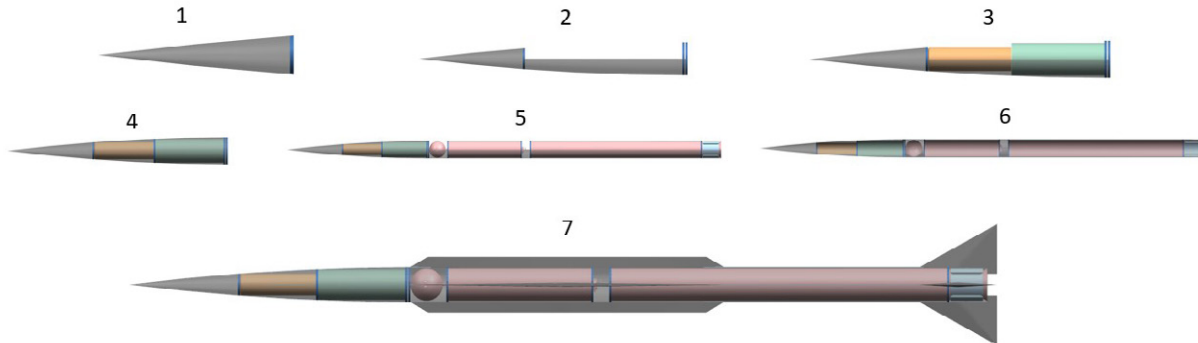


Figure 22.4: Assembly Step Procedure

22.6 Conclusions and Recommendations

The major findings from this chapter are:

- The nose cone is manufactured from slip-cast fused silica (SCFS);
- The fuselage and internal structure is manufactured from 7075 aluminum;
- The propulsion system is manufactured from A588 steel;
- The strakes and fins are manufactured from 309 stainless steel.

The authors recommend doing a stress analysis on the interconnections and fasteners between components.

23. Class II Weight and Balance

The following sections for Class II weight and balance outline how the updated component weights and center of gravity locations were determined, as well as the overall CG excursion and mass moment of inertia. CAD and (Ref. 13) were utilized for these calculations.

23.1 Weight and Balance Calculations

Detailed CAD was used to find the volume of each component, then weight was calculated based on predetermined material densities. The sum of the component weights,

Table 23.1: Class II Component Weights and Weight Fractions

Label	Component	Weight (lb)	Weight Fraction
1	GNC & Power	773	0.150
2	Nose Cone	153	0.030
3	Payload	500	0.097
4	Recovery System	155	0.030
5	Blowdown Tank	10.8	0.002
6	Liquid Oxidizer Tank	54	0.010
7	Liquid Oxidizer	2070	0.402
8	Strakes	123	0.024
9	Wires	7.3	0.001
10	Fasteners	51.4	0.010
11	Fuselage Body	311	0.060
12	Solid Fuel Tank	118	0.023
13	Solid Fuel	691	0.134
14	Actuators	37	0.007
15	Tail Fins	53.7	0.010
16	Nozzle	42	0.008
~	Total	5150	1

including payload and fuel, was taken as the takeoff weight. By dividing individual weights by the takeoff weight, the component weight fractions were calculated. The weight and weight fraction for each part of the Road Runner are displayed in Table 23.1.

23.2 CG Position and Excursion

The fuselage station correlated to each component's CG was also found by using the detailed CAD. The x-axis and z-axis locations of the CG were both measured, and the respective moments were calculated by multiplying the component weight by the CG location. Table 23.2 presents the measured CG and resulting moment for each Road Runner component.

Table 23.2: Class II Component CG Locations and Moments

Label	Component	X_{cg} (F.S.)	Moment (in*lb)	Z_{cg} (W.L.)	Moment (in*lb)
1	GNC & Power	165	127000	20	15500
2	Nose Cone	176	26000	20	3060
3	Payload	202	101000	20	10000
4	Recovery System	202	31300	20	3100
5	Blowdown Tank	232	2500	20	216
6	Liquid Oxidizer Tank	275	14900	20	1080
7	Liquid Oxidizer	275	570000	20	41500
8	Strakes	297	37000	20	2460
9	Wires	303	2220	20	146
10	Fasteners	320	16000	20	1030
11	Fuselage Body	358	111000	20	6220
12	Solid Fuel Tank	399	47100	20	2360
13	Solid Fuel	399	276000	20	13800
14	Actuators	481	18000	20	740
15	Tail Fins	483	25900	20	1070
16	Nozzle	489	20500	20	840
~	Total	~	1428000	~	103000

After all the component CGs were known, Figure 23.1 was created to

give visual assistance on the relative locations. Each individual part, as well as the overall missile are displayed.

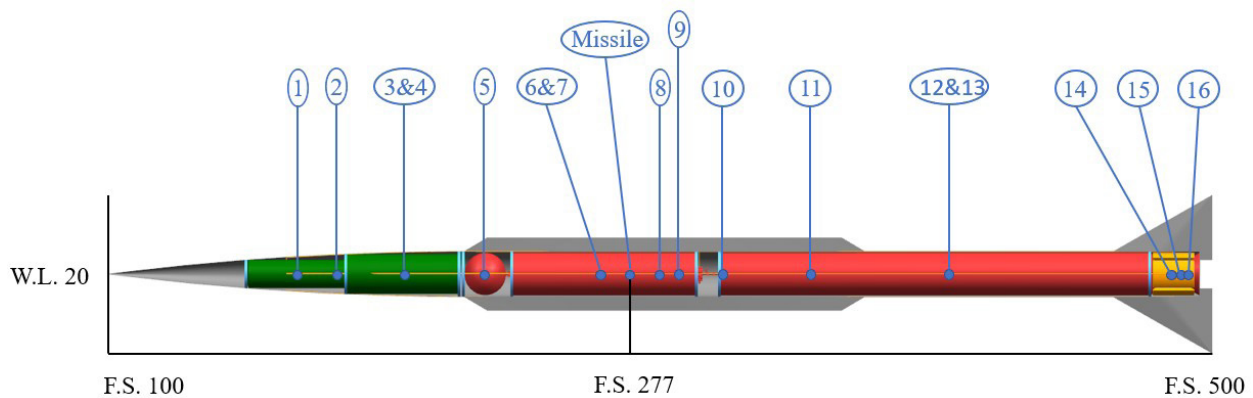


Figure 23.1: Class II Component CG Locations (1:80 Scale) (Units in Inches)

The center of gravity for the Road Runner as a whole is shown in Figure 23.2 from the front and Figure 23.3 from off-axis, giving different perspectives in addition to the view in Figure 23.1.

Figure 23.4 shows the Class II CG excursion of the final design. The four different plotted points, shown by the red dots, are the following weight conditions:

- Takeoff weight, includes payload as well as full liquid oxidizer and solid fuel;
- Empty weight, no payload and neither type of fuel;
- Payload but no fuel, simulating end of mission profile or terminal maneuver;

- Full fuel but no payload, for missions such as test flights where payload is unnecessary.

The mass moment of inertia for the Road Runner was calculated using equations from Section 4.4 of (Ref. 13). Required values for the final calculation included mass moment of inertia for the nose cone and body cylinder, the x-axis CG location for the cone and cylinder, and the x-axis CG location of the entire missile. Table 23.3 shows the calculated values for each.

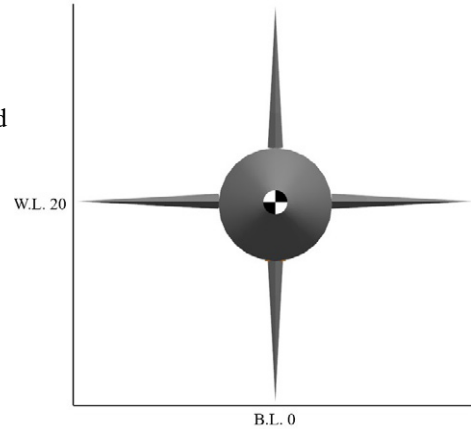


Figure 23.2: Class II Missile, Front (1:10) (Units in Inches)

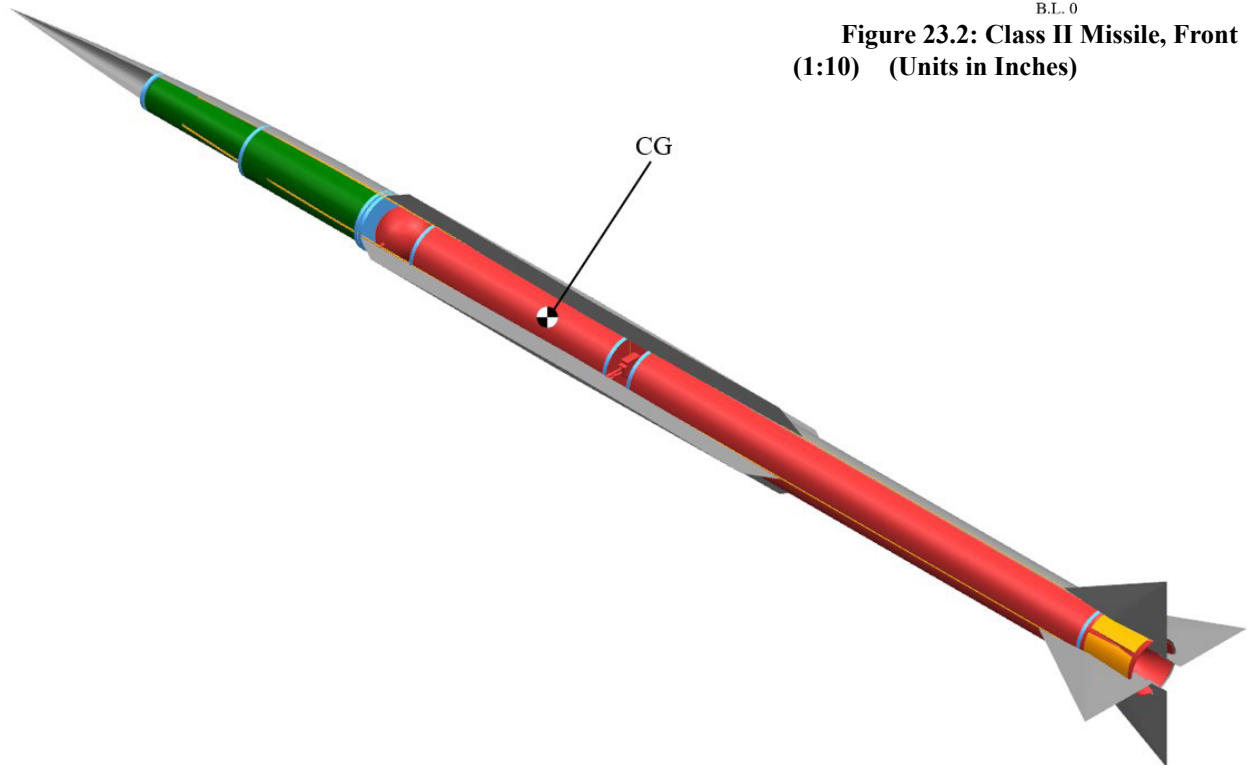
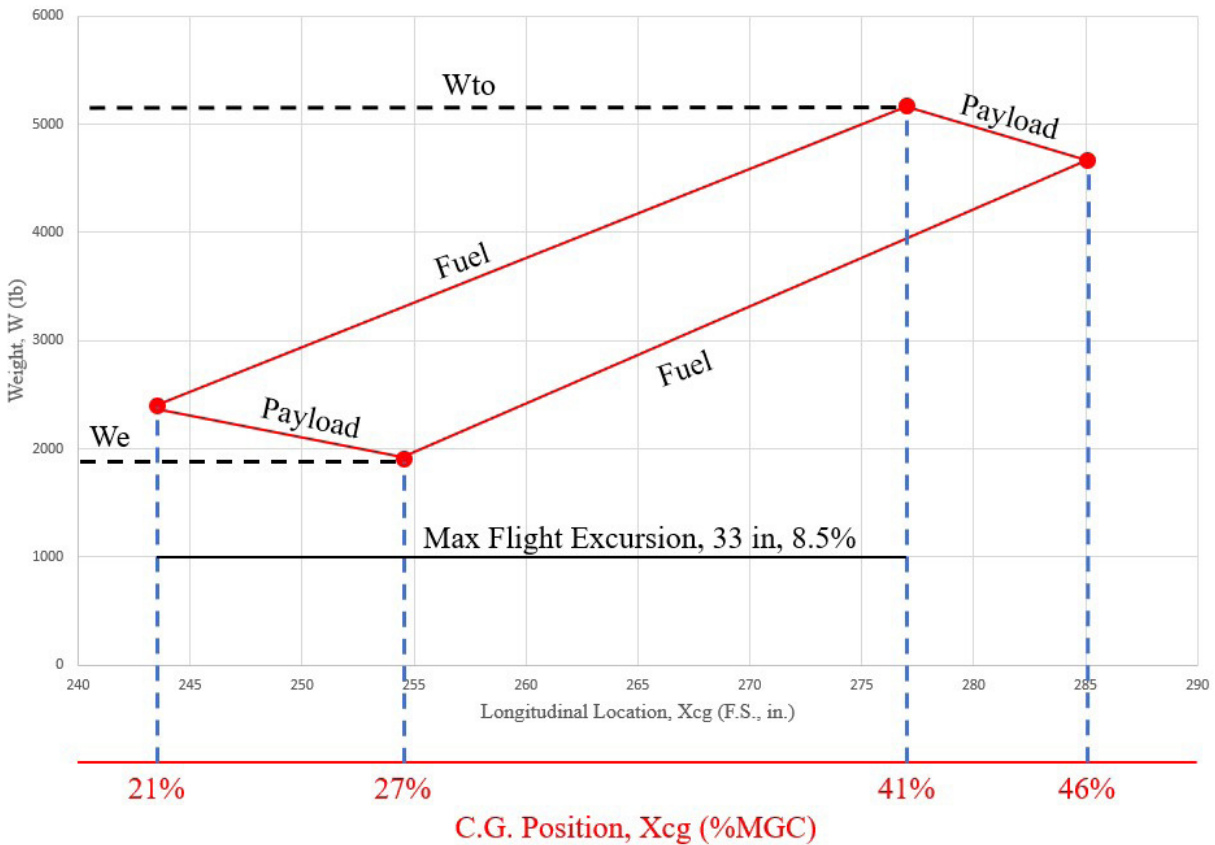


Figure 23.3: Class II Missile CG (Not to Scale)

Table 23.3: Class II Moment of Inertias

Variable	Value
$I_{yy_{cylinder}}$ (slug * ft ²)	4290
$I_{yy_{cone}}$ (slug * ft ²)	216
$X_{cg_{cylinder}}$ (F.S.)	319
$X_{cg_{cone}}$ (F.S.)	181
$X_{cg_{missile}}$ (F.S.)	277
$I_{yy_{missile}}$ (slug * ft ²)	9000



C.G. Position, Xcg (%MGC)
 Figure 23.4: Class II CG Excursion

23.3 Conclusions and Recommendations

The major conclusions from this chapter are:

- The Class II weight was 4 lbs heavier than the Class I weight;
- Takeoff CG is located at F.S. 277;
- The maximum flight CG excursion is 33 in. which is 8.5% of the overall missile length;
- The Road Runner mass moment of inertia is 9005 slug* ft^2 .

Figure 23.5: Hand Calculations

The authors recommend:

Distribute weight differently, most likely in the nose cone, to reduce the maximum flight and ground CG excursions.

24. Class II Weight and Balance Analysis

This section will analyze the Class II weight and balance calculations previously described to determine if modifications are required.

24.1 Weight and Balance Analysis

As mentioned in Section 23.3, the Road Runner CG is located at F.S. 277 after Class II weight and balance was conducted. This is the exact same F.S. that was determined from Class I calculations. The maximum CG travel for in-flight conditions is now 33 in., 8.5% of the missile length, which is 14 in. shorter than what was found in Class I. This signifies that the gains in the current will change less than those from Class I. As shown in Section 20.2, sufficient corner frequency and control bandwidth are met. The combination of these results leads to design satisfaction and no further modifications.

24.2 Conclusions and Recommendations

The major conclusions of the Class II weight and balance analysis are:

- Weight increase of 4 lbs between Class I and Class II weight and balance is not significant enough to cause stability issues or warrant modifications;
- Overall missile CG remaining at F.S. 277 after Class II dismisses any weight concerns;
- Class II maximum flight CG excursion is 33 in. which is 14 in. shorter than that from Class I;
- There is no excessive control bandwidth problem.

The authors recommend:

- Developing a dynamic model of the Road Runner so that a flight controller can be developed and the aircraft's dynamic response can be simulated.

25. Updated 3-View & Aircraft Family Summary

The MQM-1A Road Runner is designed so that it can have a variety of model variations. In this section, the different Road Runner family models will be discussed, as well as the intentions behind each design change. Figure 25.1 shows the most up to date version of the design and the basic model in the Road Runner family.

The second member of the family is MQM-10 Roadrunner. This is designed specifically for overseas sales, as it has no dedicated payload space and is solely a base level target drone. The largest change to this design will be a decrease in overall length, from a total of 33.3 feet to 21.5 feet. This will decrease the overall cost, weight, and length of the Road Runner. It will also improve the top speed and range that the design can achieve. However, it will be limited in its missile imitation capabilities without the option to carry a payload which can be a large downside to some customers. The shortened variant, the MQM-10 is show in Figure 25.2.

The final member of the family is the MQM-2A. This variant is specifically designed as a high-altitude variant of the missile. It will have no strakes in the design, as well as smaller aerodynamic control surfaces. Since the high-altitude missions require no terminal maneuvers, the tail fins will be able to easily manage and aerodynamic controls required for the Road Runners mission. This will again reduce the cost, weight, and overall size of the Road Runner. This in turn will again increase the top speed and the range of the Road Runner. The high-altitude variant,

the MQM-2A is shown in Figure 25.3.

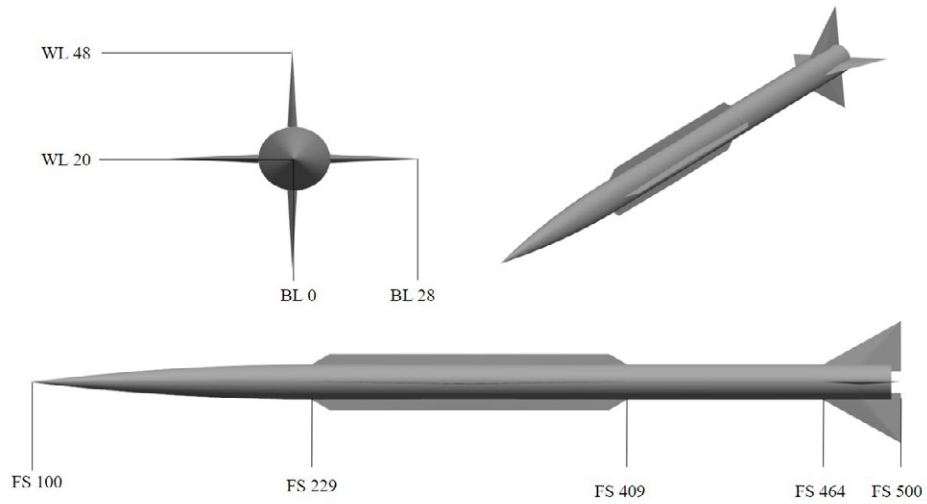


Figure 25.1: Updated Road Runner 3-View (1:80 Scale)

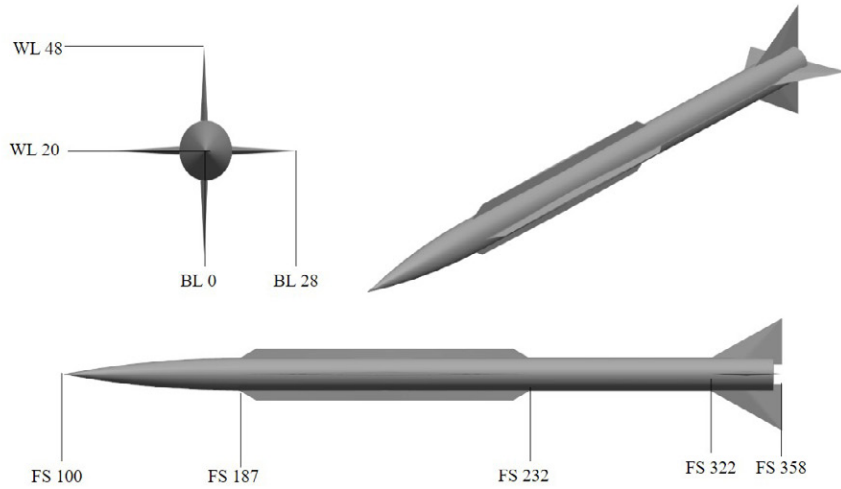


Figure 25.2: MQM-10 Road Runner 3-View (1:80 Scale)

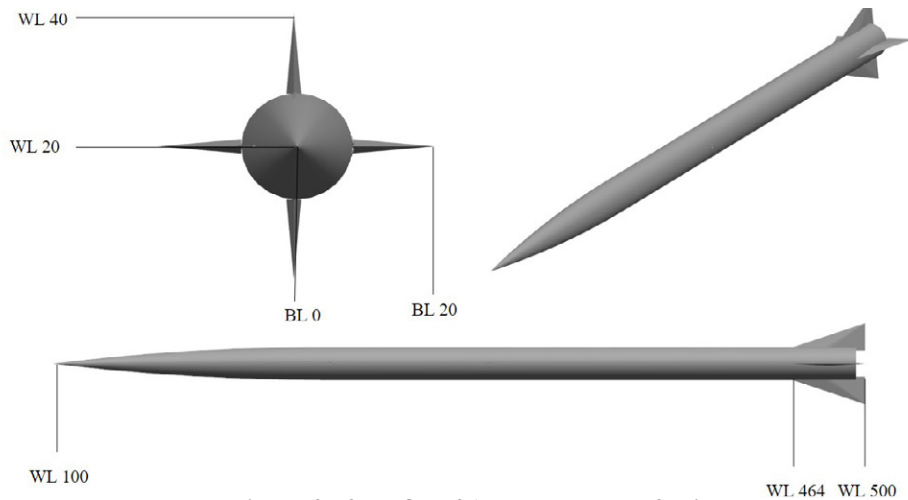
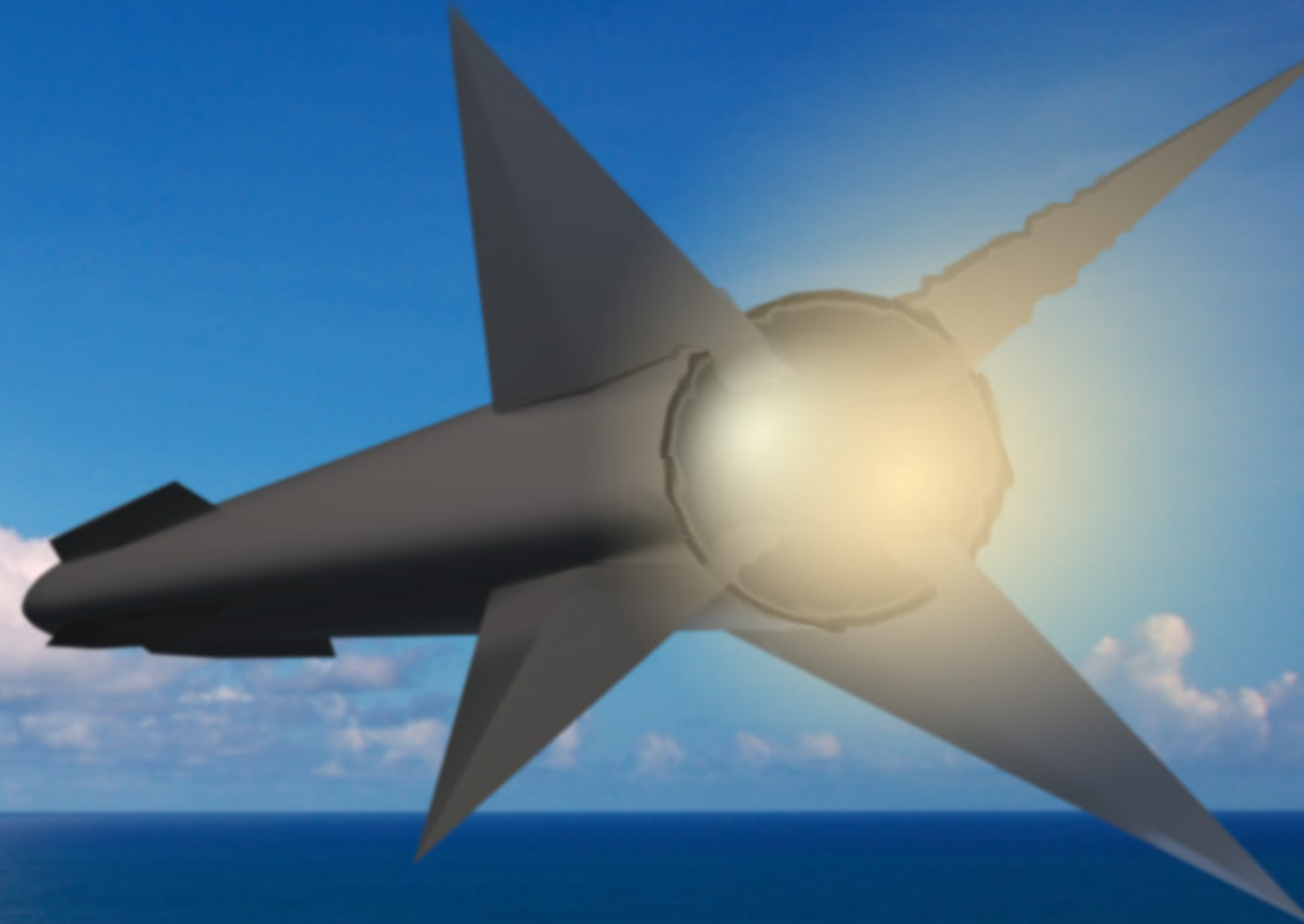


Figure 25.3: MQM-2A Road Runner 3-View

ROAD RUNNER

Road Runner is a new, high-performance target drone capable of emulating high and low altitude threats. Utilizing a state-of-the-art hybrid rocket engine that provides one-of-a-kind adaptability and maneuverability, **Road Runner was made to train the world's best pilots.**



- 65000 ft. Ceiling
- MACH 4.5
- 33-feet length
- 16-inch diameter
- 15-g Maneuverability
- Hybrid Rocket Engine
- Thrust Vectoring Capabilities
- 5150 MTOW

26. Advanced Technologies

The Road Runner is utilizing the advanced design of hybrid rockets that is not usually employed in target drones. This section will outline the reasoning for their application to the Road Runner over other engines and give a brief overview of their layout.

26.1 Hybrid Rockets

When reviewing the mission profile and comparing engine designs, the ability to have a controllable throttle was a major influence. While ramjets were initially considered in the design process, they require an assisted take-off from another engine. Since this engine would be expended on each launch new engines would need to be manufactured while a single engine design could be recovered. Liquid and solid rocket designs are time tested and reliable. The Road Runner design team instead sought to increase safety and decrease engine complexity that come with liquid rocket engines and continue to provide throttle control that is unattainable with solid rocket engines.

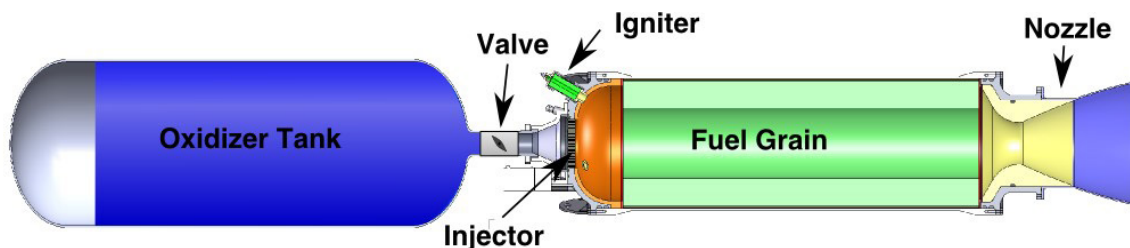


Figure 26.1: Hybrid Rocket Engine Layout

The Road Runner uses liquid oxygen as the oxidizer and uses a fuel grain of HTPB. When thrust is needed, the throttled oxidizer enters the combustion chamber and is ignited and vaporized where it then reacts to the fuel grain. Combustion within the engine occurs in the boundary layer diffusion flame on the surfaces of the fuel grain.

26.2 Conclusions and Recommendations

The authors conclude:

- A hybrid rocket is an advanced technology chosen for its ability to throttle and for its benefits compared to liquid and solid engines.

The authors recommend:

- Conducting more research into recent advancements or improvements on hybrid rocket engines and what benefits they bring.

27. Risk Mitigation

Hybrid rockets are not widely tested compared to liquid and solid fuel engines. As a result, there comes risk with using a hybrid engine. The hybrid engine also features some disadvantages to other engines that need to be accounted for to prevent risk. Another risk target drones face is a lost round. Meaning, the target drone has gone off the range and could land in populated areas.

27.1 Risk Mitigation and Implications

Hybrid rockets have gone through much less development and research time compared to the standard liquid and solid fuel engines. Some problems that surface with hybrid engines is mixture ratio and specific impulse varying during a steady flow of operations. Hybrid rockets also take on a disadvantage from its liquid and solid parts. Liquid oxygen is difficult to handle and hard to store, which can threaten damage to the Road Runner if not handled correctly. Solid fuel also presents an issue with low regression rates that impact the engine's efficiency which threatens an inability to fulfill the mission profile to full potential. The oxidizer to fuel ratio can prevent the rocket from performing at its peak, as seen in Figure 27.1, while the fuel and oxidizer also have a chance to not mix intimately, causing failures and shutdowns that will hinder the performance of the SSAT. These risks largely affect the efficiency of the engine itself and pose no dangerous threats of explosion since the fuel does not contain an oxidizer itself. The only explosion threat is blow back, which occurs when pressure changes too drastically during unstable combustion. This is only a problem with specific oxidizers and does not affect the Road Runner as it uses liquid oxygen. Many of the performance issues related to problems with the liquid and solid fuels interacting could possibly be fixed with more research and development of hybrid engines.

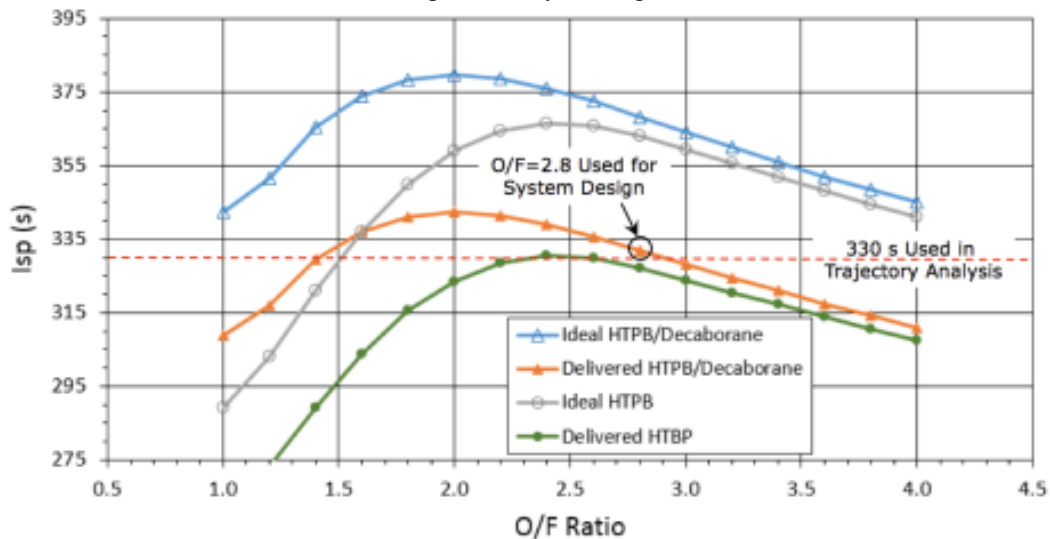


Figure 27.1: Effects of Mixture Ratio on Specific Impulse (Ref. 18)

In hopes to remove all possibilities of a lost round, the Road Runner is fitted with geo-fencing technology that doesn't allow it to leave the bounds set by the operators. If it does go outside of the geo-fenced area, the recovery sequence will begin. The missile will pull up to bleed off airspeed and deploy a parachute and fall harmlessly to the ground.

27.2 Conclusions and Recommendations

The authors conclude that:

- Proper mixture of liquid and solid fuels and proper regression rate post mild risks that

will need to be monitored to ensure safety;

- Unexpected engine explosions are unlikely, yet liquid oxygen presents issues if not stored correctly;
- The Road Runner will be equipped with geo-fencing capabilities and will enter its recovery sequence if it is found to be outside of the range.

The authors recommend:

- Significant study into the implications of low regression and poor mixture intimacy and

how this will affect the ability of the SSAT to fulfill the mission profile.

28. Manufacturing Plan

This chapter outlines the necessary steps required to produce the Road Runner. The materials and components purchased, manufacturing processes, and assembly plan will be discussed in detail. This includes a layout of the manufacturing and assembly floor.

28.1 Bill of Materials

Most components of the Road Runner will be manufactured at the associated manufacturing plant after purchasing raw materials. A few components will be purchased flight-ready due long lead times or because they are standard parts. Pre-manufactured products are shown in Table 28.1, and raw materials that will be purchased are in Table 28.2.

Table 28.1: Pre-Manufactured Components

Component	Units	Distributor
Actuators	4	Moog
Batteries	1	Wicks Aircraft Supply
Carbon-Carbon Rocket Throat	1	CFC Design

Table 28.2: Raw Materials to be Purchased

Material	Distributor
Bolts	Airparts Inc.
Rivets	Airparts Inc.
Wiring	Bulk Wire
Silica Plates	Online Metals
A558 Steel Sheets	Online Metals
Stainless Steel Sheets	Online Metals
7075 Aluminum Sheets	Online Metals
Chromate Conversion Coatings	Aircraft Spruce

28.2 Material Processing

Because this is a specialized military aircraft, most of the parts will be manufactured in-house by the associated manufacturing plant. As Table 28.2 shows, many metals will be purchased as sheets or plates and then be worked into their respective parts. After materials are received, parts are manufactured in three general steps: form-



ing, finishing, and assembly.

The fins and strakes will be machined using a mill, and the rocket nozzle will be machined using a lathe. The propellant tank and nose cone will be cast, while the fuselage skins and oxygen tank will be formed through extrusion. Lastly, because of the extremely long lead time of carbon-carbon composites, the rocket nozzle throat will be outsourced from a company specialized in carbon reinforced carbon manufacturing. This part would be laid up on a male tool as shown in Figure 28.1. The tool should be split in two parts at the point of minimum diameter and fastened before layup. Then, after the part has cured, the tool can be separated into two parts to allow for the part to be removed.

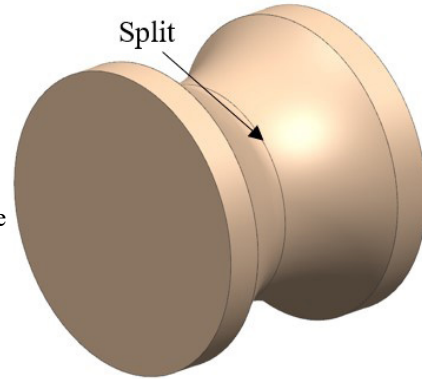


Figure 28.1: Rocket Throat Tool

After all raw materials have been formed, they will move to finishing. This stage comprises of grinding and fixing any imperfections, as well as welding the fuel tanks to ensure they are fused shut. The last finishing process is applying chromate conversion coating to metal parts are likely to experience corrosion; this step is performed in a separate facility to isolate harmful toxins.

Finally, the now completed parts will move to the assembly floor, where they will be inspected, fastened together, and then shipped off once manufacturing is complete. These processes are shown in Figure 28.2 and Figure 28.3.

The first variant of the Road Runner is that detailed in the report. These manufacturing and assembly processes allow for simple production of multiple designs. The IO variant will be shortened in length, leaving no room for a payload. This version is targeted towards foreign markets. The Road Runner-2A is designed for solely high-profile missions, and as such does not require wings to pull high-g maneuvers.

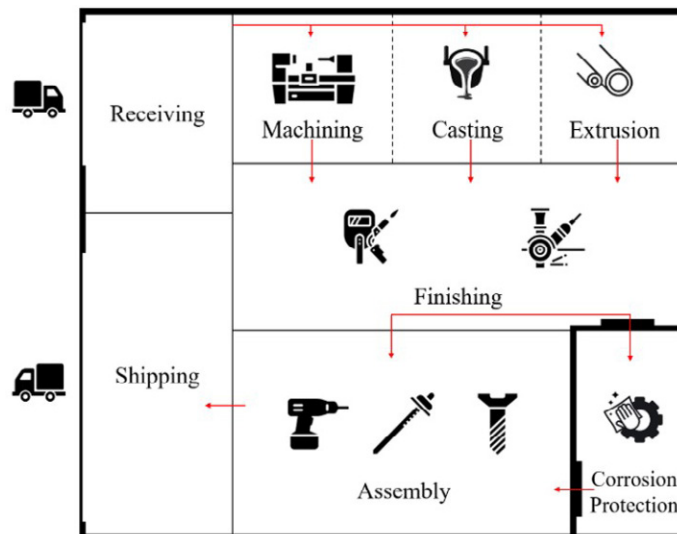


Figure 28.2: Manufacturing and Assembly Floor Plan

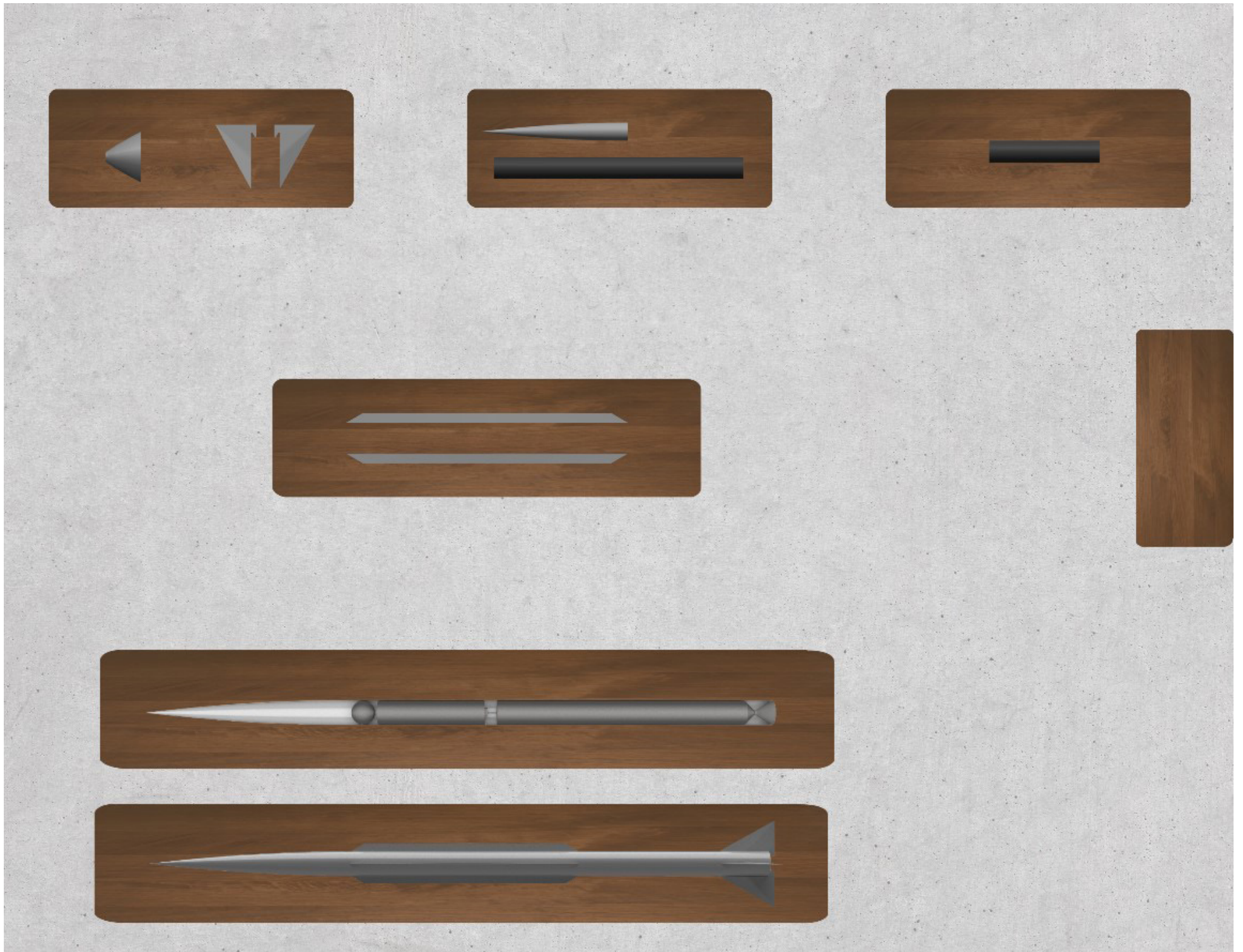


Figure 28.3: Part Flow through Manufacturing Plant

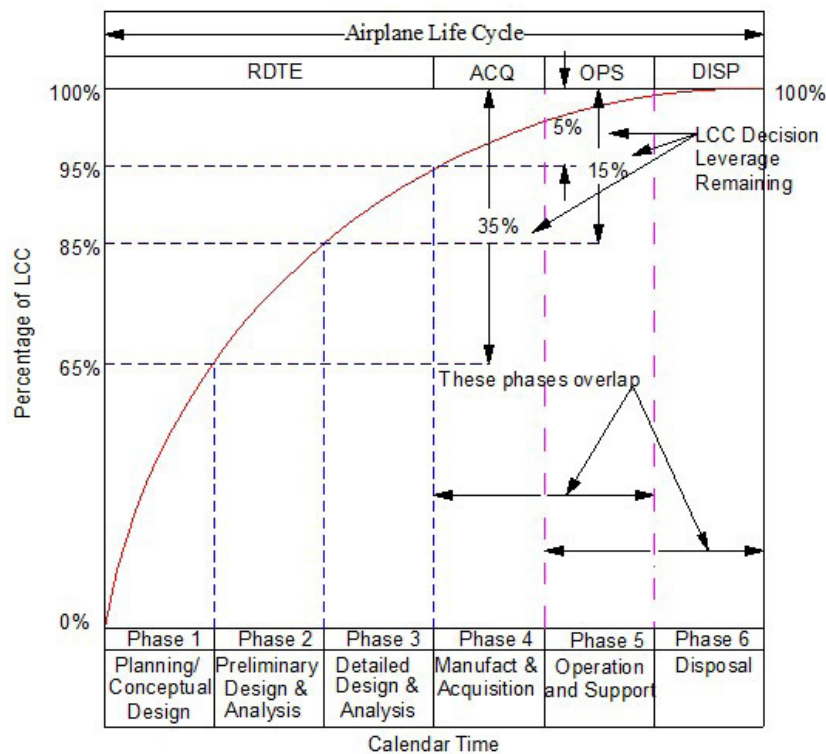
29. Cost Analysis

A cost analysis was performed following the procedures laid out in Jan Roskam’s Airplane Design Part VIII (Ref. 35), which were implemented into Advanced Aircraft Analysis (AAA), a comprehensive airplane design program.

An aircraft’s life cycle can be broken up into four distinct phases:

1. Research, Development, Testing, and Evaluation (RDTE);
2. Manufacturing and Acquisition (ACQ);
3. Operations (OPS);
4. Disposal (DISP).

For Road Runner, the disposal stage will not exist, as the aircraft’s life cycle ends when it is terminated in flight. Generally, RDTE comprises the majority of an aircraft’s life cycle cost (LCC), and the percentage of LCC decreases over the length of a program. This concept is displayed in Figure 29.1.



Impact of Airplane Program Phases on Life Cycle Cost

Figure 29.1: Impact of Aircraft Program Phases on Life Cycle Cost

The RDTE cost was investigated first. RDTE is broken into planning, preliminary design, and detailed design, and many different expenses so into calculated the total RDTE cost. Notable parameters that affect the RDTE cost are the Aeronautical Manufacturers Planning Report (AMPR) Weight, maximum

equivalent airspeed, and the number of aircraft produced for testing, which was specified as 15 in the RFP. The breakdown of expenses is shown in Table 29.1.

The next phase of the aircraft's life cycle is acquisition. This phase consists of engineering and design for manufacturing, program production, and test operations. Notable parameters for the acquisition cost

estimation were the AMPR weight, maximum equivalent airspeed, and the number of aircraft produced, which was specified as 350 in the RFP. The acquisition expenses are shown in Table 29.2.

Because the disposable phase is non-existent for Road Runner, the operations phase is the final phase of the life cycle. Road Runner will be terminated after majority of uses, so the operating costs are low. The driving factors for this price estimate were properties of the HTPB propellant and LOx oxidizer, including

weight, cost, and density. The estimates for operation costs are shown in Table 29.3, and a summary of all expenses

Table 29.3: Operation Costs

Operation Phase	
Fuel, Oil, and Lubricants	\$ 41M
Total Operating Costs	\$ 41M
Operating Cost per Hour	\$ 3800

is shown in Table 29.4.

The acquisition phase was the largest portion of the costs. This differs from the trend observed in

Figure 29.1, however, as seen in Figure 29.2, a general quadratic trendline still fits the data with some accuracy. The main reason for the increased acquisition time and cost compared to RTDE is because of the low number of target drones produced for RTDE. Additionally, less testing during the RTDE phase is required because the aircraft are

likely to be terminated after a single mission.

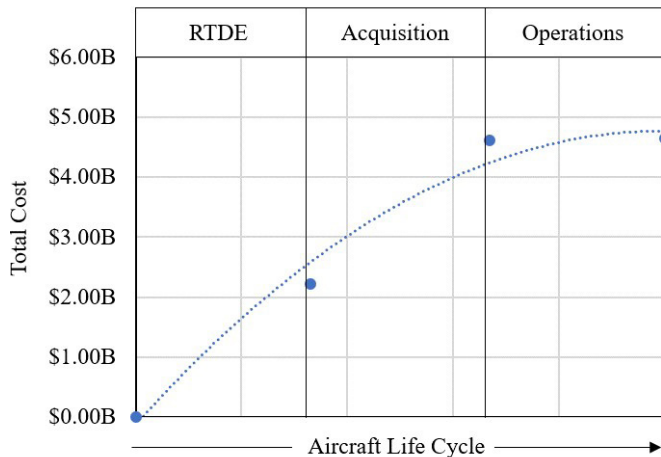


Figure 29.2: Total Cost over Road Runner's Life Cycle

Table 29.1: RDTE Costs

Research Development Testing and Evaluation Phase	
Airframe Engineering and Design	\$ 404M
Development, Support, and Testing	\$ 259M
Flight Test Aircraft	\$ 542M
Flight Test Operations	\$ 127M
Test and Simulation Facilities	\$ 444M
Financing	\$ 222M
RDTE Profit	\$ 222M
Total RDT&E Costs	\$ 2.22B

Table 29.2: Acquisition Costs

Acquisition Phase	
Airframe Engineering and Design for Manufacturing	\$ 333M
Program Production	\$ 1.47B
Production Flight Test Operations	\$ 80M
Financing	\$ 253M
Total Manufacturing Cost	\$ 2.14B
Profit	\$ 253M
Acquisition Cost	\$ 2.39B
Aircraft Selling Point	\$ 16.2M

Table 29.4: Summary of Costs

Cost Summary	
RDTE Cost	\$ 2.22B
Acquisition Cost	\$ 2.39B
Operation Cost	\$ 41.1M
Life Cycle Cost	\$ 4.65B



29.1 Conclusions and Recommendations

The main findings from this chapter are the cost and selling point for Road Runner. The target drone will incur a life cycle cost of \$4.65 billion, and will be listed at a selling point of \$16.2 million.

The methods outlined in this section offer a good preliminary estimation of costs, but the authors recommend performing a higher-fidelity investigation into the manufacturing, development, and testing processes required to produce the Road Runner.

30. Class II Stability and Control

The class II stability and control was completed using the methods presented in Airplane Design Part VII (Ref. 36), with supporting documentation from Part VI (Ref. 27). Calculations were also completed with the supporting information found in “Tactical Missile Design” by Eugene Fleeman (Ref. 13).

Dynamic stability is broken down into different regulations for specific types of aircraft. The Road Runner target drone falls under the ‘Select Weapon Systems’ sub-section of military aircraft. This states that there is no passenger limit, no weight limits, and all regulations are under Military: Appendix B. Stability regulations are classified under three different levels, Level 1 being the best and Level 3 being the worst. These levels depict the flying and handling qualities for the aircraft, along with the level of difficulty they will induce on the pilot.

30.1 Dynamic Longitudinal Stability

The dynamic longitudinal stability criteria for the missile design required being classified as one of two types of control: inherent stability or de-facto stability. For the Road Runner, de-facto stability was selected for analysis. This is due to the flight controls being controlled electronically, and not manually.

The two main stability and control criteria for the dynamic longitudinal stability are the phugoid damping and short period damping limits. These are what determine the handling quality levels for the Road Runner. The damping ratio for the phugoid mode stated that for Level 1 stability, the phugoid mode > 0.04 .

The short period stability criteria were more heavily limited within the ranges of numbers. The natural frequency in the short period mode must not be greater than 100 Hz. The short period mode itself was broken into two categories for types of flight. The target drones fell into Category A, requiring the short period damping to be greater than 0.35 and less than 1.30. Table 30.1 shows the handling qualities for both the phugoid and short period are listed.

Table 30.1: Dynamic Longitudinal Stability

Stability Criteria	Stability Limits	Road Runner Value	Handling Quality Level
ζ_p	$\zeta_p \geq 0.04$	0.07	Level 1
ω_{nsp}	$\omega_{nsp} \leq 100$ Hz	99 Hz	Level 1
ζ_{sp}	$0.35 \leq \zeta_{sp} \leq 1.3$	1.3	Level 1

With these meeting Level 1 requirements, the next check was to see if the K_α and K_q values were able to dampen the coefficient of moments due to angle of attack and pitch. One important criterion towards solving for these

values was the mass moment of inertia around the y axis. This was done in Section 24. Table 30.2 shows the values and the requirements they had to satisfy for the design.

Table 30.2: Damping Coefficients

Stability Criteria	Stability Limits	Road Runner Value
K_α	$K_\alpha \leq 3,6000 \text{ deg/deg}$	3268
K_q	$K_q \leq 18,000 \text{ deg/(deg/s)}$	3458

30.2 Dynamic Lateral-Directional Stability and Dynamic Coupling

Two major components in an aircraft stability and control are the dynamic lateral-directional stability and dynamic coupling modes that occur. These variables can cause major issues for many aircraft designs. However, the Road Runner target drone does not need to design around these two variables. This is due to the axis-symmetric nature of the design along with its control mechanism. Because of this, the lateral and longitudinal stability and control derivatives are the same, which will follow the restrictions set in Section 30.1.

30.3 Conclusions and Recommendations

The authors conclude that:

- The Road Runner properly meets all Level 1 criteria requested for a de-facto stability

controlled aircraft.

Figure 30.1: Hand Calcs

The authors recommend that:

- Further analysis and comparison of the stability and control criteria be conducted with

external software dedicated towards stability and control.

31. Advanced Performance

This chapter will use methods from Roskam's Airplane Design Part VIII (Ref. 35) to determine the Road Runner's performance in multiple flight modes.

31.1 Takeoff and Stall

Since the Road Runner is a rocket with a thrust to weight ratio greater than 2, take off will easily be obtained. Also, the road runner has enough thrust authority to fly out of any stall. However, the stall velocity during cruise would be 1734 ft/s or Mach 1.78 which is considerably slower than our flight envelope of Mach 2 to Mach 4.5.

31.2 Climb

An important characteristic of the Road Runner is its ability to climb. While in cruise, the Road Runner can climb at a rate of 8900 ft/min which is 8.9 times higher than the military requirement of 1000 ft/min. Another important factor for maneuverability is the excess power an aircraft has. Excess power is directly proportional to the throttle control at each flight phase. The MQM-1A was put to the test against an AQM-37 Jayhawk. As Figure 31.1 depicts, the Road Runner has a much greater top speed and maneuverability at high speeds. However, it is lacking in maneuverability at low speeds.

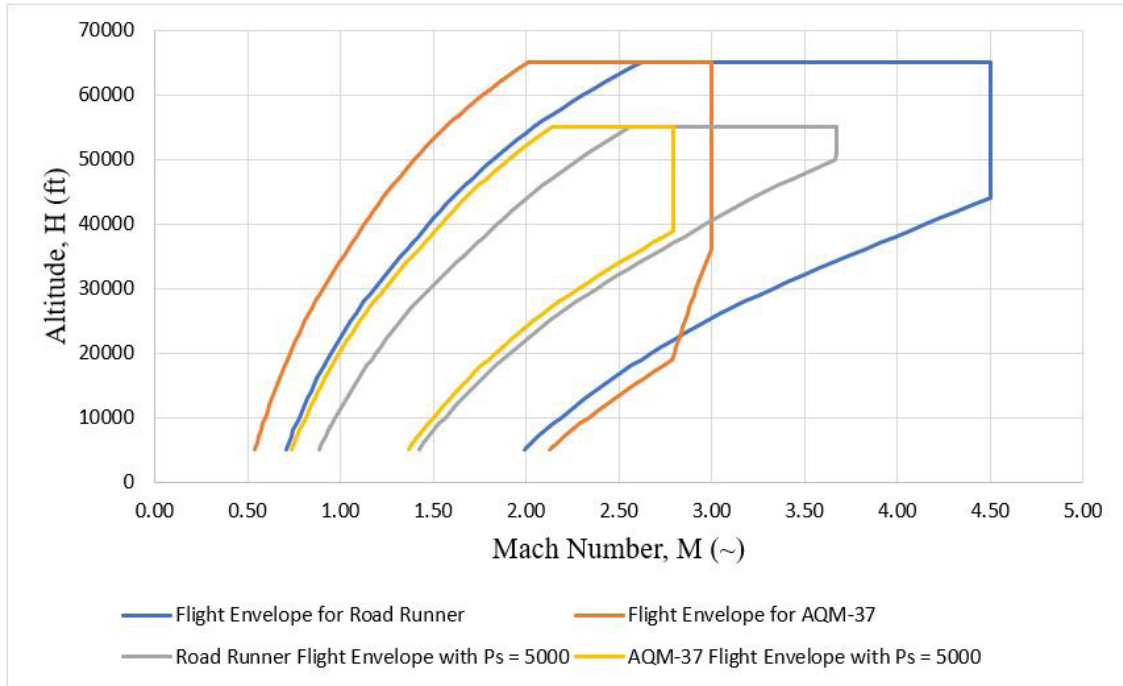


Figure 31.1: Flight Envelopes with Excess Power

31.3 Cruise, Range, and Payload Range

The Road Runner has two different cruise specifications due to its ability to perform a high diver and nap of the earth flight profile. The specifications of both can be seen in Table 31.1.

Table 31.1: Cruise Specifications

Mission Profile	Max Cruise Speed (Mach)	Max Altitude (ft)	Max Payload (lbf)
High Diver	4.5	65,000	500
Nap of the Earth	3.5	200	500

The range of the MQM-1A was found using the Breguet range equation which can be seen in Figure 31.6. The calculated range for both profiles respectively can be seen in Figure 31.2 and Figure 31.3.

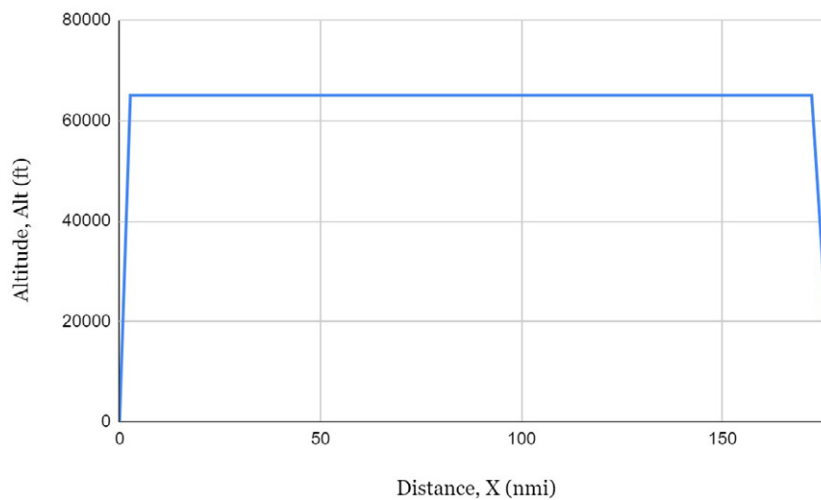


Figure 31.2: High Diver Range Profile

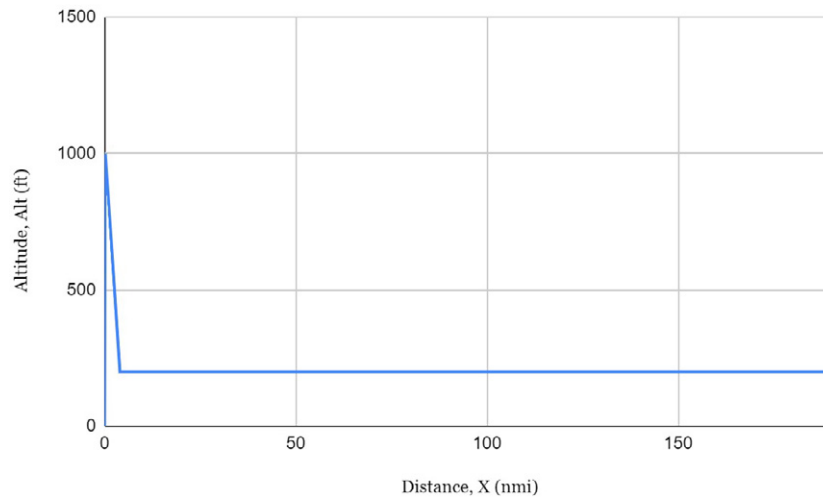


Figure 31.3: Nap of the Earth Range Profile

31.4 Endurance and Loiter

The mission of the Road Runner does not require a minimum endurance or loiter requirement. The Road Runner can last 120 seconds while full throttle which is enough time to reach a range of 87 nmi. However, with a less aggressive throttle cycle the Road Runner can reach a maximum range of 177 nmi which can be seen in Section 31.3.

31.5 Dive

As the name suggests, the high diver mission profile will feature a 75° dive at the end of the mission. As the target drone falls descends through the atmosphere the air density would exponentially increase. This increase in air density would increase the lift and drag forces that the aircraft experiences. The air temperature would also increase after the aircraft descends below 36,000 ft. This will affect the speed of sound. The dive was planned to be at a constant Mach of 3.5 and a constant

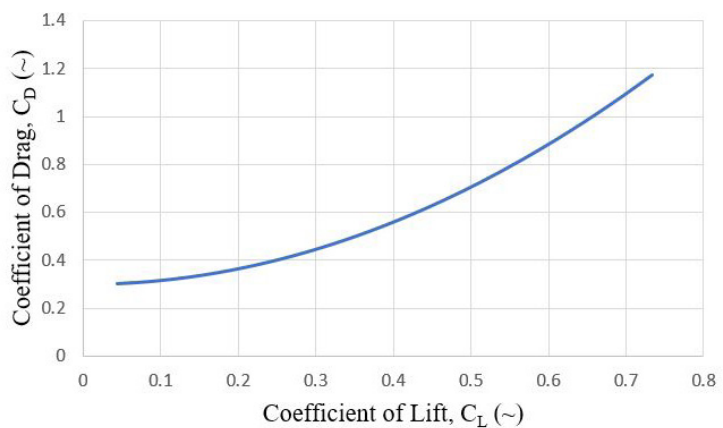


Figure 31.4: Drag Polar during Descent

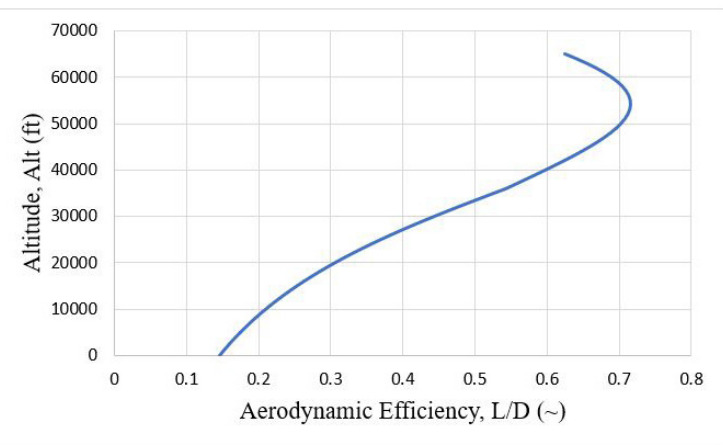


Figure 31.5: Aerodynamic Efficiency during Descent



dive angle of 75° . C_L and C_D were calculated using equations in Figure 31.6. Figure 31.4 and Figure 31.5 depict the drag polar experienced throughout the descent and the aerodynamic efficiency of the Road Runner throughout the descent.

31.6 Maneuver

The final leg of the nap of the earth mission will include a 15-g, instantaneous jiggling maneuver. Using equations from (Ref. 36), the authors were able to find the turn radius, turn rate, and bleed rate as depicted in Table 31.2. The jig will be performed at a Mach of 3.5.

Table 31.2: Maneuver Characteristics

Turn Radius	31706 ft
Turn Rate	7.06 deg/s
Bleed Rate	-126 ft/s ²

31.7 Landing

The mission of the Road Runner is to emulate a cruise missile to test defense system. Therefore, every MQM-1A should be critically damaged and most likely exploded. Because of this landing has not been modeled due to the likelihood of it not occurring. Recovery systems have been specified in Section 21.6.

31.8 Conclusions and Recommendations

The authors conclude that:

- The stall speed is 1794 ft/s, which is less than the mission envelope of Mach 2 to Mach 4.5;
- The Road Runner can outperform the AQM-37 during high speed flight, but underperforms in low speed maneuverability;
- The Road Runner is most efficient in its dive around 55,000ft;
- The MQM-1A can jig for 17 seconds before reaching a stall velocity.

Figure 31.6: Hand Calculations

The authors recommend:

- Increasing the maximum angle of thrust deflection, to decrease the stall speed;
- Jiggling at a lower speed, to decrease the turn radius;
- Decreasing the weight of the Road Runner at terminal maneuvers, to decrease the bleed rate.

Figure 31.7: Weights

32. Specification Compliance

The Roadrunner was designed to meet all RFP requirements. Table 32.1 shows the RFP requirements, the Roadrunner's specifications, whether its specifications meet the RFP requirements, and what page number in the report those specifications can be found on.

Table 32.1: Specification Compliance Check

Specification	Requirement	Expected Missile Performance	Specification Met?	Page #
Low Altitude				
Altitude	15 - 200 ft	15	✓	15
Cruise Mach	2 – 3.5	3.5	✓	15
Lateral Maneuvers	15 g's	15 g's	✓	41
Vertical Maneuvers	7 g's	15 g's	✓	41
High Altitude				
Altitude	5,000 – 65,000 ft	65,000 ft	✓	15
Cruise Mach	2 – 4.5	2.0	✓	15
Terminal Dive Angle	10° - 75°	10° - 75°	✓	74
Both				
Range	150 nmi	177 nmi	✓	74
Course Deviation	< 1500 ft	< 1500 ft	✓	44
CEP Diameter	50 ft	45 ft	✓	44
Payload Bay Size	3.5 ft long, 10 in diameter	3.5 ft long, 10 in diameter	✓	18
Payload Weight	500 lbs	500 lbs	✓	18

33. Marketing Plan and Path Forward

The selling point of the MQM-1A Road Runner is its ability to meet all RFP requirements while minimizing cost. The ability to recover and reuse the payload held in the nose of the missile, the use of aluminums and steels in all surfaces besides those exposed to extreme heat, and simplifying manufacturing processes all contribute to cost savings.

Another selling point is that the Roadrunner comes in modular designs. To capitalize on overseas sales MQM-10 has no payload bay which reduces the overall length by over ten feet. This will reduce the cost of the missile and improve its range and top

speed. The MQM-2A is a model that is specifically designed for missions without high G maneuvers. A combination of both domestic and foreign sales will allow for the company producing the Road Runner to re-invest in the development of new airborne weapon systems. Figure 33.1 shows the Road Runner’s revenue and expenditures over time.

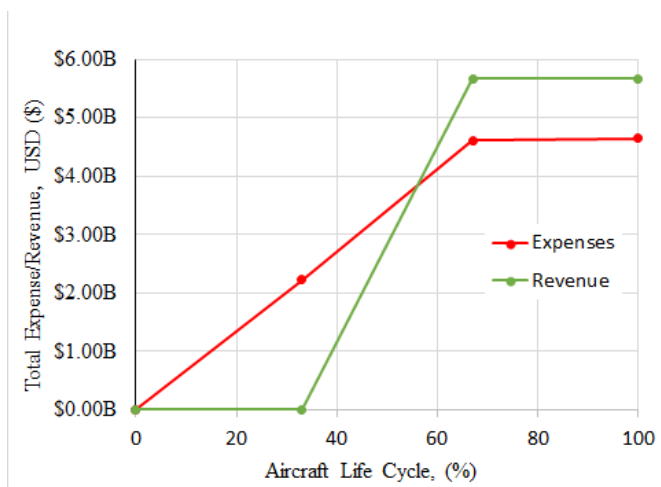


Figure 33.1: Road Runner Life Cycle Revenue and Expenses

References

1. Anon, “2019-2020 Graduate Team Missile Systems Design Competition – Supersonic Aerial Target” AIAA Design Competitions, Web Site, [https://www.aiaa.org/docs/default-source/upload-edfiles/education-and-careers/university-students/design-competitions/34771-mstc_graduate_design_competition.pdf?sfvrsn=588f9774_0] American Institute of Aeronautics and Astronautics, Reston, VA 2019, 9 September 2019
2. Roskam, Jan, “Airplane Design: Part 1, Preliminary Sizing of Airplanes,” DARcorporation, Lawrence, KS, 2005.
3. Anon, “GQM-163A Coyote Supersonic Sea Skimming Target [Fact Sheet].” 2018, https://www.northropgrumman.com/Capabilities/SupersonicMissileTargets/Documents/Coyote_Factsheet.pdf
4. Parsch, Andreas. “Lockheed Q-5/AQM-60 Kingfisher” Lockheed AQM-60 Kingfisher, 2002, www.designation-systems.net/dusrm/m-60.html.
5. Anon, “Beechcraft AQM-37A Jayhawk” Naval Air Museum Barbers Point, 2019, www.namp.org/beechna-air-museum/aqm-37a-jayhawk.com
6. Parsch, Andreas, “Nord/Bell CT.41/PQM-56” PQM-56, 2003, <http://www.designation-systems.net/dusrm/m-56.html>
7. Anon, “Meteor Beyond Visual Range Air-to-Air Missile [Fact Sheet].” MBDA Missile Systems, 2018, <https://www.mbda-systems.com>
8. Parsch, Andreas, “Raytheon (General Dynamics) RIM-67 Standard ER” Rim-67, 2003, <http://www.designation-systems.net/dusrm/m-67.html>
9. Carter, R., “Missile Sketches,” University of Kansas Department of Design., 2019.
10. Farokhi, S., “Engine Design and Design Vector Consultation,” The University of Kansas Aerospace Engineering Department, 10:00-11:00 am , 11 September 2019.
11. Keshmiri, S., “Aerodynamics and Design Vector Consultation,” The University of Kansas Aerospace Engineering Department, 10:00-11:00 am , 10 September 2019.
12. Barrett, R.M., “Statistical Time and Market Predictive Engineering Design (STAMPED) Techniques for Aerospace System Preliminary Design. J Aeronaut Aerospace Eng 3:” 2018, e121. doi:10.4172/2168-9792.1000e121.
13. Fleeman, E., “Tactical Missile Design,” 1st ed., American Institution of Aeronautics and Astronautics, Reston, VA, 2001.
14. Taghavi, R., “Engine Selection and Technical Parameter Discussion,” The University of Kansas Aerospace Engineering Department, 10:00-10:45 am , 13 September 2019.
15. Stivers, L. “Studies of Optimum Body Shapes at Hypersonic Speeds.” National Aeronautics and Space Administration. Washington D.C. 1967.
16. Humble, Ronald W., “et al. Space Propulsion Analysis and Design.” McGraw-Hill, 2007.

17. Story, George. "Fundamentals of Hybrid Rocket Combustion and Propulsion." *Fundamentals of Hybrid Rocket Combustion and Propulsion*, by Martin J. Chiaverini and Kenneth K. Kuo, American Institute of Aeronautics and Astronautics, 2007, pp. 513–592.
18. Sutton, George P., and Oscar Biblarz. "Rocket Propulsion Elements." John Wiley & Sons Inc., 2017.
19. Barrett, RM, "AE521_SSAT_RB2a" University of Kansas, 2019, <https://vimeo.com/360444990>
20. Roskam, Jan, "Airplane Design: Part 2, Preliminary Preliminary Configuration Design and Integration of the Propulsion System," DARcorporation, Lawrence, KS, 2005.
21. Nowell Jr., J., "Missile Total and Subsection Weight and Size Estimation Equations," Naval Postgraduate School, June 1992.
22. Roskam, Jan, "Airplane Design: Part V, Component Weight Estimation," DARcorporation, Lawrence, KS, 2005.
23. Roskam, Jan, "Flight Dynamics Part II", DARcorporation, Lawrence, KS, Reprint 2009.
24. Barrett, RM, "AE521_SSAT_RB4_movie" University of Kansas, 2019, <https://vimeo.com/370004970>
25. Jorgensen, Leland, H., "A Method for Estimating Static Aerodynamic Characteristics for Slender Bodies of Circular and Noncircular Cross Section Alone and With Lifting Surfaces At Angles of Attack From 0° to 90°," Ames Research Center, April 1973.
26. Darling, John, A., "Handbook of Blunt-Body Aerodynamics Volume 1 Static Stability," Naval Ordnance Laboratory, December 1973.
27. Roskam, Jan, "Airplane Design: Part VI, Preliminary Calculation of Aerodynamic, Thrust, and Power Characteristics," DARcorporation, Lawrence, KS, 2005.
28. Barrett, RM, "AE521_SSAT_RB5a" University of Kansas, 2019, <https://vimeo.com/372897889>
29. Harasani, W., "A Survey of Subscale Aircraft Primary Flight Control Actuator Dynamic Response Characteristics," King Abdulaziz University, 2015.
30. Robinson, Trevor, "Choosing the Electric Power System for a Short Range Missile," Northrop Corporation Norair Division, 1966
31. Anon, "G-12 Cargo Parachute Assembly." Mills Manufacturing, Mills Manufacturing Web Site, Asheville, NC, <https://www.millsmanufacturing.com/products/g-12-parachute/#tab-id-2>
32. Roskam, Jan, "Airplane Design: Part III, Layout Design of Cockpit, Fuselage, Wing and Empennage: Cutaways and Inboard Profiles," DARcorporation, Lawrence, KS, 2005.
33. Kouroupis, James, "Flight Capabilities of High-Speed-Missile Radome Materials," APL Technical Digest, 1992
34. Roskam, Jan, "Airplane Design: Part IV, Layout Design of Landing Gear and Systems," DARcorporation, Lawrence, KS, 2005.
35. Roskam, Jan, "Airplane Design: Part VIII, Airplane Cost Estimation: Design, Development, Manufacturing and Operating," DARcorporation, Lawrence, KS, 2005.

36. Roskam, Jan, "Airplane Design: Part VII, Determination of Stability, Control and Performance Characteristics: FAR and Military Requirements," DARcorporation, Lawrence, KS, 2005.